# BIOACTIVE CONDUCTING POLYMER COATINGS FOR IMPLANTABLE NEURAL AND COCHLEAR ELECTRODES

by

Jeffrey L. Hendricks

A dissertation submitted in partial fulfillment
of the requirements for the degree of
Doctor of Philosophy
(Biomedical Engineering)
in The University of Michigan
2008

Doctoral Committee:

Professor David C. Martin, Chair
Professor Daryl R. Kipke
Associate Professor Joerg Lahann
Assistant Professor Joseph M. Corey

This dissertation is dedicated to the future generations of scientists and engineers. Let your curiosity and knowledge guide you to leave a better world than we inherited.

## Acknowledgements

First, I would like to thank my advisor, Dr. David Martin for the opportunity to be a part of this amazing research. He has provided support, motivation, and sage guidance throughout my doctoral studies while pushing me to set the highest standards for myself. He has taught me more about science and life than I ever could have imagined.

I am especially grateful to the members of my doctoral committee, Dr. Joseph Corey, Dr. Daryl Kipke, and Dr. Joerg Lahann, for their time and advice throughout my studies and for keeping the doors to their labs open for me. I would also like to thank Dr. Douglas Noll for valuable discussion and advice.

This interdisciplinary research would not have been possible without the help of many extraordinary colleagues and collaborators. My sincere thanks to Dr. Yehoash Raphael, Dr. Bryan Pfingst, Jen Chikar and Dr. Mark Crumling in the Kresge Hearing Research Institute. Thanks to Dr. Steve Yalisove for educating me about the finer points of laser machining and coffee preparation and to Joel McDonald for his encouragement, insight and friendship throughout the dissertation process. My thanks to Andres Lasagni for great feedback as well. Chris Pacheco has been a great friend, teacher, and supporter throughout.

Many people supported this work in other ways. The technology transfer office at UM has supported our research and have made possible its commercial development. I am particularly grateful to Allied Minds for supporting and guiding our research in crucial ways. I am indebted to the staff of the Biomedical Engineering and Materials Science and Engineering Departments. And to John Roos, who has supplied motivation in many forms.

My thanks go to the entire Martin Research group—my lab family—for creating a stimulating and supportive environment to work in. I have learned from each and every one of you. My sincere appreciation goes to the many students that have directly assisted with my research. I am especially grateful to Sarah Richardson-Burns for her great friendship, generosity, and mentoring throughout so much of this unexpected journey. Thanks also to Charles Shaw for great conversation over many delicious cups of coffee.

I am extremely grateful for the immense talent, patience and support of my girlfriend, Caitlyn Cody Gertz. She has kept me on the path to happiness and graduation. I can only hope to give her as much support throughout her graduate studies as she has given me. My appreciation to Bella for great walks in all seasons.

Last but certainly not least, it is not possible to thank my mom, dad, and brother Steven enough for their endless support and love. I am immensely appreciative of their patience, sacrifices, and encouragement. Everything that I have achieved has been made possible by them.

# Table of Contents

# List of Figures

**Figure**

# List of Tables

**Table**

## Abstract

Neural prostheses facilitate communication with the nervous system for the diagnosis, treatment, and functional recovery from neurological illness or trauma. These devices require electrodes that can be permanently implanted, provide a stable electrical connection to the nervous system for reliable interaction, and do not produce adverse effects. Unfortunately, the immune and inflammatory reaction to implanted electrodes often leads to the formation of fibrous tissue that limits charge transfer and renders longterm performance unreliable.

This dissertation presents the development and characterization of a number of novel electrode coatings designed to promote enhanced functional integration at the tissue-electrode interface. The primary constituent of these coatings is the conducting polymer poly(3,4-ethylene dioxythiophene) (PEDOT). PEDOT is a suitable material for interfacing electrodes with tissue because it is biocompatible, conducts both electronic and ionic charge, is easily functionalized with cells and biomolecules, and mediates the mechanical mismatch often found when metallic or ceramic probes are implanted in soft tissue. In addition, PEDOT-based coatings can be rapidly and reproducibly deposited on individual electrode sites.

To form electrode coatings containing live cells or cellular components, PEDOT was deposited around living neuroblastoma and primary cortical neurons. These coated electrodes had 73% lower 1 kHz impedance than uncoated metal while delivering live cells to direct the tissue response. Spongy coatings and tissue engineering scaffolds were made from PEDOT deposited in alginate hydrogel containing live cells and were capable of delivering over 25 times more current at the same voltage than the same electrode without PEDOT.

Laser patterning of PEDOT films was performed to produce electrode coatings capable of directing neuronal orientation and elongation. Laser interference patterning of 825 nm thick PEDOT coatings with channels of period 7.82 μm resulted in the alignment of up to 87% of neurites in the direction of the pattern without compromising the improved electrical properties of the coating.

Finally, evaluation of conducting polymer and hydrogel coatings on cochlear implants was performed. Coatings on cochlear electrodes reduced the electrode impedance by 80 and 99% at 1 kHz and 10.7 Hz, respectively. These coated electrodes also delivered BDNF directly within the cochlea, increasing levels of the neurotrophin to 30.3 ng/ml after one week compared to 1.7 ng/ml in animals that received control implants without BDNF. When implanted into deafened guinea pigs, coated cochlear implants had reduced failure than uncoated implants and had a final average 1 kHz impedance of 5870 Ω compared to $1.2*10^6$ Ω for uncoated implants after 6 months.

Bioactive conducting polymer electrode coatings offer the ability to direct the tissue reaction and promote integration at the neuron-electrode interface while providing improved electrical transfer. Results from *in vitro* and *in vivo* testing indicates that these materials may be able to increase the specificity, reliability, and safety of clinical neural prostheses and thus enable the longterm use of next-generation neural prosthetic devices.

# Chapter 1

# Introduction and overview

## 1.1 Neural prostheses

### 1.1.1. Overview

Neural prostheses facilitate communication with the nervous system for the diagnosis, treatment, and functional recovery from neurological illness or trauma. In order to treat many chronic neurological diseases and conditions, it is necessary to have neural prosthetic devices that include electrodes that can be permanently implanted and that will provide a stable electrical connection to the nervous system for reliable interaction without adverse effects. Unfortunately, the tissue reaction to implanted electrodes often leads to encapsulation with fibrous tissue that limits charge transfer and renders longterm performance unreliable. Efforts to direct the tissue reaction and promote integration at the neuron-electrode interface using biomimetic and bioactive materials may result in increased specificity, reliability, and safety of clinically available devices and could provide the necessary tools to enable the use of next-generation neural prosthetic devices.

Currently, there are different kinds of neural prosthetic devices that have achieved clinical success treating neurological deficits using implanted

stimulating electrodes. Cochlear implants (CIs) have successfully provided auditory function to roughly 100,000 adults and children with severe deafness since FDA approval in 1985 [1-3]. These devices collect sound using an external microphone and transmit the signals to an electrode array placed within the cochlea that stimulates nearby neuronal processes. Deep brain stimulation (DBS) was recommended for use by the FDA in 1997 to control the tremors and motor dysfunction associated with Parkinson's disease and movement disorders [4, 5]. Similar to most neural prosthetic systems, the DBS system consists of an implantable pulse generator (IPG) which houses the battery and processors and connects via a lead to the implanted electrodes that communicate electrically with nervous tissue. The electrodes constantly deliver electrical pulses to the brain in order to control aberrant motor activity. Testing is also underway to use DBS for patients with drug resistant forms of epilepsy, chronic pain, obsessive-compulsive disorder, addiction, depression, Tourette syndrome, and restoration of consciousness from a vegetative state [6-9]. Vagal nerve stimulation is FDA-approved for epileptic seizure prevention, and is of interest for the treatment of depression and heart failure [8, 10]. Neural prosthetic devices are also available to treat chronic pain disorders using electrodes implanted within the spine [11]. In addition, a number of neural prosthetic devices can help paralyzed patients regain control of vital organ functions. Diaphragm pacing by phrenic nerve stimulation can serve as a long-term substitute for mechanical ventilators to regulate breathing [12], and other functional electrical stimulation devices are used for bladder and bowel control [13, 14]. The use of neural prosthetic devices for sensory, psychiatric, neurological, and homeostatic applications has transformed many lives in the past 25 years and has improved the quality of life for many patients.

Despite the great successes of clinical neural prosthetic devices, there are significant adverse effects and limitations associated with them. Electrical stimulation can unintentionally activate nearby structures that produce muscle spasms and the sensation of pain or heat [15]. Applying excessive voltages with an electrode may produce harmful reaction byproducts such as salt deposits or

gas bubbles, damaging tissue near the electrode [16]. Many studies have also shown that local neuronal viability is compromised due to implanted neural electrodes [15, 17]. Many neural prosthetic devices in development for new applications have unreliable chronic performance, precluding clinical use.

Visual prosthetics, auditory implants in the central nervous system, and permanent neural recording electrodes operate with small electrical signals and are therefore most susceptible to variations in the tissue composition and conductivity around the electrode site. Efforts to direct the tissue reaction near implanted neural electrodes are expected to improve the integration between electrodes and neurons, while preserving neural activity. A number of promising material-based technologies including drug delivery, cell delivery, hydrogels, micropatterned surfaces and conducting polymers may make this possible. These improvements will bring experimental devices closer to human use and will enable improvements in the function and safety of clinical devices.

### 1.1.2. Auditory prostheses

Auditory prostheses (APs) are some of the most widely-used neural prosthetic devices. By electrically stimulating components of the auditory neural pathway, they can restore auditory function. A wide variety of currently available and experimental APs serve to treat a broad range of clinical conditions. They can improve the hearing of patients with moderate hearing loss or hearing loss specific to certain frequencies, and can restore auditory function in patients with complete deafness. The success and effectiveness of AP therapy depends on many factors including electrode placement, device design, stimulus waveform, proximity of electrodes to neurons, auditory system pathology, integrity of neural pathways, and extent of fibrous tissue [18-20]. Animal studies have shown that the number of intact nerve fibers is an important indicator of cochlear implant (CI) success [21, 22]. Thus, methods capable of preventing degeneration of the auditory pathways, limiting fibrous tissue encapsulation and increasing neuronal viability after trauma or device insertion can improve the therapeutic benefits of APs.

A number of APs are available for patients with different physiological sources and degrees of hearing loss. For patients with significant residual hearing, hearing aids and middle ear implants can reliably improve hearing by amplifying sounds acoustically or mechanically, respectively [23, 24]. Damage to the conductive hearing structures of the middle ear can be circumvented using bone-anchored hearing aids which vibrate the entire temporal bone and cochlea. CIs have had great clinical success particularly with restoring speech perception for patients with extensive sensorineural hearing loss (SNHL) at the level of the cochlea [1-3, 25]. CI electrodes, shown in Figure 1-1, are placed directly into the cochlea to electrically stimulate the neuronal processes of the cochlear nerve. When the cochlear nerve is damaged or inoperable, auditory brainstem implants (ABIs) and auditory midbrain implants (AMIs), also shown in Figure 1-1, can be used to stimulate targets of the central auditory pathway including the cochlear nucleus (CN) and the inferior colliculus (IC) [26-30]. In order for APs to send rich acoustic information covering broad tonal and dynamic ranges, they must be coupled to a large, healthy population of neurons [19, 21, 31-35]. Unfortunately, as hearing loss progresses and less neural input is received, degeneration of auditory neurons and their processes occurs [36-39]. In addition, surgical implantation of CIs and devices in the central nervous system can cause trauma, inflammation, infection and reduction in the health and availability of target neurons near the implant [15, 35, 40]. While APs have been used to treat a variety of auditory system conditions, they still face various performance and safety limitations including immune rejection, infection, fibrous and bony tissue growth, encapsulating tissue response, device migration, and degeneration of the auditory nervous system. Improvements made at the neural interface can also improve place-pitch discrimination, tonal range and resolution, dynamic range and resolution, and power consumption.

### 1.1.3. Tissue reaction to implanted neural electrodes

Key to developing appropriate pharmacological and materials interventions to improve neural prosthesis integration and function is an

understanding of the tissue reaction to electrodes implanted in the central and peripheral nervous systems. In the brain, there is a multiple-stage response to implanted microelectrodes which is shown in Figure 1-2 [41]. The initial insertion of an electrode or array into the soft tissue causes trauma including tearing of neurons, glia and blood cells. The early tissue response typically lasts 2-4 weeks and includes inflammation, increased astrocyte proliferation, the presence of reactive astrocytes and growth of astrocytes within 100-200 µm of the implant. The severity of the early response is related to the magnitude of insertion trauma which correlates with the device size and geometry. The early response is followed by a sustained tissue response which is independent of the implant size or shape. The sustained response is characterized by the formation of a dense and compact fibrous sheath, composed of reactive astrocytes and reactive microglia. The dense fibrous tissue which is typically in place 6 weeks after insertion, reduces electro-ionic conduction between the electrode and neurons. In addition, a neuronal "kill zone" with decreased neuronal viability extends approximately 100-200 µm from the implant [17, 42, 43]. Unfortunately, during neural recording, microelectrodes sample only from a maximum distance of approximately 130 µm [44, 45].

Lenarz et al. [15] described the tissue reaction of cats implanted with AMIs in the IC. As shown in Figure 1-3 (A), after 2 months a fibrillary sheath about 60 µm thick was present around the implants. Reactive glial cells were also present in both stimulated and non-stimulated animals within 500 µm from the implant (Figure 1-3 (B)). The graph in Figure 1-3 (C) is evidence of the "kill zone", the area of decreased neuronal viability seen within 100 µm of the implant. A human brainstem implant removed due to infection showed coverage with a dense, collagen-rich sheath after 22 months of use [46]. The leads of the device were also covered by a sheath of connective tissue 150 to 430 µm thick. A study by Quester et al. [47] examined the local tissue reaction in rats to polyethylene terephthalate (PET) meshes used as electrode carriers in ABIs. The study again demonstrated the presence of a fibrous sheath around the meshes beginning 2 weeks after implantation, but also discussed the importance of fibrous tissue in

preventing the migration of implanted devices. In addition, other adverse effects were observed including fatal lesioning of brainstem structures and infections including meningitis. While cellular encapsulation is often necessary to prevent migration of the implant and to sequester foreign materials from tissue, it can also block critical device components such as electrodes and retard charge transfer at the electrode interface. This research highlights the importance of using soft materials which are less likely to cause lesioning once implanted, and using drug treatments such as anti-inflammatory and anti-bacterial agents in conjunction with implants to reduce the risk of infection and cell death.

The tissue reaction in the cochlea differs from that in the CNS primarily due to the bony structure of the cochlea. The cochlea is a fluid-filled bony spiral which houses spiral ganglion neurons (SGN) and processes as well as the sensory hair cells which transduce mechanical vibrations into electrical impulses. The bony structure may be partially responsible for the success of cochlear implants since it is more resistant to trauma than the soft tissue of the brain and helps isolate the electrode from other delicate structures. The insertion of CI electrodes into the scala tympani of the cochlea can cause trauma to the basilar membrane, spiral ligament, osseous spiral lamina, and lateral wall of the scala tympani leading to acute inflammation. The longterm effects of implantation include chronic inflammation, fibrous encapsulation, new bone growth, and further hearing loss [48, 49]. The amount of trauma to the lateral cochlear wall during the initial insertion has been shown to correlate with the amount of fibrous tissue and bone growth seen later [40]. In turn, the extent of fibrous tissue and bony growth has been associated with higher stimulation thresholds, reduced dynamic ranges, and decreased SGN viability [18, 50], although there is some debate on the subject [40]. It is widely agreed upon, however, that new bony and fibrous tissue in the cochlea limits subsequent treatment options including reimplantation and regeneration strategies [51]. Studies have mostly shown that electrical stimulation can help preserve SGNs, although there are a number of other factors which influence SGN viability including the initial surgical trauma, and subsequent bony and fibrous tissue formation [52-55]. However, the

administration of electrical stimulation to the cochlea can also increase the inflammation and encapsulation around the electrode in the scala tympani [56]. Variations in tissue response with respect to location, time since implantation, and between individuals can lead to significant differences in performance and can necessitate repeated doctor's visits or in extreme cases, removal and re-implantation of the auditory prosthesis.

## 1.2 Engineering the neuro-electrode interface

### 1.2.1. Overview and goals

In order for implanted neural prosthetic devices to communicate effectively and reliably with the human nervous system, the neuro-electrode interface must meet certain criteria. Ideally the components of the interface should be mechanically integrated, biologically functional, electrically conductive and permanent so that useful information can be transmitted throughout the lifetime of the device. In addition, if a neural prosthesis can interact selectively with a diverse group of neurons, then the functional range of the device, such as the tonal range of an auditory prosthesis, should improve. In most cases, implantable neural prosthetic devices are intended to last for the life of the patient, thus the composition of the interfacial tissue and neuronal population should ideally remain constant for decades. If the implant is able to move it may cause repeated trauma and inflammation to nearby tissue, and the electrodes will come into contact with varying neuronal populations. For the safe and efficient exchange of electrical information between the electrode and target neurons, it is desirable to have interfacial tissue which easily conducts charge. It is also important that the device is able to sample and interact with functional tissue. If the implanted device causes degeneration of nearby tissue or can only access unhealthy cells, it will reduce the effectiveness of stimulation and recording. Additionally, increased electrode selectivity, such as the ability to stimulate small clusters of cochlear neurons which correspond with specific frequencies, will

increase the functional range of the device while reducing unwanted stimulation. For recording, ultimately it is desirable to decipher the activity of individual neurons for the highest resolution and most accurate information. While it may be possible to achieve clinically useful treatment without achieving all of these goals, as we take steps towards making the neuron-electrode interface well integrated, permanent, and functional, the capabilities and safety of neural prosthetic devices will improve.

Many differences exist among the materials used for neural prostheses and the tissue into which they are implanted. Biomedical device materials are typically inert, dry, relatively stiff, flat, and electronically conductive while the tissues of the central and peripheral nervous systems are moist, alive, soft, rough or fuzzy, and ionically conductive. Neural prostheses are typically made from inert and biocompatible materials designed to elicit minimal chronic tissue reaction. Electrodes are often made from platinum, iridium, gold, or other noble metals [16]. Other non-reactive metals such as medical grade titanium and stainless steel as well as silicon are used for structural components. Soft, biocompatible polymers such as polydimethylsiloxane (PDMS or silicone) and polyurethanes are used for leads and other flexible components. While these materials are selected for their non-reactivity and stability, when implanted they still elicit a foreign body response which often leads to the formation of a fibrous capsule around the implant as shown upon removal of the device or histological evaluation [57]. This fibrous sheath may be useful for segregating the body from the implanted materials and for anchoring the device to prevent migration; however, this response can be problematic and restrict electrical charge transfer at the tissue-electrode interface. Especially at the tissue-electrode interface, it is desirable to prevent the fibrous tissue response and promote integration with viable neuronal structures. In order to achieve the aforementioned desirable interface properties, it is necessary to have materials which have properties similar to the tissue into which they are implanted. Bioactivity, including drug delivery and surface functionalization is the first step in using the body's own signaling cues to direct tissue adhesion, proliferation and migration. The

materials currently used for neural prosthetic devices are much stiffer than the tissues into which they are implanted. The brain has an elastic modulus of roughly 100 kPa while that of silicon is around 100 GPa [58]. Even the polysiloxane elastomer silicone has a modulus of 2 MPa, 20 times stiffer than brain tissue [59]. This modulus mismatch has been shown to create tremendous interfacial strains which can produce a chronic inflammatory response [60]. Part of the reason for the low modulus of neural tissue is their high water content. The materials traditionally used for medical devices are dry. A group of materials called hydrogels, used for wound repair and scaffolds have extremely high water content similar to tissue and may be useful for delivering cells or drugs and for buffering the tissue from the stiff probe. Another disparity between device materials and nervous tissue involves charge carriers. In the electrical components of neural prosthetic devices, including metals and doped silicon, charge is carried by electrons and holes. In our bodies charge is carried predominantly by ions, including $Na^+$, $K^+$, $Ca^{2+}$, $Mg^{2+}$, $Cl^-$, $HCO_3^-$ as well as organic anions [61]. The ionic charge carriers move more slowly than their electronic counterparts, and require an aqueous medium for conduction. The differences between the properties of man-made implanted neural prosthetic devices and the nervous system are most apparent at the interface between the two where the largest discrepancies exist. By conferring some of the mechanical, electrical, and bioactive properties of the nervous system to neural prosthetic device materials, it may be possible to facilitate integration and reduce the chronic immune and inflammatory responses that are in large part responsible for the failure of many devices.

### 1.2.2. Conducting polymers for biomedical applications

Conducting polymers are a class of materials made from small organic molecules that when linked together conduct charge due to overlapping electron orbitals along the conjugated polymer backbone. They include polyacetylene, polyaniline, polypyrrole (PPy), polythiophene, and their derivatives shown in Figure 1-4. These synthetic molecules have similar structures to melanin, a

naturally occurring ionic conductor found in our skin, brain and cochlea. The conducting polymer PPy has been studied most extensively for biomedical applications due to its biocompatibility and electrical properties [62, 63]. Cui et al. [64] demonstrated the ability to tailor the attachment of different cell types onto neural electrodes that had coatings of PPy containing various adhesion polypeptides. When implanted into the brain of guinea pigs, electrodes with PPy coatings containing the amino acid adhesion sequence DCDPGYIGSR produced increased neurofilament staining, indicative of connection with neuronal structures [65]. Recently there has been interest in poly(3,4-ethylene dioxythiophene) (PEDOT) and its derivatives for biomedical applications because of its increased chemical stability, conductivity, and processability [66-70]. Fuzzy and highly conductive PEDOT electrode coatings can also help mediate the mechanical mismatch by offering an intermediate stiffness between the brain and metallic electrode [71]. In addition, the morphology and conductivity of PEDOT electrode coatings can be varied by altering the counterion used during electrochemical deposition. Extremely high surface area structures can be made using polymeric counterions or surfactants [72, 73]. PEDOT has also been deposited around templates such as degradable microspheres to create porous films or into hydrogels to create diffuse polymer networks [74-76].

Research on the use of conducting polymers for neural engineering applications has demonstrated their biocompatibility, desirable electrical properties, including low impedance and high charge injection density, and ability to actuate upon application of electrical bias [77, 78]. Electrical stimulation of conducting polymer substrates has been shown to promote neurite outgrowth from cultured cells [79]. Upon application of charge, drug-loaded conducting polymers have been shown to expel minute quantities of ions, growth factors, corticosteroids or other compounds [80, 81]. Release of charged species from the conducting polymer matrix is thought to occur by charge compensation during electrical stimulation. When an electrical bias is applied to the pharmaceutical-loaded conducting polymer, mobile compounds with the same charge are expelled in order to balance the applied charge [82-85]. Conducting

polymers have also been functionalized with enzymes and used for biosensing applications which may offer a useful method for monitoring the chemical environment of the auditory system [66, 86, 87]. Recent studies detailed hereafter suggest that conducting polymers including PEDOT, PPy, polyaniline, and their derivatives may offer useful methods for directing the tissue reaction to neural electrodes while improving charge transfer between electrode and tissue.

Nerve growth factor (NGF) has been incorporated into conducting polymers for enhancing neural interactions. Kim et al. [88] immobilized NGF in both PPy and PEDOT using electrochemical co-deposition. The NGF in the films increased the attachment and neurite extension of PC12 (rat pheochromocytoma) cells. Covalent attachment of NGF to the surface of PPy also promoted neurite growth from PC12 cells. Co-administration of electrical stimulation in addition to the tethered NGF provided the most significant neurite elongation [89]. Thompson et al. [90] described the incorporation of neurotrophin-3 (NT-3) into PPy films during electrochemical deposition. The films were electrically stimulated using a variety of methods including cyclic voltammetry, pulsed potential, and pulsed current to determine the optimum release protocol. During the first day, there was a burst of neurotrophin release from all of the samples, including un-stimulated samples. Subsequently, diffusion from the un-stimulated sample was extremely low, while the electrically stimulated films continued to secrete neurotrophin [90]. The effect of these NT-3-containing PPy films on cochlear cells was further investigated by Richardson et al. [91], where the incorporation and delivery of NT-3 in PPy and its effects on explanted SGNs was assessed. Spiral ganglion explants cultured on the NT-3-containing PPy substrate exhibited 1.5 times more neurite outgrowth than explants grown on PPy without NT-3 or on tissue culture polystyrene. When biphasic pulses were applied to the coated electrodes for 1 hour, the cells responded with a 2.2-fold increase in neurite extension. Unstimulated samples containing NT-3 released roughly 2.1 ng of NT-3 within the first 24 hours. The study confirmed that NT-3 was being delivered from PPy substrates over 4 days, and that stimulation increased the delivery of neurotrophin.

Using conducting polymer actuators, it is possible to achieve repeatable, active release of pharmacological agents. One approach is to use bi-layer actuators built from conducting polymers to open small valves in order to release drugs from a reservoir [92]. Another approach is to coat drug-loaded fibers with conducting polymers that are then stimulated to release the drug contents within. Upon application of 1 V, drug is eluted from the conducting polymer-fiber coating. This process was shown to be effective at actively delivering dexamethasone at 54 days and beyond [80]. Actuators based on the expansion and contraction of conducting polymers due to the movement of ions can also be used to guide the placement of CIs. By attaching a conducting polymer actuator either into the lumen of a commercially available implant or onto the back of it, it is possible to create a steerable CI. This allows insertion and placement of the electrode closer to the target cells and with less damage to the outer wall of the scala tympani [93].

### 1.2.3. Micropatterning of conducting polymers

In addition to the biochemical cues at the surface of an electrode, the surface morphology plays an equally important role in controlling tissue adhesion and integration. Electrochemically deposited conducting polymers typically have a rough surface which has been shown to be compatible for the attachment of neural, glial, and cardiac cells [72, 77, 94]. In order to direct the growth of cells in a specific direction or to differentially adhere different cell types, methods to pattern conducting polymers at and below the scale of the cells, from approximately 100 nm to 10 µm, are necessary. Patterned conducting polymer surfaces can be used both *in vivo* or *in vitro* to align neural processes and direct cells towards electrodes or other targets.

A variety of methods have been used to pattern and template conducting polymers. Traditional photolithography has been used to create micron-scale conducting polymer features for microelectronic applications [95-97]. E-beam lithography has been used to create features as small as 50 nm with conducting polymers [98, 99]. Soft lithography techniques including microcontact printing

can be used to direct conducting polymer deposition from solution, resulting in features from 250 nm up to 50 µm such as those seen in Figure 1-5 (A) [100, 101]. Inkjet printing and surface energy-assisted inkjet printing are useful methods to pattern water soluble conducting polymers at and below the micron scale [102-104]. The use of self-assembled monolayers or polymer brushes in conjunction with other techniques can direct conducting polymer patterning such as the PPy features shown in Figure 1-5 (C) [105, 106]. Electrochemically deposited conducting polymers can be grown around various templating materials such as degradable polymer spheres that can be self-assembled onto the electrode surface prior to electrochemical polymerization. When the spheres are then removed, the conducting polymer is left intact with hexagonally-packed pores, as shown in Figure 1-5 (D) [74, 75].

Laser-modification can be used to pattern conducting polymer substrates with sub micron resolution. The laser can be used to initiate polymerization of photopolymerizable precursors or to remove material from the surface [107]. The low ablation threshold of conducting polymers can also be harnessed to selectively ablate the polymer without disturbing the underlying substrate [108]. Pulsed lasers provide the additional benefit of very low thermal distribution which helps to make more delineated features.

### 1.2.4. Hydrogels for neural prostheses

Hydrogels are materials composed of at least 90 % (w/v) water held together by a lightly crosslinked network of polymer chains. They are an ideal scaffold material for tissue engineering due to their 3-D porosity and high water content. Many types of gels have been used *in vitro* and *in vivo* for a number of uses and are FDA approved [109]. They can be made from either natural or synthetic sources and their biodegradability can be tailored from fully degradable to permanent [110, 111]. Since they are predominantly made of water, hydrogels are suitable as vehicles for the delivery of water soluble drugs or cells and can be tailored for delivering other compounds using emulsifying agents [112]. Hydrogels have been used extensively as surgical repair materials for otological

and neural applications. For neural prostheses they may be loaded with pharmaceuticals and applied during surgery to the implant site to reduce inflammation and stimulate neuronal growth, applied as a coating to the device to release their drug loads once implanted [113], or used to deliver cells on devices [114].

For cochlear and CNS drug delivery hydrogels are often used in the form of beads or sponges loaded with pharmaceutical compounds. A variety of growth factors have been delivered to the inner ear using hydrogels placed over the round window membrane (RWM). Noushi et al. used beads of alginate hydrogel to deliver NT-3 and found that release from the beads was nearly complete by 5 days. When these beads were implanted in guinea pig cochleae, there was minimal tissue inflammation or fibrous reaction. In deafened animals treated with 1.5 μg of NT-3 in alginate hydrogel beads placed on the RWM, the density of SGNs surviving after 28 days was significantly higher than controls [115]. Hydrogels loaded with BDNF have also been implanted in the middle ear to prevent SGN degeneration. After 1 week, animals implanted with BDNF-containing collagen hydrogels had significantly lower (improved) electrically-evoked auditory brainstem response thresholds, a significantly higher density of surviving SGN, and perilymph levels of BDNF over 100 times higher than control animals treated with saline [116, 117]. Both collagen-glutaraldehyde hydrogels and gelatin hydrogels have been used to deliver recombinant human insulin-like growth factor 1 to the inner ear to prevent noise-induced damage [118, 119]. Animals with these gels had lower auditory brainstem response thresholds and higher SGN survival than animals that received control gels. Burdick et al. [120] incorporated and delivered ciliary-neurotrophic factor (CNTF), NT-3, and BDNF into degradable hydrogels based on polyethylene glycol and polylactic acid to stimulate the outgrowth of sensory neurites. Neurotrophin release could be tailored by altering the concentration of polymer, as well as the loading conditions and polymer degradability. Functionalization of hydrogels with ECM components or adhesion molecules such as collagen, polylysine and laminin-1 may also help to promote stable tissue fixation at the interface, while minimizing fibrous

encapsulation [121]. Hydrogels have been shown to be effective for the delivery of cells, neurotrophins and other compounds to reduce inflammation and promote neuronal survival and may also find uses as scaffolds to direct desirable tissue adhesion to the implant surface.

### 1.2.5. Drug delivery for neural prostheses

The ability to locally deliver bioactive compounds including pharmaceutical agents and biological factors can alter the tissue response to implanted neural prostheses. Localized delivery from the implant can produce high concentrations of pharmaceutical agents using small quantities and without exposing the entire body to the drug. Many useful compounds can be delivered to optimize the properties of the tissue-electrode interface. Pharmaceutical agents such as the anti-inflammatory steroid dexamethasone are used to suppress the inflammatory and immune responses that lead to increased stimulation thresholds of cardiac devices [122, 123]. Antibacterial and antimicotic agents are used to reduce the risk of infection and direct the tissue reaction. The use of antibacterial agents with neural electrodes shows increased recording quality and longevity [124]. Adhesion peptides and molecules can be incorporated onto the surface to promote the attachment of desirable cell types such as endothelial cells or neurons [125, 126]. Growth factors can be immobilized or secreted to increase neurite extension and promote neuronal survival [88, 91]. Other compounds which show promise for improving the viability of target neurons in the CNS and PNS include anti-apoptotic agents, neurotransmitters and their agonists, antioxidants and hormones [127, 128]. By selecting and delivering the appropriate compounds in a controlled and localized manner, the tissue response can be tailored for optimal device performance.

For optimal pharmacological effect with fewest adverse effects, it is desirable to maintain constant concentrations within the therapeutic window. In order to achieve this, controlled, localized, and sustained delivery is necessary. Methods to achieve this include microfluidic delivery, degradable and non-

degradable materials for sustained release, surface functionalization, reservoirs, iontopheresis, and the aforementioned conducting polymers.

### 1.2.6. Cell delivery for neural prostheses

Cell-based therapies, including the delivery of stem cells and other cell types, is of interest for the repair, regeneration and protection of neuronal and sensory tissue [129]. There are two primary cell transplant options. The first is to implant cells that produce protective or therapeutic molecules either naturally, through differentiation, or by genetic modification. With genetic modification, cells are transfected with a genetic vector and then secrete specific proteins which can promote the health of endogenous tissue. The second treatment modality is to deliver cellular replacements for damaged or permanently lost cells including sensory hair cells, SGN, and neurons in the central nervous system. Progenitor cells can be implanted directly or within a support scaffold, such as hydrogel or other porous matrices, in order to rebuild damaged sections of the auditory or nervous system [130, 131]. The potential benefits of cell delivery for neural prostheses are to increase the viability of neurons and support cells or to replace entirely the missing cells required for processing and transduction of neural signals from implants to the brain. These techniques can affect not only prosthetic senses, but may improve natural sensory function as well.

Genetic modification of the transplant cells can be accomplished by various methods. Viral vectors including retroviruses, adenoviruses, and adeno-associated viruses can deliver genetic material to the cells of choice both *in vivo* and *ex vivo* [132]. Non-viral gene delivery methods including lipophilic delivery systems, electroporation, cationic polymers, ligand-mediated vehicles, and nanoparticles tend to be less cell-specific than viral methods. Warnecke et al. [133] demonstrated the ability of brain-derived neurotrophic factor (BDNF) secreted by lentivirus-transduced fibroblast cell lines to improve the survival and neurite outgrowth of SGNs in culture. Rejali et al. [114] used an adenovirus to transfer genetic materials to fibroblasts. The ability of these BDNF-secreting cells transplanted into the scala tympani within a hydrogel scaffold on a cochlear

implant to promote the survival of SGNs *in vivo* was confirmed. Transfected fibroblasts have also been used to deliver BDNF to the central nervous system. The transplantation of transfected fibroblasts prevented degeneration of dopaminergic neurons in a rat model of Parkinson's Disease [134]. Transplanted BDNF-secreting fibroblasts also helped reduce neuronal degeneration following ischemia [135]. These results suggest that the delivery of genetically modified cells can be used to prevent the degeneration associated with implantation trauma, lack of sensory input, or toxic conditions.

Olivius et al. [136] transplanted dorsal root ganglion (DRG) sensory neurons to the cochlea in order to restore damaged cochlear nerve pathways. Many cells survived transplantation into the scala tympani and attached near the organ of Corti. Infusions of BDNF and CNTF significantly increased the survival of transplanted cells in the cochlea. In further studies they confirmed the survival of transplanted DRGs in the cochlea, as well as the survival of transplanted embryonic and adult stem cells [137]. They found that embryonic stem cells showed the best survival, and that all cells required exogenous trophic factor support.

Stem cells have been of great interest for transplantation because they may provide an endogenous source of cells which can be differentiated into numerous phenotypes for cell replacement and delivery of trophic factors [138]. The major rationale for the use of stem cell-based therapies is that they provide a multipotent, endogenous survival and regeneration source for inner ear neurons and hair cells that do not regenerate naturally. The transplantation of mesenchymal stem cells into the inner ear has been shown to promote hearing recovery in a rat model of SNHL [139]. Parker et al. [140] have shown that neural stem cells, following transplantation into the scala tympani, expressed markers for key auditory cell types, including hair cells and SGNs.

While promising, cell-based strategies to direct the tissue response at the neuro-electrode interface present many difficulties in both research and clinical applications. These include the reliability of donor cell sources, knowledge of the cell differentiation process, compatibility of the delivered cells with the target

environment, and delivery of the appropriate cell type. Often in diseased and degenerative states many of the critical factors for survival of implanted cells are absent [131]. Strategies to differentiate stem cells into appropriate cell types have made progress [141, 142], but more research is needed to reliably produce the desired phenotype, and the risk of stem cell implants forming tumors still exists [143]. The studies above suggest that cell transplantation can improve neural prosthesis function by restoring components of the neural pathway, and in conjunction with other approaches such as tissue engineering and gene therapy, may help restore natural sensory function in hearing loss patients by replacing lost sensory hair cells.

## 1.3 Acknowledgements

Portions of this chapter are in press for publication in: Hendricks, J.L., J.A. Chikar, M.A. Crumling, Y. Raphael, D.C. Martin, *Localized cell and drug delivery for auditory prostheses*. Hearing Research, 2008. 242(1-2).

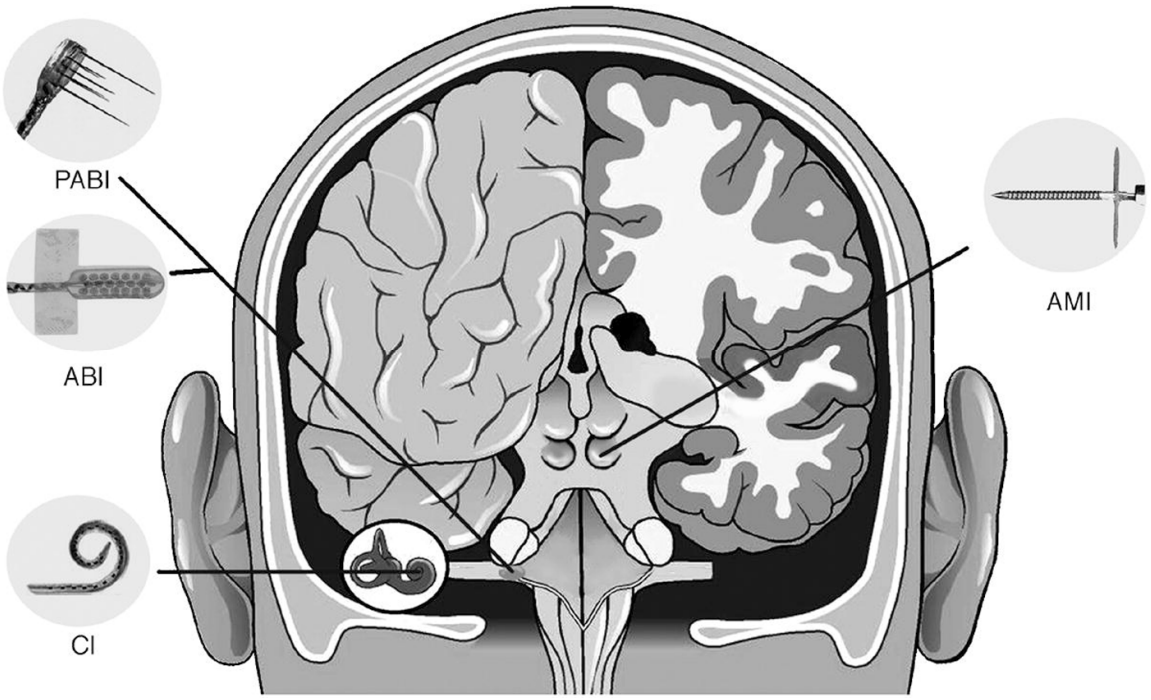


Figure 1-1. Schematic of auditory prostheses in the cochlea and central auditory pathway. The cochlear implant (CI) is used to stimulate cochlear nerve processes from within the cochlea. The auditory brainstem implant (ABI) is composed of a grid of surface electrodes to stimulate the cochlear nucleus. The penetrating auditory brainstem implant (PABI) is better able to access the tonotopic structures of the cochlear nucleus which lie parallel to the surface of the cochlear nucleus. The target of the auditory midbrain implant (AMI) is the inferior colliculus. (Lenarz et al., 2006)

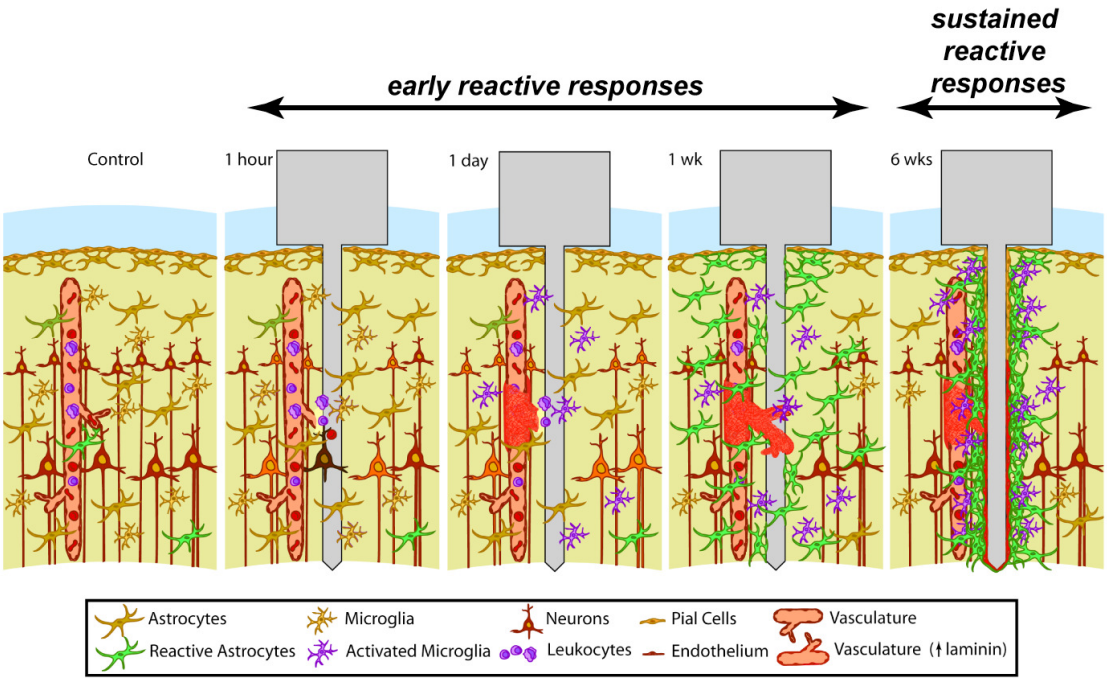


Figure 1-2. Schematic showing the components of the injury response to microfabricated silicon neural implants. Courtesy of William Shain, Wadsworth Center, Albany, NY.

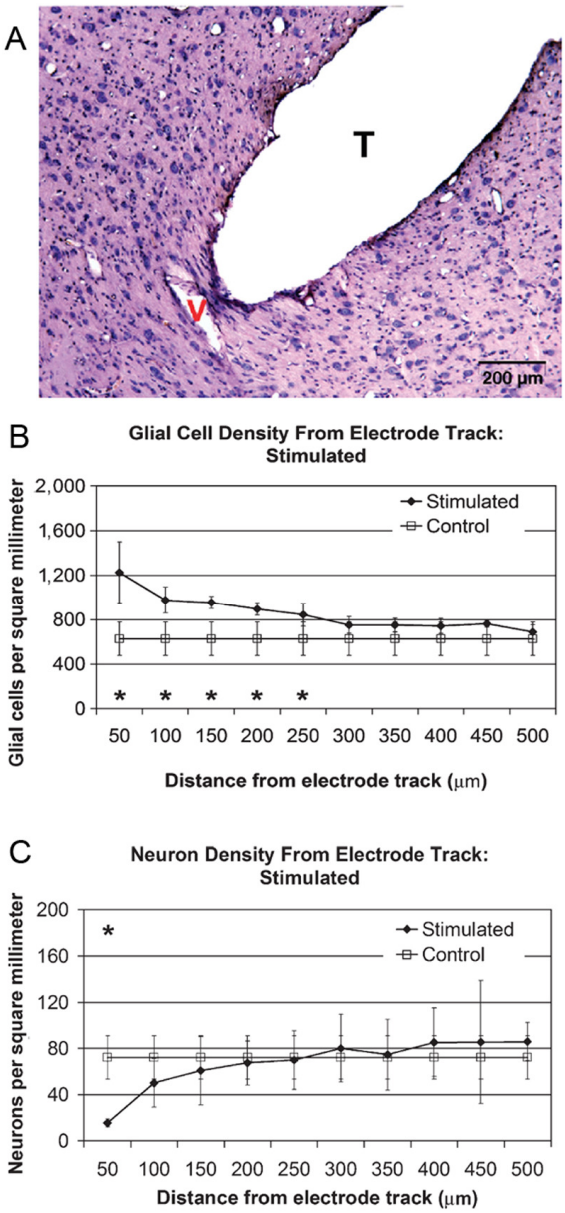


Figure 1-3. Tissue response to auditory midrain implant (AMI). (A) Histological section of feline inferior colliculus showing implant track, *T*, from an AMI that had been in place for 3 months and electrically stimulated for the final 2 months. Dense tissue around implant track is fibrous encapsulation of electrode and shows vascularization, *V*, and increased staining for glial fibrillay acidic protein suggesting presence of astrocytes around the implant. (B) Average glial cell density around the probe show elevated glial populations for up to 500 µm from the implant site. The difference is statistically significant for 50-250 µm (*) (4 animals). (C) The average density of neurons in the tissue surrounding the implant site is lower than in the control, unimplanted inferior colliculus. At 50 µm the difference in neuronal density is statistically significant (*), and around 200 µm from the implant no difference is seen (4 animals). (Lenarz et al., 2007)

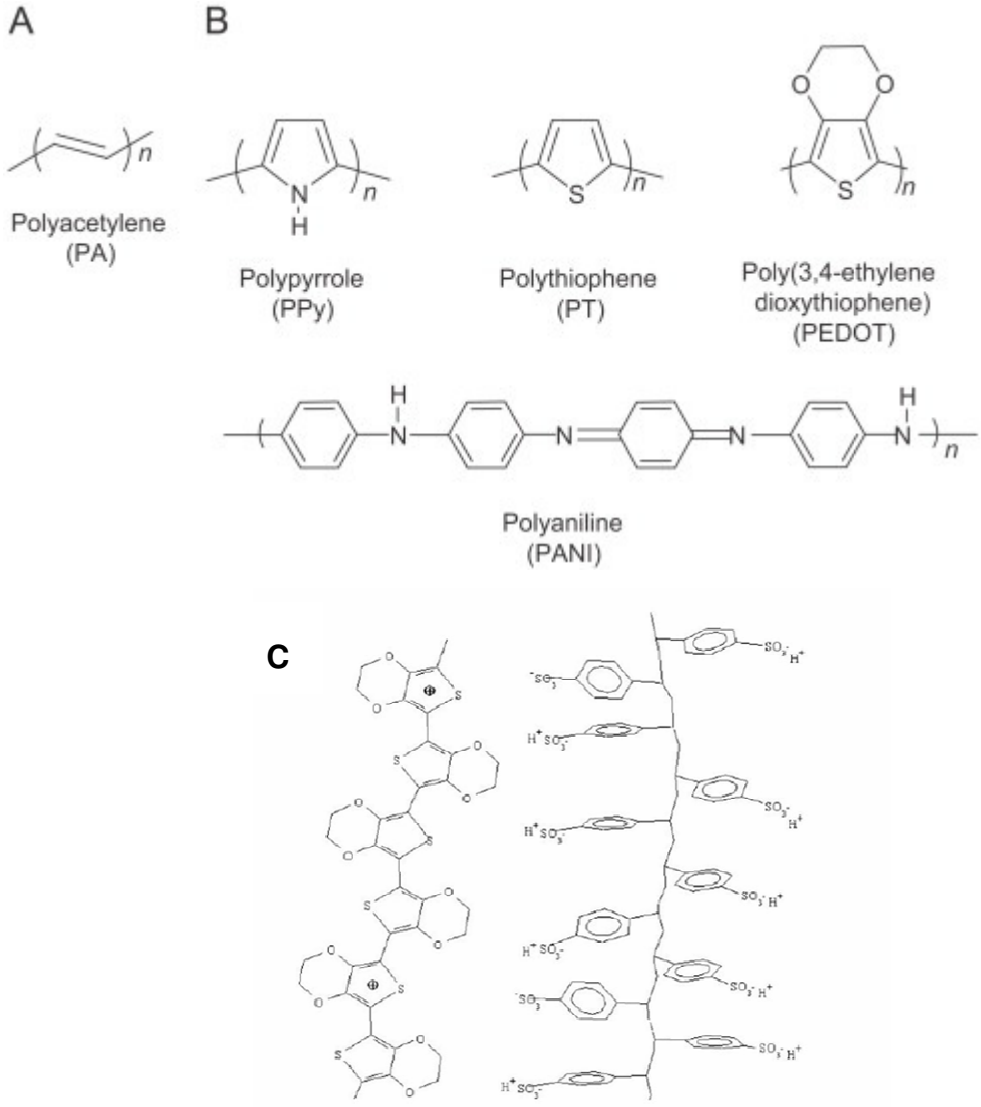


Figure 1-4. Molecular structures of various conducting polymers (A) Polyacetylene (PA), the first synthetic conducting polymer discovered. (B) Conducting polymers used in biomedical applications, including polypyrrole (PPy), polythiophene (PT), poly(3,4-ethylene dioxythiophene) (PEDOT) and polyaniline (PANI). (Guimard et al., 2007) (C) Postulated structure of PEDOT-PSS (Crispin et al., 2003).

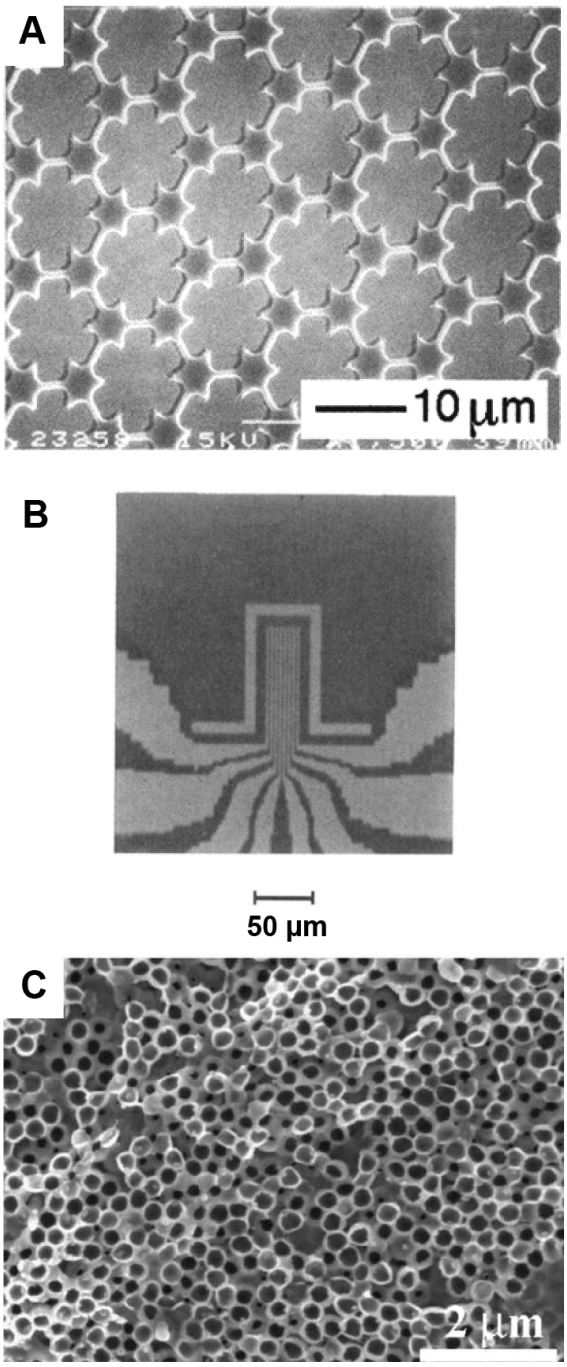


Figure 1-5. Micropatterned conducting polymers. (A) Polyaniline patterned using soft lithography. (Beh et al., 1999) (B) Polypyrrole electrodeposited onto a monolayer selectively irradiated to pattern conducting polymer growth. (Rozsnyai et al., 1995) (C) PEDOT-$LiClO_4$ electrochemically deposited around 300 nm polystyrene spheres which were then removed. (Yang et al., 2004)

# References


1. Cervera-Paz, F.J. and M.J. Manrique, *Traditional and emerging indications in cochlear and auditory brainstem implants.* Rev Laryngol Otol Rhinol (Bord), 2005. **126**(4): p. 287-92.

2. Deggouj, N., et al., *Today's indications for cochlear implantation.* B-ENT, 2007. **3**(1): p. 9-14.

3. Di Girolamo, S., et al., *Functional outcome of auditory implants in hearing loss.* Acta Neurochir Suppl, 2007. **97**(Pt2): p. 425-9.

4. Pena, C., K. Bowsher, and J. Samuels-Reid, FDA-approved neurologic devices intended for use in infants, children, and adolescents. Neurology, 2004. **63**(7): p. 1163-7.

5. Pena, C., et al., An overview of FDA medical device regulation as it relates to deep brain stimulation devices. IEEE Trans Neural Syst Rehabil Eng, 2007. **15**(3): p. 421-4.

6. Theodore, W.H. and R. Fisher, *Brain stimulation for epilepsy.* Acta Neurochir Suppl, 2007. **97**(Pt 2): p. 261-72.

7. George, M.S., et al., *Brain stimulation for the treatment of psychiatric disorders.* Curr Opin Psychiatry, 2007. **20**(3): p. 250-4; discussion 247-9.

8. Alexopoulos, A.V., et al., Electrical stimulation and gene-based neuromodulation for control of medically-refractory epilepsy. Acta Neurochir Suppl, 2007. **97**(Pt 2): p. 293-309.

9. Kern, D.S. and R. Kumar, *Deep brain stimulation.* Neurologist, 2007. **13**(5): p. 237-52.

10. Goodnick, P.J., et al., *Vagus nerve stimulation in depression.* Expert Opin Pharmacother, 2001. **2**(7): p. 1061-3.

11. Falowski, S., A. Celii, and A. Sharan, *Spinal cord stimulation: an update.* Neurotherapeutics, 2008. **5**(1): p. 86-99.

12. Exner, G. and G.A. Baer, Functional electrical stimulation in paralyzed respiratory muscles: International workshop in Hamburg, Germany. Neuromodulation, 2000. **3**(4): p. 211-217.

13. Ragnarsson, K.T., Functional electrical stimulation after spinal cord injury: current use, therapeutic effects and future directions. Spinal Cord, 2008. **46**(4): p. 255-74.

14. Peckham, P.H. and J.S. Knutson, *Functional electrical stimulation for neuromuscular applications.* Annu Rev Biomed Eng, 2005. **7**: p. 327-60.

15. Lenarz, M., et al., Auditory midbrain implant: histomorphologic effects of long-term implantation and electric stimulation of a new deep brain stimulation array. Otol Neurotol, 2007. **28**(8): p. 1045-52.

16. Merrill, D.R., M. Bikson, and J.G. Jefferys, *Electrical stimulation of excitable tissue: design of efficacious and safe protocols.* J Neurosci Methods, 2005. **141**(2): p. 171-98.

17. Biran, R., D.C. Martin, and P.A. Tresco, Neuronal cell loss accompanies the brain tissue response to chronically implanted silicon microelectrode arrays. Exp Neurol, 2005. **195**(1): p. 115-26.

18. Kawano, A., et al., Intracochlear factors contributing to psychophysical percepts following cochlear implantation. Acta Otolaryngol, 1998. **118**(3): p. 313-26.

19. Incesulu, A. and J.B. Nadol, Jr., Correlation of acoustic threshold measures and spiral ganglion cell survival in severe to profound sensorineural hearing loss: implications for cochlear implantation. Ann Otol Rhinol Laryngol, 1998. **107**(11 Pt 1): p. 906-11.

20. Blamey, P.J., et al., Factors predicting postoperative sentence scores in postlinguistically deaf adult cochlear implant patients. Ann Otol Rhinol Laryngol, 1992. **101**(4): p. 342-8.

21. Pfingst, B.E. and D. Sutton, *Relation of cochlear implant function to histopathology in monkeys.* Ann N Y Acad Sci, 1983. **405**: p. 224-39.

22. Pfingst, B.E., et al., Relation of psychophysical data to histopathology in monkeys with cochlear implants. Acta Otolaryngol, 1981. **92**(1-2): p. 1-13.

23. Weber, P.C., Medical and surgical considerations for implantable hearing prosthetic devices. Am J Audiol, 2002. **11**(2): p. 134-8.

24. Backous, D.D. and W. Duke, *Implantable middle ear hearing devices: current state of technology and market challenges.* Curr Opin Otolaryngol Head Neck Surg, 2006. **14**(5): p. 314-8.

25. Wilson, B.S., Cochlear implants: A remarkable past and a brilliant future. Hearing Research, In press.

26. Lim, H.H., et al., The auditory midbrain implant: Effects of electrode location. Hear Res, In press.

27. McCreery, D., A. Lossinsky, and V. Pikov, Performance of multisite silicon microprobes implanted chronically in the ventral cochlear nucleus of the cat. IEEE Trans Biomed Eng, 2007. **54**(6Pt1): p. 1042-52.

28. Seki, Y., N. Samejima, and A. Komatsuzaki, Auditory brainstem implants: current state and future directions with special reference to the subtonsillar approach for implantation. Acta Neurochir Suppl, 2007. **97**(Pt2): p. 431-5.

29. McCreery, D.B., *Cochlear nucleus auditory prostheses.* Hearing Research, In press.

30. Middlebrooks, J.C. and R.L. Snyder, Intraneural stimulation for auditory prostheses: Peripheral and intra-cranial stimulation sites. Hearing Research, In press. **In press**.

31. Fayad, J., et al., Cochlear implants: histopathologic findings related to performance in 16 human temporal bones. Ann Otol Rhinol Laryngol, 1991. **100**(10): p. 807-11.

32. Sutton, D., *Cochlear implant effects on the spiral ganglion.* Ann Otol Rhinol Laryngol, 1983. **92**(3 Pt 1): p. 316.

33. Khan, A.M., et al., Effect of cochlear implantation on residual spiral ganglion cell count as determined by comparison with the contralateral nonimplanted inner ear in humans. Ann Otol Rhinol Laryngol, 2005. **114**(5): p. 381-5.

34. Nadol, J.B., Jr., et al., *Histopathology of cochlear implants in humans.* Ann Otol Rhinol Laryngol, 2001. **110**(9): p. 883-91.

35. Leake-Jones, P.A. and S.J. Rebscher, *Cochlear pathology with chronically implanted scala tympani electrodes.* Ann N Y Acad Sci, 1983. **405**: p. 203-23.

36. Nadol, J.B., Jr., Degeneration of cochlear neurons as seen in the spiral ganglion of man. Hear Res, 1990. **49**(1-3): p. 141-54.

37. Nadol, J.B., Jr., Patterns of neural degeneration in the human cochlea and auditory nerve: implications for cochlear implantation. Otolaryngol Head Neck Surg, 1997. **117**(3 Pt 1): p. 220-8.

38. Dodson, H.C. and A. Mohuiddin, Response of spiral ganglion neurones to cochlear hair cell destruction in the guinea pig. J Neurocytol, 2000. **29**(7): p. 525-37.

39. Shepherd, R.K. and N.A. Hardie, Deafness-induced changes in the auditory pathway: implications for cochlear implants. Audiol Neurootol, 2002. **6**(6): p. 305-18.

40. Li, P.M.M.C., et al., Analysis of intracochlear new bone and fibrous tissue formation in human subjects with cochlear implants. Annals of Otology Rhinology and Laryngology, 2007. **116**(10): p. 731-738.

41. Szarowski, D.H., et al., *Brain responses to micro-machined silicon devices.* Brain Res, 2003. **983**(1-2): p. 23-35.

42. Biran, R., M.D. Noble, and P.A. Tresco, *Characterization of cortical astrocytes on materials of differing surface chemistry.* J Biomed Mater Res, 1999. **46**(2): p. 150-9.

43. Cheung, K.C., *Implantable microscale neural interfaces.* Biomed Microdevices, 2007. **9**(6): p. 923-38.

44. Drake, K.L., et al., Performance of planar multisite microprobes in recording extracellular single-unit intracortical activity. IEEE Trans Biomed Eng, 1988. **35**(9): p. 719-32.

45. Henze, D.A., et al., Intracellular features predicted by extracellular recordings in the hippocampus in vivo. J Neurophysiol, 2000. **84**(1): p. 390-400.

46. Terr, L.I., J.P. Mobley, and W.F. House, Biocompatibility of the central electroauditory prosthesis and the human cochlear nuclei. Am J Otol, 1989. **10**(5): p. 339-42.

47. Quester, R., et al., Polyester meshes and adhesive materials in the brain: comparative research in rats to optimize surgical strategy. J Neurosurg, 2002. **96**(4): p. 760-9.

48. James, D.P., et al., Effects of round window dexamethasone on residual hearing in a Guinea pig model of cochlear implantation. Audiol Neurootol, 2008. **13**(2): p. 86-96.

49. Nadol, J.B., Jr. and D.K. Eddington, *Histopathology of the inner ear relevant to cochlear implantation.* Adv Otorhinolaryngol, 2006. **64**: p. 31-49.

50. Hanekom, T., Modelling encapsulation tissue around cochlear implant electrodes. Med Biol Eng Comput, 2005. **43**(1): p. 47-55.

51. Somdas, M.A., et al., Quantitative evaluation of new bone and fibrous tissue in the cochlea following cochlear implantation in the human. Audiol Neurootol, 2007. **12**(5): p. 277-84.

52. Leake, P.A., et al., Chronic intracochlear electrical stimulation induces selective survival of spiral ganglion neurons in neonatally deafened cats. Hear Res, 1991. **54**(2): p. 251-71.

53. Leake, P.A., et al., Chronic intracochlear electrical stimulation in neonatally deafened cats: effects of intensity and stimulating electrode location. Hear Res, 1992. **64**(1): p. 99-117.

54. Hartshorn, D.O., J.M. Miller, and R.A. Altschuler, *Protective effect of electrical stimulation in the deafened guinea pig cochlea.* Otolaryngol Head Neck Surg, 1991. **104**(3): p. 311-9.

55. Lousteau, R.J., Increased spiral ganglion cell survival in electrically stimulated, deafened guinea pig cochleae. Laryngoscope, 1987. **97**(7 Pt 1): p. 836-42.

56. Shepherd, R.K., et al., Cochlear pathology following chronic electrical stimulation of the auditory nerve: II. Deafened kittens. Hear Res, 1994. **81**(1-2): p. 150-66.

57. Grill, W.M. and J.T. Mortimer, *Electrical properties of implant encapsulation tissue.* Ann Biomed Eng, 1994. **22**(1): p. 23-33.

58. Miller, K. and K. Chinzei, *Constitutive modelling of brain tissue: experiment and theory.* J Biomech, 1997. **30**(11-12): p. 1115-21.

59. Lontz, J.F., Schweige.Jw, and A.W. Burger, *Modifying Stress-Strain Profiles of Polysiloxane Elastomers for Improved Maxillofacial Conformity.* Journal of Dental Research, 1974. **53**(Feb): p. 277-277.

60. Subbaroyan, J., D.C. Martin, and D.R. Kipke, A finite-element model of the mechanical effects of implantable microelectrodes in the cerebral cortex. J Neural Eng, 2005. **2**(4): p. 103-13.

61. Kandel, E.R., J.H. Schwartz, and T.M. Jessell, *Principles of Neural Science*. 4th ed. 2000: McGraw-Hill.

62. Ateh, D.D., H.A. Navsaria, and P. Vadgama, *Polypyrrole-based conducting polymers and interactions with biological tissues.* J R Soc Interface, 2006. **3**(11): p. 741-52.

63. Ramanaviciene, A., et al., *Biocompatibility of polypyrrole particles: an in-vivo study in mice.* J Pharm Pharmacol, 2007. **59**(2): p. 311-5.

64. Cui, X., et al., Surface modification of neural recording electrodes with conducting polymer/biomolecule blends. J Biomed Mater Res, 2001. **56**(2): p. 261-72.

65. Cui, X.Y., et al., *In vivo studies of polypyrrole/peptide coated neural probes.* Biomaterials, 2003. **24**(5): p. 777-787.

66. Kros, A., N.A.J.M. Sommerdijk, and R.J.M. Nolte, *Poly(pyrrole) versus poly (3,4-ethylenedioxythiophene): implications for biosensor applications.* Sensors and Actuators B-Chemical, 2005. **106**(1): p. 289-295.

67. Cui, X.Y. and D.C. Martin, Electrochemical deposition and characterization of poly(3,4-ethylenedioxythiophene) on neural microelectrode arrays. Sensors and Actuators B-Chemical, 2003. **89**(1-2): p. 92-102.

68. Xiao, Y.H., et al., Electrochemical polymerization of poly(hydroxymethylated-3,4-ethylenedioxythiophene) (PEDOT-MeOH) on multichannel neural probes. Sensors and Actuators B-Chemical, 2004. **99**(2-3): p. 437-443.

69. Xiao, Y.H., X.Y. Cui, and D.C. Martin, *Electrochemical polymerization and properties of PEDOT/S-EDOT on neural microelectrode arrays.* Journal of Electroanalytical Chemistry, 2004. **573**(1): p. 43-48.

70. Xiao, Y.H., et al., Surface modification of neural probes with conducting polymer poly(hydroxymethylated-3,4-ethylenedioxythiophene) and its biocompatibility. Applied Biochemistry and Biotechnology, 2006. **128**(2): p. 117-129.

71. Yang, J.Y. and D.C. Martin, Impedance spectroscopy and nanoindentation of conducting poly(3,4-ethylenedioxythiophene) coatings on microfabricated neural prosthetic devices. Journal of Materials Research, 2006. **21**(5): p. 1124-1132.

72. Yang, J., et al., Ordered surfactant-templated poly(3,4-ethylenedioxythiophene) (PEDOT) conducting polymer on microfabricated neural probes. Acta Biomater, 2005. **1**(1): p. 125-36.

73. Yang, J., K. Lipkin, and D.C. Martin, Electrochemical fabrication of conducting polymer poly(3,4-ethylenedioxythiophene) (PEDOT) nanofibrils on microfabricated neural prosthetic devices. J Biomater Sci Polym Ed, 2007. **18**(8): p. 1075-89.

74. Yang, J.Y. and D.C. Martin, Microporous conducting polymers on neural microelectrode arrays II. Physical characterization. Sensors and Actuators a-Physical, 2004. **113**(2): p. 204-211.

75. Yang, J.Y. and D.C. Martin, Microporous conducting polymers on neural microelectrode arrays - I - Electrochemical deposition. Sensors and Actuators B-Chemical, 2004. **101**(1-2): p. 133-142.

76. Kim, B.C., et al., Preparation and characterisation of processable conducting polymer-hydrogel composites. Reactive & Functional Polymers, 2000. **44**(1): p. 31-40.

77. Guimard, N.K., N. Gomez, and C.E. Schmidt, *Conducting polymers in biomedical engineering.* Progress in Polymer Science, 2007. **32**(8-9): p. 876-921.

78. Smela, E., *Conjugated polymer actuators for biomedical applications.* Advanced Materials, 2003. **15**(6): p. 481-494.

79. Schmidt, C.E., et al., *Stimulation of neurite outgrowth using an electrically conducting polymer.* Proc Natl Acad Sci U S A, 1997. **94**(17): p. 8948-53.

80. Abidian, M.R., Kim, D.H., Martin, D.C., *Conducting-Polymer Nanotubes for Controlled Drug Release.* Advanced Materials, 2006. **18**(4): p. 405-409.

81. Massoumi, B. and A. Entezami, Controlled release of sulfosalicylic acid during electrochemical switching of conducting polymer bilayers. European Polymer Journal, 2001. **37**(5): p. 1015-1020.

82. Wadhwa, R., C.F. Lagenaur, and X.T. Cui, Electrochemically controlled release of dexamethasone from conducting polymer polypyrrole coated electrode. Journal of Controlled Release, 2006. **110**(3): p. 531-541.

83. Kontturi, K., P. Pentti, and G. Sundholm, *Polypyrrole as a model membrane for drug delivery.* Journal of Electroanalytical Chemistry, 1998. **453**(1-2): p. 231-238.

84. Zhou, Q.X., L.L. Miller, and J.R. Valentine, Electrochemically Controlled Binding and Release of Protonated Dimethyldopamine and Other Cations from Poly(N-Methylpyrrole) Polyanion Composite Redox Polymers. Journal of Electroanalytical Chemistry, 1989. **261**(1): p. 147-164.

85. Pernaut, J.M. and J.R. Reynolds, Use of conducting electroactive polymers for drug delivery and sensing of bioactive molecules. A redox chemistry approach. Journal of Physical Chemistry B, 2000. **104**(17): p. 4080-4090.

86. Nien, P.C., T.S. Tung, and K.C. Ho, Amperometric glucose biosensor based on entrapment of glucose oxidase in a poly(3,4-ethylenedioxythiophene) film. Electroanalysis, 2006. **18**(13-14): p. 1408-1415.

87. Geetha, S., et al., *Biosensing and drug delivery by polypyrrole.* Analytica Chimica Acta, 2006. **568**(1-2): p. 119-125.

88. Kim, D., et al., Effect of Immobilized Nerve Growth Factor on Conductive Polymers: Electrical Properties and Cellular Response. Advanced Functional Materials, 2007. **17**(1): p. 79-86.

89. Gomez, N. and C.E. Schmidt, Nerve growth factor-immobilized polypyrrole: Bioactive electrically conducting polymer for enhanced neurite extension. Journal of Biomedical Materials Research Part A, 2007. **81A**(1): p. 135-149.

90. Thompson, B.C., et al., Optimising the incorporation and release of a neurotrophic factor using conducting polypyrrole. J Control Release, 2006. **116**(3): p. 285-94.

91. Richardson, R.T., et al., The effect of polypyrrole with incorporated neurotrophin-3 on the promotion of neurite outgrowth from auditory neurons. Biomaterials, 2007. **28**(3): p. 513-23.

92. Tsai, H.K.A., et al., *Development of integrated protection for a miniaturized drug delivery system.* Smart Materials & Structures, 2007. **16**(2): p. S295-S299.

93. Zhou, D., et al., *Actuators for the cochlear implant.* Synthetic Metals, 2003. **135**(1-3): p. 39-40.

94. Kmecko, T., et al., *Nanocomposites for Neural Interfaces.* Mater. Res. Soc. Symp. Proc., 2006. **926**.

95. Lowe, J. and S. Holdcroft, Synthesis and Photolithography of Polymers and Copolymers Based on Poly(3-(2-(Methacryloyloxy)Ethyl)Thiophene). Macromolecules, 1995. **28**(13): p. 4608-4616.

96. Renak, M.L., G.C. Bazan, and D. Roitman, *Microlithographic process for patterning conjugated emissive polymers.* Advanced Materials, 1997. **9**(5): p. 392-&.

97. Hauser, B.T., T.S. Bergstedt, and K.S. Schanze, Photolithographically Defined Electropolymerized Films - Fabrication of an Electrochemically Switchable Diffraction Grating Comprised of Poly-(Bpy)(2)Ru(Vpy)(2)(2+). Journal of the Chemical Society-Chemical Communications, 1995(19): p. 1945-1946.

98. Persson, S.H.M., P. Dyreklev, and O. Inganas, *Patterning of poly(3-octylthiophene) conducting polymer films by electron beam exposure.* Advanced Materials, 1996. **8**(5): p. 405-&.

99. Angelopoulos, M., et al., *Water-Soluble Conducting Polyanilines - Applications in Lithography.* Journal of Vacuum Science & Technology B, 1993. **11**(6): p. 2794-2797.

100. Beh, W.S., et al., Formation of patterned microstructures of conducting polymers by soft lithography, and applications in microelectronic device fabrication. Advanced Materials, 1999. **11**(12): p. 1038-1041.

101. Zhang, F.L., T. Nyberg, and O. Inganas, *Conducting polymer nanowires and nanodots made with soft lithography.* Nano Letters, 2002. **2**(12): p. 1373-1377.

102. Xue, F.L., Y. Su, and K. Varahramyan, *Modified PEDOT-PSS conducting polymer as S/D electrodes for device performance enhancement of P3HT TFTs.* Ieee Transactions on Electron Devices, 2005. **52**(9): p. 1982-1987.

103. Bao, Z.N., et al., *High-performance plastic transistors fabricated by printing techniques.* Chemistry of Materials, 1997. **9**(6): p. 1299-&.

104. Wang, J.Z., et al., Dewetting of conducting polymer inkjet droplets on patterned surfaces. Nature Materials, 2004. **3**(3): p. 171-176.

105. Rozsnyai, L.F. and M.S. Wrighton, *Selective Deposition of Conducting Polymers Via Monolayer Photopatterning.* Langmuir, 1995. **11**(10): p. 3913-3920.

106. Zhou, F., et al., Selective electrodeposition and etching on polymer brush template prepared by patterned monolayer surface initiated polymerization. Chemistry Letters, 2004. **33**(5): p. 602-603.

107. Baumann, R. and J. Bargon, *Conducting polymer patterns via laser processing.* Applied Surface Science, 1996. **106**: p. 287-292.

108. McDonald, J.P., et al., Femtosecond pulsed laser patterning of poly(3,4-ethylene dioxythiophene)-poly(styrenesulfonate) thin films on gold/palladium substrates. Journal of Applied Physics, 2007. **102**(1): p. -.

109. Potter, W., R.E. Kalil, and W.J. Kao, *Biomimetic material systems for neural progenitor cell-based therapy.* Front Biosci, 2008. **13**: p. 806-21.

110. Broder, K.W. and S.R. Cohen, *An overview of permanent and semipermanent fillers.* Plast Reconstr Surg, 2006. **118**(3 Suppl): p. 7S-14S.

111. Babensee, J.E., L.V. McIntire, and A.G. Mikos, *Growth factor delivery for tissue engineering.* Pharm Res, 2000. **17**(5): p. 497-504.

112. Xiong, X.Y., K.C. Tam, and L.H. Gan, *Polymeric nanostructures for drug delivery applications based on Pluronic copolymer systems.* J Nanosci Nanotechnol, 2006. **6**(9-10): p. 2638-50.

113. Williams, J.C., et al., *Multi-site incorporation of bioactive matrices into MEMS-based neural probes.* Journal of Neural Engineering, 2005. **2**(4): p. L23-L28.

114. Rejali, D., et al., Cochlear implants and ex vivo BDNF gene therapy protect spiral ganglion neurons. Hear Res, 2007. **228**(1-2): p. 180-7.

115. Noushi, F., et al., *Delivery of neurotrophin-3 to the cochlea using alginate beads.* Otol Neurotol, 2005. **26**(3): p. 528-33.

116. Ito, J., et al., *A new method for drug application to the inner ear.* ORL J Otorhinolaryngol Relat Spec, 2005. **67**(5): p. 272-5.

117. Endo, T., et al., Novel strategy for treatment of inner ears using a biodegradable gel. Laryngoscope, 2005. **115**(11): p. 2016-20.

118. Iwai, K., et al., Cochlear protection by local insulin-like growth factor-1 application using biodegradable hydrogel. Laryngoscope, 2006. **116**(4): p. 529-33.

119. Lee, K.Y., et al., Novel therapy for hearing loss: delivery of insulin-like growth factor 1 to the cochlea using gelatin hydrogel. Otol Neurotol, 2007. **28**(7): p. 976-81.

120. Burdick, J.A., et al., Stimulation of neurite outgrowth by neurotrophins delivered from degradable hydrogels. Biomaterials, 2006. **27**(3): p. 452-9.

121. Zhong, Y., et al., Stabilizing electrode-host interfaces: a tissue engineering approach. J Rehabil Res Dev, 2001. **38**(6): p. 627-32.

122. Deshmukh, P., et al., Stable electrical performance of high efficiency pacing leads having small surface, steroid-eluting pacing electrodes. Pacing Clin Electrophysiol, 1999. **22**(11): p. 1599-603.

123. Schuchert, A., K.H. Kuck, and T. Meinertz, [Modern electrodes with and without steroid: effects on stimulation current of cardiac pacemakers]. Z Kardiol, 1995. **84**(4): p. 289-95.

124. Rennaker, R.L., et al., Minocycline increases quality and longevity of chronic neural recordings. J Neural Eng, 2007. **4**(2): p. L1-5.

125. Chang, J.C., G.J. Brewer, and B.C. Wheeler, A modified microstamping technique enhances polylysine transfer and neuronal cell patterning. Biomaterials, 2003. **24**(17): p. 2863-70.

126. Cui, X., et al., *In vivo studies of polypyrrole/peptide coated neural probes.* Biomaterials, 2003. **24**(5): p. 777-87.

127. Richardson, R.T., F. Noushi, and S. O'Leary, *Inner ear therapy for neural preservation.* Audiol Neurootol, 2006. **11**(6): p. 343-56.

128. Wang, J.Y., et al., Dual effects of antioxidants in neurodegeneration: direct neuroprotection against oxidative stress and indirect protection via suppression of glia-mediated inflammation. Curr Pharm Des, 2006. **12**(27): p. 3521-33.

129. Nakagawa, T. and J. Ito, *Cell therapy for inner ear diseases.* Curr Pharm Des, 2005. **11**(9): p. 1203-7.

130. Sekiya, T., et al., *Cell transplantation to the auditory nerve and cochlear duct.* Exp Neurol, 2006. **198**(1): p. 12-24.

131. Sekiya, T., et al., *Rebuilding lost hearing using cell transplantation.* Neurosurgery, 2007. **60**(3): p. 417-33; discussion 433.

132. Tresco, P.A., R. Biran, and M.D. Noble, *Cellular transplants as sources for therapeutic agents.* Adv Drug Deliv Rev, 2000. **42**(1-2): p. 3-27.

133. Warnecke, A., et al., The biological effects of cell-delivered brain-derived neurotrophic factor on cultured spiral ganglion cells. Neuroreport, 2007. **18**(16): p. 1683-1686.

134. Levivier, M., et al., Intrastriatal implantation of fibroblasts genetically engineered to produce brain-derived neurotrophic factor prevents degeneration of dopaminergic neurons in a rat model of Parkinson's disease. J Neurosci, 1995. **15**(12): p. 7810-20.

135. Ferrer, I., et al., Brain-derived neurotrophic factor reduces cortical cell death by ischemia after middle cerebral artery occlusion in the rat. Acta Neuropathol, 2001. **101**(3): p. 229-38.

136. Olivius, P., et al., Allografted fetal dorsal root ganglion neuronal survival in the guinea pig cochlea. Brain Res, 2003. **979**(1-2): p. 1-6.

137. Ulfendahl, M., et al., *A cell therapy approach to substitute neural elements in the inner ear.* Physiology & Behavior, 2007. **92**(1-2): p. 75-79.

138. Altschuler, R.A., K.S. O'Shea, and J.M. Miller, *Stem cell transplantation for auditory nerve Replacement.* Hear Res, This issue. **This issue**.

139. Kamiya, K., et al., Mesenchymal stem cell transplantation accelerates hearing recovery through the repair of injured cochlear fibrocytes. Am J Pathol, 2007. **171**(1): p. 214-26.

140. Parker, M.A., et al., Neural stem cells injected into the sound-damaged cochlea migrate throughout the cochlea and express markers of hair cells, supporting cells, and spiral ganglion cells. Hear Res, 2007. **232**(1-2): p. 29-43.

141. Shi, F.X., et al., BMP4 induction of sensory neurons from human embryonic stem cells and reinnervation of sensory epithelium. European Journal of Neuroscience, 2007. **26**(11): p. 3016-3023.

142. Coleman, B., M.G. de Silva, and R.K. Shepherd, Concise review: the potential of stem cells for auditory neuron generation and replacement. Stem Cells, 2007. **25**(11): p. 2685-94.

143. Matsui, J.I., et al., *Regeneration and replacement in the vertebrate inner ear.* Drug Discov Today, 2005. **10**(19): p. 1307-12.

# Chapter 2

# Interactions of bioactive, biomimetic neural electrode coatings with living cells

## 2.1 Introduction

Bio-electrodes enable electrical communication with neural cells for diagnostic, therapeutic, and research purposes. They are used in devices to treat epilepsy, Parkinson's disease, paralysis, chronic pain and other neurological disorders, as well as to sense abnormal electrical activity. Bio-electrodes can also be functionalized for use as biosensors to detect toxins, pathogens, unhealthy cells, medications, and indicators of severe medical conditions. The ability of these electrodes to safely treat neurological disorders, accurately sense pathologies, and provide reliable data on cell function relies on their ability to efficiently transfer charge between the electrodes and target tissue. Thus, the composition and conductivity of the tissue/electrode interface and proximity of target tissue to the electrode play crucial roles in the success of these devices, whether they are implanted electrodes in the brain or microelectrode arrays used for *in vitro* applications.

For single unit neural recording in the central nervous system, it is necessary for the electrodes to have desirable electrical properties including low impedance and spatial resolution on the order of the size of a neuron—which

usually necessitates the use of arrays of microelectrodes placed as close to target cells as possible [1, 2]. In order to reduce the inflammatory cell response and fibrous cell encapsulation as a result of electrode implantation that can block signal transfer, many electrode materials and designs have been examined. These include the use of biocompatible materials [3, 4], the use of materials with mechanical properties more similar to brain tissue's [5-9], and the release of anti-inflammatory agents from the electrode site [10, 11]. In conjunction with reducing the inflammatory and fibrous responses, approaches to promote the viability and proximity of target neurons have examined the use of neurotrophins [12-14], and adhesion molecules [15, 16] as well as biomimetic surface topographies [17, 18]. To achieve high spatial resolution, it is necessary to employ electrodes with small footprints [2, 19]. Unfortunately as the surface area of metallic electrodes is reduced, their impedance increases, reducing the signal-to-noise ratio of recordings, and reducing their sensitivity.

Research on the use of conducting polymers for bio-electrodes has produced coatings which reduce the impedance of bio-electrodes by many orders of magnitude without increasing the overall dimensions of the electrode [20-23]. These coatings are biocompatible and can easily be functionalized and loaded with biomolecules for passive release, active delivery, and surface functionality [24]. Coatings made from conducting polymers and hydrogels are much softer than the metals and ceramics typically used in these applications, and have morphologies which are extremely fuzzy and have more in common with biological tissue than engineered materials [6, 25]. Conducting polymers also help to bridge the gap between ionically-conductive tissue and electronically-conductive metals and silicon due to their ability to transport both ionic and electronic charge [26, 27]. When conducting polymers are used in conjunction with hydrogels, they produce low-impedance electrode extensions which are extremely soft, wet and highly porous. These materials offer methods for improving the integration of bio-electrodes with cells and tissue while facilitating charge transport between the two.

Cell-based therapies have also been employed experimentally to help in recovery from traumatic injury or neurological disease [28-30]. Cells are implanted into the patient either alone or within a scaffold, such as a hydrogel, which helps to control cell proliferation and growth. The implanted cells replace damaged tissue or help to promote healing by release of biochemical molecules. In the case of implanted electrodes in the brain, where there is either an existing area of damaged cells such as in Parkinson's disease, or the insertion and presence of the electrode causes a new injury, it may be useful to combine cell delivery therapies with electrical devices to promote the viability of target cells.

Our objective is to improve mechanical and electrical integration between neural electrodes and live cells using conducting polymer coatings. By depositing conducting polymers directly around cells cultured on electrodes or in hydrogel scaffolds, it is possible to encapsulate the cells within extensions of the electrode. We will examine the health and viability of the cells after their incorporation into the conducting polymer electrode, study the morphology of the resulting complex, and characterize its electrical properties.

## 2.2 Experimental

### 2.2.1. Biomedical electrodes

Electrodes were fabricated in-house by sputtering gold-palladium (AuPd) onto plastic coverslips (Fisher Scientific) using a Hummer IV sputter coater. Approximately 1600 Å of AuPd was sputtered through a mask to create 6 mm diameter electrodes. Electrodes were also made by sputtering approximately 1600 Å AuPd onto 5 x 5 mm silicon wafers. Other electrodes used in these studies include commercially available electrode arrays for cell culture and implantable electrical devices. Advanced BioPhysics (ABP) ECIS electrodes were purchased and have 250 µm gold electrode sites at the bottom of an 8 x 8 mm cell culture well. Microfabricated silicon neural probes were acquired from NeuroNexus Technologies and from the Center for Neural Communication

Technologies at the University of Michigan. These silicon probes typically have 8 individually addressable 40 µm diameter gold electrode sites. For conducting polymer in hydrogel experiments, polytetrafluoroethylene (PTFE)-coated gold microwire (A-M systems) with diameter of 75 µm was cut into desirable lengths with a razor blade and used. Electrodes were sterilized prior to cell culture by immersion in 70 % (v/v) ethanol for 15 min and then airdrying in a hood for 15 min.

### 2.2.2. Electrochemical polymerization

Conducting polymers were electrochemically deposited from aqueous monomeric solutions containing counterions and dopants. Poly(3,4-ethylene dioxythiophene)-poly(styrenesulfonate) (PEDOT-PSS) was deposited from a solution containing 0.1 % (w/v) ethylene dioxythiophene (EDOT; H.C. Starck) and 0.2 % (w/v) poly(styrenesulfonate) sodium salt (PSS; Acros Organics) in deoinized water. For deposition of conducting polymer films around living cells, the deionized water was replaced by phosphate-buffered saline (PBS; HyClone Media) or Hank's Balanced Salt Solution (HBSS; HyClone Media) and the solution was sterilized using a 0.45 µm syringe filter (Millipore). The electrode was immersed into the monomer solution and served as the working electrode (anode). A 6 x 6 mm platinum foil served as the counter electrode (cathode). Galvanostatic currents of 0.5 – 10 mA/cm$^2$ were then applied using an AutoLab PGStat12 Potentiostat/Galvanostat (EcoChemie).

### 2.2.3. Hydrogel coatings

Calcium-alginate hydrogel coatings were made by dip-coating. Electrodes were first dipped into a solution of 0.5 – 2 % (w/v) Pronova MVG alginate (FMC Biopolymer) in PBS and then dipped into a solution of 1 – 2 % (w/v) calcium chloride ($CaCl_2$; Sigma-Aldrich) in PBS. The process is repeated to build thicker coatings. RGD-functionalized alginate gels were provided by Dr. David Mooney at Harvard University and were used in a similar fashion.

### 2.2.4. Cell culture

SH-SY5Y neuroblastoma cell lines (SY5Y) were obtained from Dr. Joseph Corey and Dr. Eva Feldman at the University of Michigan and used at passages between 30 and 60. SY5Y were maintained at 37℃ in a humid incubator with 5 % $CO_2$ in media consisiting of Dulbecco's Modified Eagle's Medium (DMEM with glucose, L-glutamine; Gibco/Invitrogen) supplemented with 10 % (v/v) fetal bovine serum (FBS; Gibco/Invitrogen) and 1 % (v/v) antibiotic-antimicotic solution (Gibco/Invitrogen). Cell media was replaced every four days, and cells were passaged every 7 days. SY5Y were passaged using a solution of 0.25 % trypsin and 1 mM ethylenediaminetetraacetic acid (EDTA) in PBS. Rat pheochromocytoma cell lines (PC-12) were obtained from Dr. Christine Carter-Su at the University of Michigan and were used between passages 10 and 20. PC-12 were maintained at 37 ℃ in a humid incubator with 5 % $CO_2$ in media consisting of DMEM supplemented with 10 % (v/v) horse serum (Gibco/Invitrogen), 5 % (v/v) FBS, 1 % (v/v) L-glutamine (200 mM; Gibco/Invitrogen), and 1 % (v/v) antibiotic-antimicotic solution. Cell media was replaced every four days, and cells were passaged every 7 days. PC-12 were passaged using a solution of PBS with 0.25 % (v/v) trypsin and 1 mM EDTA. Differentiation media consisted of DMEM with 2 % (v/v) horse serum, 1 % (v/v) FBS, and 1 % (v/v) L-glutamine. When PEDOT was deposited around living cells, the cells were first cultured for 24 – 48 h on the electrodes. After polymerization of PEDOT around living cells, some cells were removed by exposure to 100 mM trypsin-versene (HyClone Media) for 2 h at 37℃. Mouse primary dissociated cortical cultures (MCC) were prepared from embryonic days 18–20 (E18–20) mice. The brains were removed and submerged in ice-cold Hank's buffered saline solution (HBSS; without calcium chloride, magnesium chloride, magnesium sulfate, or phenol red; Invitrogen), the neocortex was dissected, the meninges were removed, tissue was washed in ice-cold HBSS then manually dissociated with a 1 ml pipette tip. MCC were maintained in Neurobasal media supplemented with 0.5mM L-glutamine and 2% serum-free nutritional supplement B27 (Invitrogen) at 37 1C in 5% CO2. A third of the media

was replaced every 4 days, and cells were allowed to mature for at least 7 days before use in experiments.

### 2.2.5. Cell viability assay

The cytotoxicity of the monomer solution was measured using a colorimetric 3-(4,5-dimethylthiazol-2-yl)-2,5-diphenyltetrazolium bromide (MTT) assay for cell survival and proliferation (Chemicon International Inc.). At 12, 24, 48, and 72 hours after cells were exposed to solutions of 0.001 – 1 M EDOT, the MTT assay was performed and read at 570 nm using a plate reader. Hoechst 33342 (Molecular Probes/Invitrogen) was used to label all nuclei, and propidium iodide (Molecular Probes/Invitrogen) was used to label cells with compromised plasma membranes. Cell cultures were immunostained for the apoptosis-associated protease, activated caspace-3 (Cell Signaling Technologies).

### 2.2.6. Staining

Cells were fixed in 4 % paraformaldehyde in PBS for 1 hour at room temperature. The actin cytoskeleton was stained by incubating samples in Phallodin-Oregon Green (Molecular Probes/Invitrogen), diluted 1:300 in PBS with 0.1 % (w/v) Triton X (PBSX) for 1 hour at 4°C. They were then counterstained with Hoeschst 33342 (Molecular Probes/Invitrogen), rinsed with PBS, and mounted in Fluoromount G (Fisher). For α-caspace-3 staining, the primary antibody was diluted to 1 % (v/v) in a blocking solution of PBSX and 3 % (w/v) bovine serum albumin to prevent non-specific binding. Samples were incubated with the primary antibody overnight at 4°C and then rinsed with PBSX. They were then incubated with the secondary antibody, diluted to 1:300 in the blocking buffer solution, rinsed again with PBSX, counterstained with Hoechst in PBS and mounted in Fluoromount G. Scanning electron microscope (SEM) samples were fixed using 1 % (w/v) glutaraldehyde, rinsed in deionized water, dehydrated in consecutive ethanol baths (50 %, 75 %, 95 %, and 100 %) for 10 minutes each, and then dried overnight in hexamethyldisilazane (HMDS; Ted Pella, Inc.). Environmental scanning electron microscope (ESEM) samples were fixed in 4 %

(w/v) paraformaldehyde in PBS for 1 hour at room temperature, kept in PBS at 4 ℃, and rinsed in deionized water prior to imaging. Transmission electron microscope (TEM) samples were first fixed in 2.5 % (w/v) gluataraldehyde in PBS overnight. They were then rinsed twice in PBS and then incubated in 1 % (w/v) osmium tetrachloride in PBS for 1 hour at room temperature. They were then rinsed twice in distilled water and incubated in 3 % (w/v) uranyl acetate in distilled water for 1 hour at room temperature. Subsequently the samples were dehydrated by soaking in 50 %, 70 %, 90 %, and 100 % ethanol each for 15 minutes. The samples were infiltrated with 25 % resin in ethanol for 1 hour, then 50 % resin in ethanol for 1 more hour, and finally in 75 % resin in ethanol overnight. They were then infiltrated with 100 % resin which was changed three times, and inserted into removable TEM molds and placed in the vacuum desiccator for 4 hours. The samples were then placed in a 60 ℃ oven for 24 hours to solidify the resin. The hard samples were sectioned to 70 nm using an ultramicrotome and placed on copper TEM grids.

### 2.2.7. Microscopy

Samples were imaged optically using a Nikon OptiPhot POL microscope with SPOT RT digital camera with either transmitted or reflected light. Fluorescent and phase contrast images were captured using either a Nikon TE-2000U inverted microscope with Hammamatsu CCD camera and Simple PCI imaging software (courtesy of Dr. Shuichi Takayama) or an Olympus BX-51 upright microscope with Olympus CCD camera and Olympus imaging software (University of Michigan Morphology and Imaging Analysis Core Laboratory). SEM was performed using a FEI Nova 200 Nanolab Dualbeam FIB (University of Michigan Electron Microbeam Analysis Laboratory (EMAL)). Samples were first sputtered with approximately 10 Å of gold prior to SEM imaging. Environmental scanning electron microscopy (ESEM) was performed using a FEI Quanta 3D Dualbeam FIB operating under low vacuum. Transmission electron microscopy (TEM) was performed using a Phillips CM-100 operating at an accelerating

voltage of 60 kV (University of Michigan Morphology and Imaging Analysis Core Laboratory).

### 2.2.8. Electrochemical analysis

The electrochemical properties of the electrodes were characterized before and after coating with conducting polymers. Electrochemical impedance spectroscopy (EIS) was performed using the AutoLab PGstat 12. A three electrode setup was used in which the coated electrode served as the working electrode, a 6 mm x 6 mm platinum foil as the counter electrode, and a saturated calomel electrode (SCE) as the reference electrode. The electrolyte used was room temperature PBS (pH = 7.4). The impedance was measured at frequencies from 1 – 1,000,000 Hz upon application of a 5 mV RMS sine wave between the working and counter electrode. Cyclic voltammetry was performed to measure the charge storage and transfer properties of the electrodes. The equipment and three-electrode setup described above were used. The current was measured as the voltage was cycled from +1.0 to -1.0 V versus SCE at a rate of 0.1 V/s.

## 2.3 Results and discussion

### 2.3.1. Polymerization around living cells

Figures 2-1 (A-F) show the resulting structure of PEDOT-PSS-PBS deposited around live SH-SY5Y neuroblastoma cultured on a metallic electrode. Cells are cultured on the metallic electrode for 24 hours prior to the electropolymerization process. The polymer film covers many neural processes and is deposited directly against the cell body. As shown in figure 2-2 (A) the electrode with cultured cells is electrically connected and submerged into a bath containing the conducting polymer monomer, EDOT, as well as counterions and dopants. The primary role of the counterions, which are often polyanions such as

PSS, heparin, or other negatively charged molecules, is to balance the positive charge of the polymer as it is oxidized during electropolymerization. Additionally, some counterions may have secondary roles as dopants which contribute to mechanical stability, biological function, morphological templating, or improved conduction to the resulting conducting polymer films. Other dopants present in the monomer solution and resulting polymer films are used solely for their mechanical, morphological, electronic, electro-active or biological function and do not contribute to charge balance. Biological dopants including salts and buffers were used for deposition of PEDOT around living cells to promote the viability of cells throughout the deposition process. Both phosphate-buffered saline (PBS) and Hank's Balanced Salt Solution (HBSS) were used in the monomer solution to maintain the viability of cells. Other biological dopants may be used to promote cell adhesion, viability and differentiation.

Electropolymerization is initiated by applying a current through the monomer solution from the submerged electrode with cells serving as the anode to a platinum foil which acts as the cathode. The current drives the oxidation of the EDOT monomer from the solution and results in the deposition of a fuzzy, dark-blue PEDOT conducting polymer film on the anode. When live cells are present on the anode, PEDOT is deposited between the cells but curiously, not underneath the cells or where they are in direct contact with the metallic substrate as illustrated in Figure 2-2 (B). As shown in Figures 2-1 (A) and 2-1 (B) smaller cell processes such as neurites are quickly encased in PEDOT as polymerization proceeds, and entire cells can become buried if deposition is carried out long enough. The amount of conducting polymer is related to the overall deposition charge, which is the product of the deposition current and time. Time-lapse imaging (not shown) of the electropolymerization process shows that initially cells are free to move around on the substrate, but that the deposition of PEDOT around the cells immobilizes them to the substrate and reduces their movement. Figures 2-1 (C) and 2-1 (D) show that the electrochemical deposition of PEDOT around living cells forms very intimate contact between the cells and underlying electrode through the conducting polymer coating. The process

allows for very precise localization and connection between small electrodes and target cells. The direct electrode-cell contact also reduces the distance between the two, thereby improving recording and stimulation signal integrity and minimizing signal loss for use with cells cultured on electrodes or even implantable devices. The immobilization of genetically-modified cells in conducting polymer coatings can also be used to build electrodes which can secrete growth factors or other biomolecules. After formation of the conducting polymer-cell-electrode complex, the electrode complex can be re-submerged in media and returned to the cell culture incubator.

To form biomimetic, cell-templated conducting polymer electrode coatings, PEDOT is first deposited around cells so that it doesn't fully encase them. The cells are then removed from the PEDOT film using either enzymatic removal or mechanical removal by sonication in deionized water or a combination thereof as illustrated in Figure 2-2 (C). After removal of the cells, cell-templated holes and tunnels are exposed in the PEDOT film—essentially creating a mold of the lower portion of the cell as shown in Figures 2-1 (E) and 2-1 (F).

### 2.3.2. Cytotoxicity of EDOT

In order to demonstrate the cytocompatability of depositing PEDOT around living cells it was necessary to verify the cytotoxicity of the monomer, EDOT, and the other chemicals present in the monomer solution used for deposition. The cytocompatability of PBS and HBSS is well known as they are used routinely in cell culture. The cytotoxicity of EDOT and PSS was quantified by exposing SY5Y cells to EDOT and PSS in their cell media and measuring cell viability for up to 72 hours using an MTT assay. EDOT was mixed into the cell media at concentrations of 0.001 M, 0.01 M, 0.1 M, and 1 M. Throughout the study the concentration of PSS was kept at 0.2 % (w/v) or 0.01 M, the concentration used during deposition. Figure 2-3 shows the effects of EDOT-PSS in the media on SY5Y viability. At EDOT concentrations of 1 mM, cell viability never drops below 90 % over 72 hours. With 10 mM EDOT, 87 % of cells are viable after 24 hours, and 76 % are viable after 72 hours. For

deposition, the concentration of EDOT is typically 0.1 % (w/v) or 7.0 mM and the cells are exposed to the monomer solution for 5 – 20 minutes. At these conditions, nearly 100 % of the SH-SY5Y cells remain viable according to the MTT assay.

### 2.3.3. Cellular response to deposition of PEDOT around live cells

Initial assessment in the first few hours after PEDOT deposition around SY5Y reveals cells which appear to be viable despite being partially encased in conducting polymer. As shown in figure 2-5 (B), nuclear staining (Hoechst 33342) show intact nuclei 24 hours after deposition, indicating that the cells are not undergoing necrotic or lytic death. There is evidence that the cell membranes are permeabilized during the electrochemical deposition process, as shown by staining with propidium iodide immediately after deposition to label cells with compromised membranes (data not shown). The permeabilization appears to be transient, as 24 hours after electrochemical deposition the fraction of cells labeled with propidium iodide has returned to basal levels. As early as 5 minutes after PEDOT deposition around cells, disruption of the actin cytoskeletal structure can be seen. The actin filaments, labeled with Phalloidin-Oregon Green (Molecular Probes/Invitrogen) are well defined fibers prior to deposition, but become cloudy, diffuse and poorly defined after the deposition process (Figure 2-5 (B)). These effects were still present after 72 hours.

The longterm effects on cell viability caused by polymerizing PEDOT around cells were studied by measuring the fraction of apoptotic cells (Figure 2-4). At incremental times up to 120 h after electrochemical deposition, the SY5Y were fixed and labeled with an immunocytochemical marker for activated caspase-3, a protease present in cells undergoing apoptosis. The experiments were repeated with primary mixed cortical neurons to verify the trends observed with neuronal cell lines. The fraction of apoptotic cells in PEDOT was compared to the fraction of apoptotic cells that had been exposed to the current alone in a PBS solution. Beginning 24 h after the deposition process, the fraction of apoptotic SY5Y cells encased in PEDOT is 2 % compared to 0 % of the cells

which were exposed to current alone. 72 h after deposition, the difference between the experimental group and control group becomes more pronounced. The fraction of apoptotic SY5Y cells encased in PEDOT was 10 %, 11 % and 19 % respectively at 72, 96, and 120 hours after electrochemical deposition, whereas the control group had only 1 %, 1% and 2% apoptotic cells at the same time points. Similar increases in apoptotic cell fraction over time were observed with primary cortical neurons. The fraction of apoptotic primary cortical neurons was 2 %, 4 %, 5 %, 21 %, 20 %, and 32 % at 0, 1, 2, 3, 4, and 5 days after deposition, respectively. Primary cortical neurons not encased in PEDOT had a maximum apoptotic fraction of 5 % at 5 days after culturing of cells.

### 2.3.4. Cellular adhesion to cell-templated PEDOT

Cell adhesion to the cell-templated conducting polymer electrode coatings was assayed to investigate biomimetic surface effects. SY5Y cells were cultured on PEDOT films which had been deposited around a previous batch of living SY5Y which were then removed using EDTA. The cells cultured onto the cell-templated conducting polymer film readily adhere to the textured film without the need for adhesion molecules and prefer this surface over the bare electrode surface. The cells find some of the features left by the original cells but tend not to occupy the identical vacancies left by the original cells (Figure 2-6).

### 2.3.5. Electrical properties of PEDOT around live cells

Electrochemical impedance spectroscopy was used to measure the impedance of electrodes with cells and conducting polymer coatings across a broad frequency range. Impedance spectroscopy is a useful technique because it gives information about charge transport processes which occur across a large range of rates. It also provides useful information about the type of charge transfer occurring at the electrode interface—whether the processes are faradaic (i.e., resistive and involving redox reactions) or non-faradaic (i.e., capacitive or inductive and not involving redox reactions). For neural recording, frequencies of 0.1 Hz to 1 kHz are typically used in order to provide enough temporal resolution

to observe electro-chemical cellular activity [31]. As shown in Figure 2-7 (A) and (B), the impedance of bare gold electrode sites on commercially available Applied Biophysics (ABP) electrodes decrease with increasing frequency and exhibit primarily capacitive behavior at frequencies below approximately 10 kHz as shown by phase angles of 75° to 85°, with 90° being completely capacitive. At 1 kHz the impedance of the bare site is 4487 Ω. When SY5Y neuroblastoma are cultured on these electrodes there are small shifts in the impedance and the phase angle increases slightly closer to 90°, possibly due to the capacitive nature of their lipid bilayers. The impedance at 1 kHz with SY5Y on the gold electrode is 2691 Ω. PEDOT deposition around the SY5Y cells leads to a large decrease in the impedance, most noticeably at frequencies below 500 Hz, and a decrease in the phase angle. This is consistent with previous data pm conducting polymer coatings that have a tendency to reduce the impedance of metallic electrodes, often by 99 % or more [8, 20, 23, 25]. At 1 kHz the impedance of the electrode with PEDOT grown around the SY5Y is 1230 Ω, a 73 % decrease from the bare electrode. After removal of the cells from the PEDOT film, the impedance and phase angle are both lowered again, presumably due to the removal of capacitive cell membrane components. The impedance of this cell-templated electrode coating is 705 Ω, 84 % lower than the initial bare electrode. For comparison, we deposited PEDOT onto bare electrodes with no cells and then performed impedance spectroscopy. These coatings had the lowest impedances and phase angles of the group with a 1 kHz impedance of 231 Ω. It is possible that the PEDOT grown directly onto the bare electrodes with no cells present has a more regular surface morphology and thus has a higher surface area leading to lower impedances.

The electrical properties of the films were further characterized using cyclic voltammetry to measure their charge storage properties. As the voltage is cycled between + 1 and – 1 volt, with respect to the saturated calomel electrode (SCE), at a rate of 0.1 V/s, the current is monitored. In the resulting plot, the area within the curve is proportional to the amount of charge that is stored and released during a cycle. The peaks also represent reactions which occur at

corresponding voltages. For the bare metallic electrode, there is very little charge storage as shown by the flat trace in Figure 2-8. The addition of SY5Y cells increases the charge storage by a small amount. But it is the deposition of PEDOT around these cells which allows significantly more current to pass through the electrode. When the cells are removed, the charge storage capacity, proportional to the area in the curve, is further increased, and is similar in shape and almost as large as the curve corresponding to PEDOT grown directly onto the bare electrode with no cells. The cyclic voltammetry results suggest that these conducting polymer coatings can increase the amount of current and charge transferred through these electrodes over the same time period and voltage window. These properties are relevant to the ability to effectively stimulate neural tissue without causing pain or damage.

### 2.3.6. Application of conducting polymer, cell-loaded hydrogels to neural electrodes

Hydrogel coatings can also be used to facilitate integration of bioelectrodes with cells and tissue. Hydrogels are composed almost entirely of water held in a lightly crosslinked polymer network. Hydrogels are ideal materials for cells since they are similar in structure to the extracellular matrix, are wet, and highly porous which allows diffusion of nutrients and waste products. They have been used extensively as biomaterials for neural tissue engineering and cell delivery applications [28, 32, 33]. It has also been shown that hydrogels can be used as scaffolds to grow three-dimensional conducting polymer electrode extensions [6, 7].

Figure 2-9 (A) shows an unmodified microfabricated neural probe used for acute neural recordings from animals. The probe tip is made of microfabricated silicon and has a series of metallic microelectrodes along its shank. It is mounted onto the green circuit board assembly in order to facilitate handling and connection. When coated with cell-loaded hydrogel along the shank, as shown in Figure 2-9 (B), the coating provides a buffer between the stiff probe and the soft brain tissue. In addition, the SY5Y neural cells incorporated in the probe

coating demonstrate the feasibility of delivering cells to the implant site via the probe. Cells including stem cells or cells genetically modified to secrete growth factors or other compounds can be used to direct the tissue response to the implanted probe. Similar coatings have been used to deliver transfected cells on cochlear electrodes to promote neural regeneration of cochlear neurons [34].

The microscale porosity of the alginate network seen in Figure 2-10 (A) contributes significantly to macroscopic properties including softness, high water retention, and ability to transport cell nutrients and waste products. In order for the hydrogel to retain its desirable mechanical properties and usefulness as a cell scaffold material, it is necessary that it retain significant porosity when PEDOT networks are deposited within. According to transmission electron microscopy analysis, the porosity of alginate hydrogel is retained when PEDOT is deposited within, as shown in Figure 2-10 (B). Instead of obscuring the pores between alginate fibers, PEDOT congregates around the fibers themselves, making them slightly thicker. The mean thickness from 10 alginate fibers with no PEDOT in Figure 2-10 (A) is 5.1 nm with a standard deviation of 1.2 nm. Once PEDOT has been electrochemically deposited into the hydrogel scaffold, the voids remain unfilled while the fibers thicken to a mean diameter of 7.5 nm with a standard deviation of 1.8 nm.

### 2.3.7. Electrical properties of PEDOT in cell-seeded hydrogel

Deposition of PEDOT within the hydrogel produces an electrically connected scaffold which can be used to sense or stimulate cell activity. Figure 2-11 shows the effects on impedance spectroscopy of PEDOT deposition and cell loading within the hydrogel scaffold. The loading of SY5Y cells into the scaffold leads to a small shift in the impedance, with an increase in the 1 kHz impedance from 7744 Ω in the bare hydrogel to 8820 Ω in the hydrogel with cells. Across all frequencies there is a decrease in the phase angle of 5 – 15 °. When PEDOT is deposited into the hydrogel network there is a large decrease in impedance across all frequencies measured. At 1 kHz the impedance is 526 Ω, a decrease of 93 % from the bare hydrogel. The current flow also becomes less

capacitive as the phase angles drop across all frequencies by up to 63 °. When PEDOT is deposited for the same amount of time into a cell-loaded hydrogel scaffold, the impedance is lower than either alginate alone, or the cell-loaded alginate, but is slightly higher than PEDOT deposited into a hydrogel without cells. At 1 kHz the impedance of PEDOT in an SY5Y loaded scaffold is 1130 Ω. The increase in impedance could be due to the cells obscuring some of the current flow pathways. The phase angle of PEDOT in SY5Y-loaded alginate is similar to PEDOT in unloaded alginate for frequencies above 35 Hz, but below that point is higher when cells are present.

The charge storage capabilities of these conducting polymer-hydrogel scaffolds are dramatically increased over the bare hydrogels, indicating that larger currents and charges can be transferred through the scaffolds when the conducting polymer is present. In Figure 2-12 the voltammagrams show the current flow while cycling the voltage between + 1 V and – 1 V. In both cases when PEDOT is present in the scaffold, significantly higher currents can be passed through the hydrogels. The total charge storage capacities, the sum of the charge stored during the anodic and cathodic sweeps, increases slightly when cells are present in the gel, and increases dramatically with the deposition of PEDOT in the hydrogel. The charge storage capacities of the wire electrodes in alginate alone and in alginate with SY5Y are 47.8 µC and 125.9 µC, respectively. When PEDOT is deposited into alginate scaffolds, the charge storage capacities increase to 1157 µC in hydrogel alone, and 913 µC in hydrogel seeded with SY5Y. The maximum current flows through these coated electrodes are increased as impedance is lowered. Over the voltage range of +1 V to -1 V, the maximum current of the wire in alginate is 3.8 µA. When cells are present in the alginate, the maximum current increases to 10.3 µA, and with the addition of PEDOT to alginate alone and alginate with cells the maximum currents are 97.9 µA and 81.4 µA, respectively. The addition of electrochemically deposited conducting polymers in alginate makes possible the creation of electrically-connected neural cell scaffolds with reduced impedance across a broad frequency range, and increased currents and charge capabilities.

## 2.4 Conclusions

The novel process of electrochemical polymerization around living cells can be used to improve the integration of neural interfaces for numerous applications. Implantable electrodes can be coated with cells and conducting polymers to help promote healing around the electrode sites while improving charge transfer. Cell-templated electrode coatings can be made to direct adhesion and promote the viability of neural cells to electrodes for use *in vitro* and *in vivo*. Conducting polymers grown in cell-seeded hydrogels can also be made for use as either tissue engineering scaffolds for electrically conductive cells or soft hydrogel coatings on electrodes to facilitate recording past the glial scar. In each of these applications, cells are directly interfaced with extensions of the electrode to form intimate connections for efficient charge transfer. The resulting electrodes have both low impedance and high charge storage capacities. They can also operate at higher current levels than uncoated electrodes while remaining at safe voltages. These materials and processes present a method to impart bioactivity to electrodes while also improving the electrical properties for recording or stimulation.

## 2.5 Acknowledgements

The author would like to thank Dorothy Sorenson at the MIL for her assistance with TEM sample preparation. Portions of this chapter have been previously published in: Richardson-Burns, S.M., J.L. Hendricks, B. Foster, L.K. Povlich, D.H. Kim, D.C. Martin, Polymerization of the conducting polymer poly(3,4-ethylenedioxythiophene) (PEDOT) around living neural cells. Biomaterials, 2007. **28**(8): p. 1539-52. And in: Richardson-Burns, S.M., J.L. Hendricks, and D.C. Martin, Electrochemical polymerization of conducting polymers in living neural tissue. J Neural Eng, 2007. **4**(2): p. L6-L13.

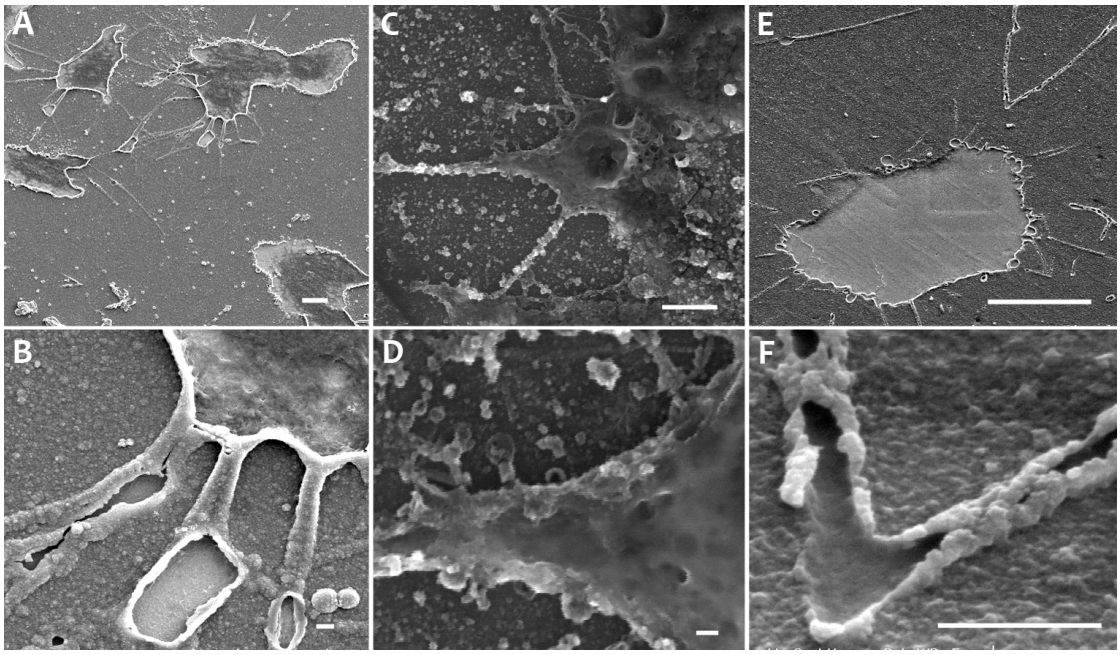


Figure 2-1. Conducting polymer deposited around living neural cells. (A) and (B) are SEM images showing PEDOT deposited around living cells. (C) and (D) show PEDOT deposited around a hydrated living cell in the environmental scanning electron microscope (ESEM). (E) and (F) show PEDOT deposited around living cells which were subsequently removed. For images (A), (C), (E) the scale bar is 10 μm; for images (B), (D), (F) the scale bar is 1 μm.

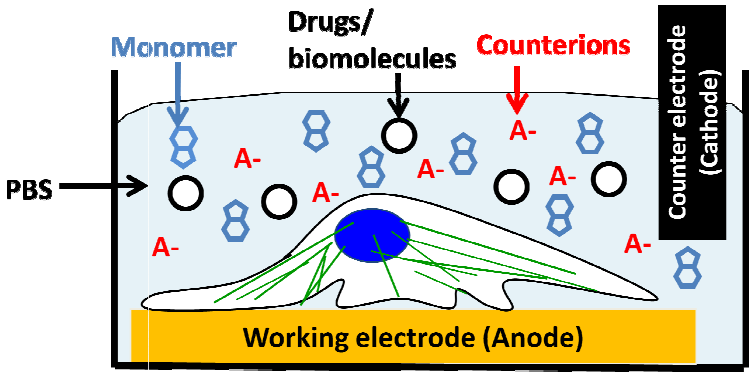


A. Before electrochemical deposition

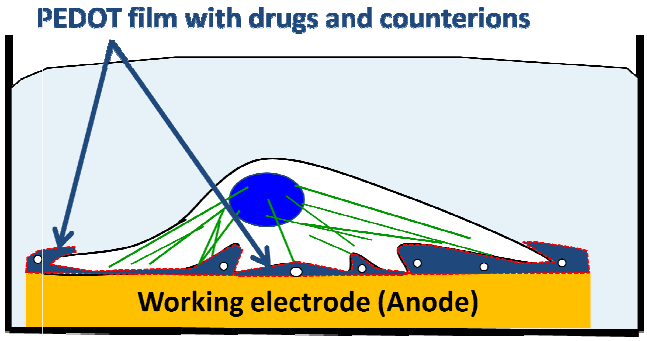


B. After electrochemical deposition

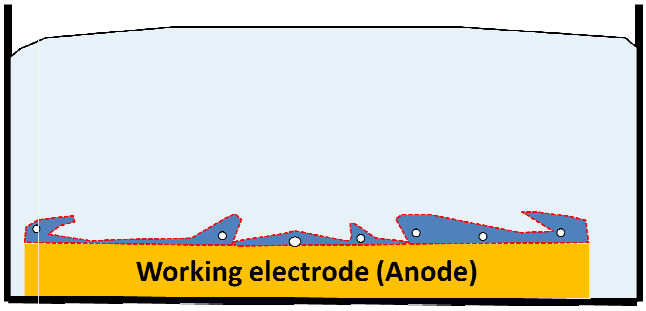


C. After mechanical or biochemical cell removal

Figure 2-2. (A) Cells are cultured on a metallic electrode and submerged into an aqueous solution with monomer and counterions. (B) After electrochemical deposition of conducting polymer around living cells, a dark film is deposited around the cells on the metallic anode. (C) By removing cells either mechanically or biochemically from the conducting polymer, a cell-templated electrode coating is created.

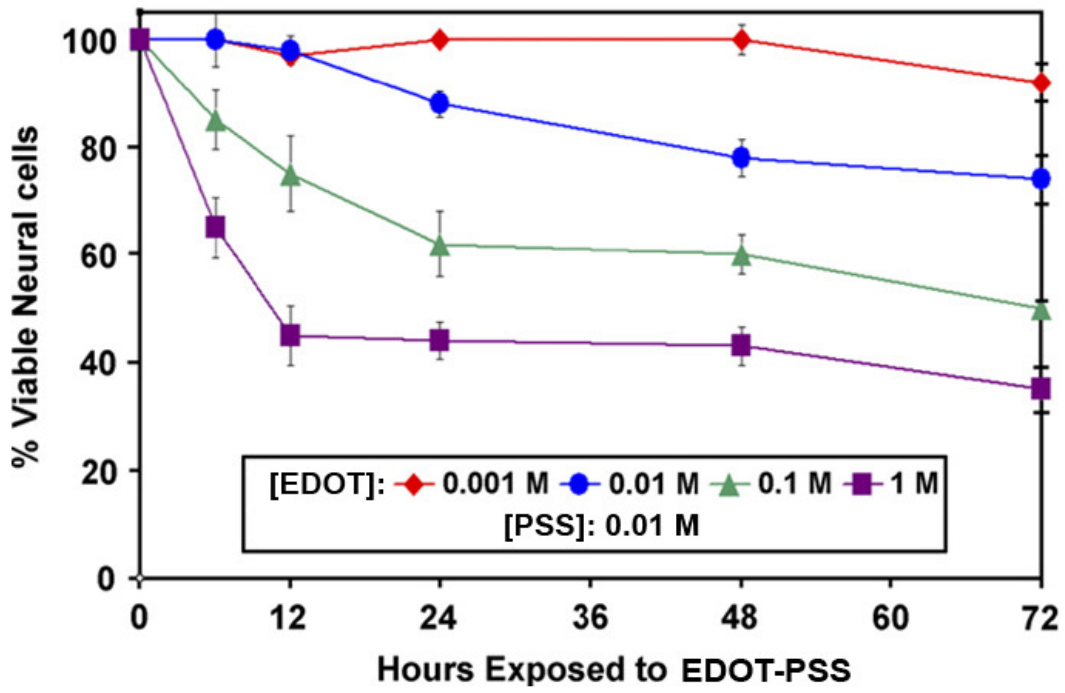


Figure 2-3. Viability of SH-SY5Y neuroblastoma after exposure to EDOT-PSS in cell media.

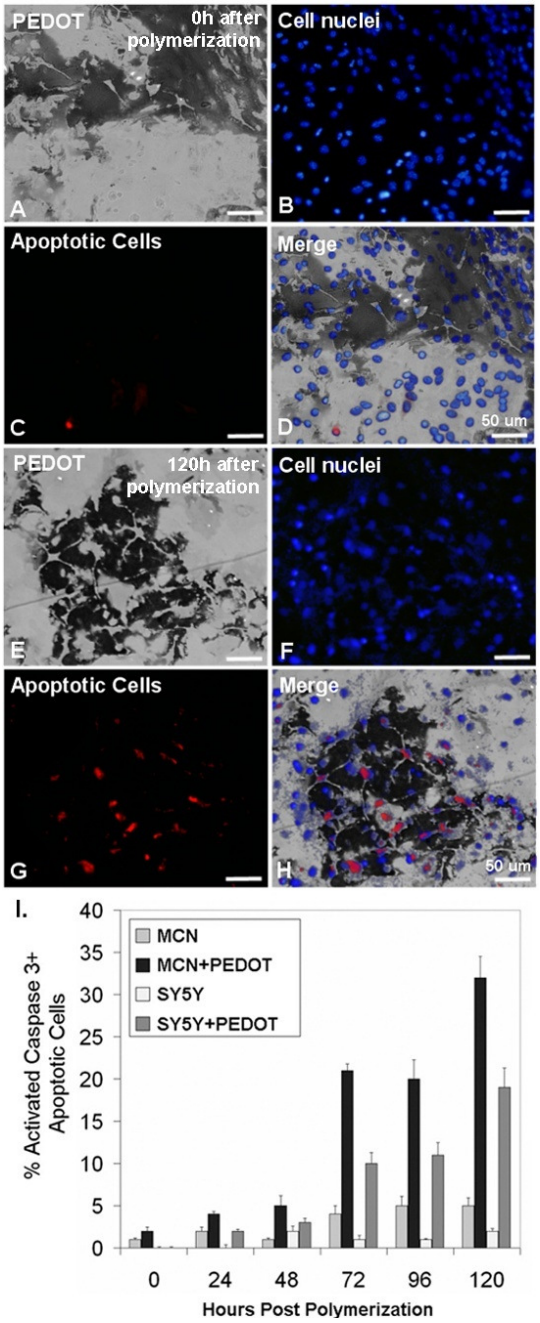


Figure 2-4. Viability of primary mixed cortical neurons (MCN) and SH-SY5Y cells after PEDOT has been electrochemically deposited around them. (A) – (D) are representative images of MCN directly after deposition. (E) – (H) are representative images of MCN 120 h after deposition. (A) and (E) are phase contrast images of PEDOT and cells. (B) and (F) show cell nuclei labeled with Hoechst 33342 (blue). (C) and (G) show apoptotic cells labeled with α-caspace-3 antibody (red). (D) and (H) show the merged phase contrast image with nuclear and α-caspace-3 labeling. (I) Quantification of apoptotic cells after PEDOT polymerization.

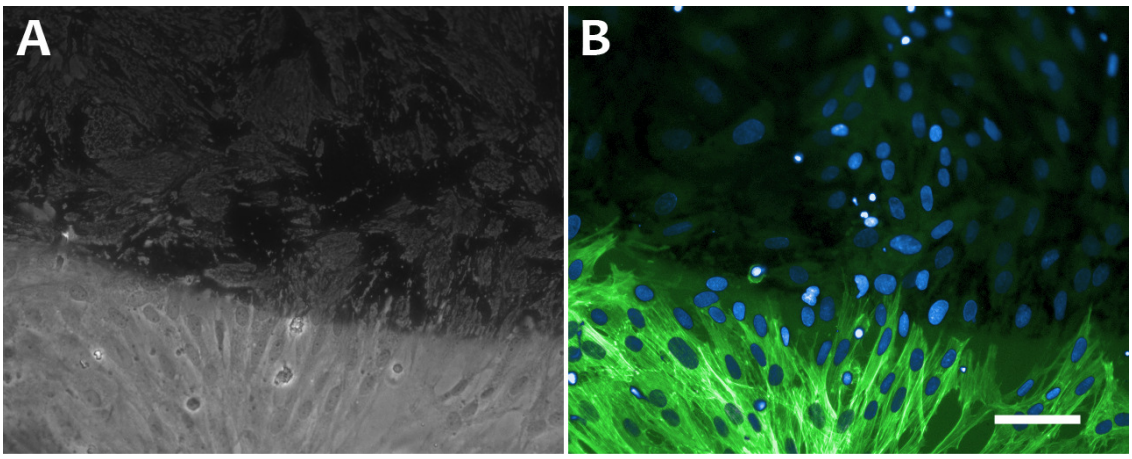


Figure 2-5. Cell morphology of SH-SY5Y 24 hours after electrochemical polymerization of PEDOT-PSS. (A) Brightfield image of cells with dark regions indicating PEDOT-PSS coating. (B) Cell nuclei are stained with Hoechst 33342 (blue) and actin filaments are stained with Phalloidin-Oregon Green (green) (Scale bar = 20 µm).

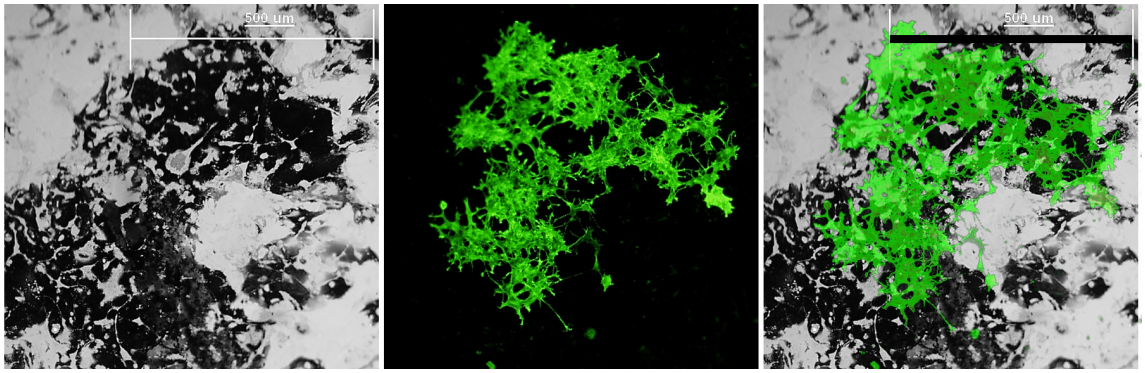


Figure 2-6. Adhesion of SH-SY5Y neuroblastoma to PEDOT films that had been previously templated with primary mixed cortical culture. Actin filaments are stained with Phalloidin-Oregon Green. (Scale bar = 500 µm)

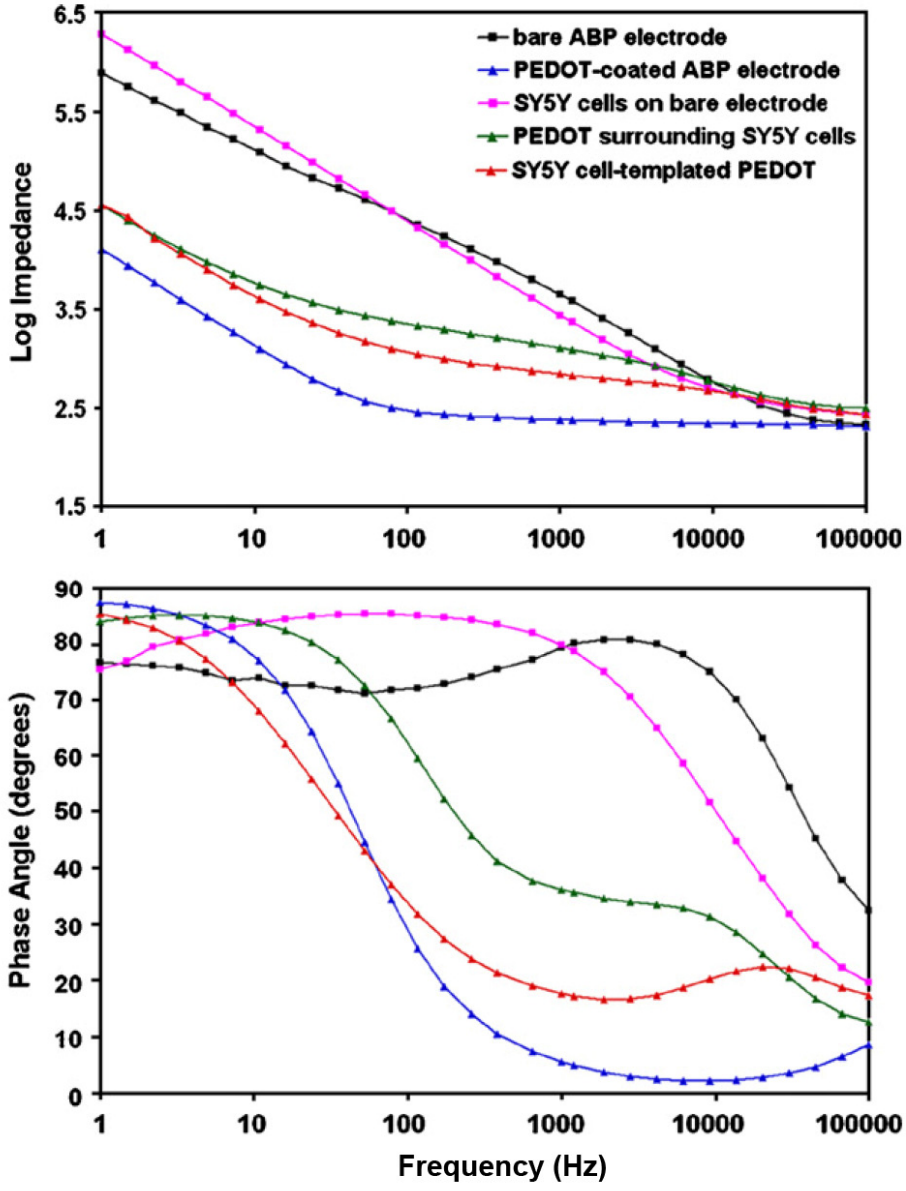


Figure 2-7. Electrochemical impedance spectroscopy and phase angle of PEDOT deposited around living SY5Y neuroblastoma on ABP electrodes.

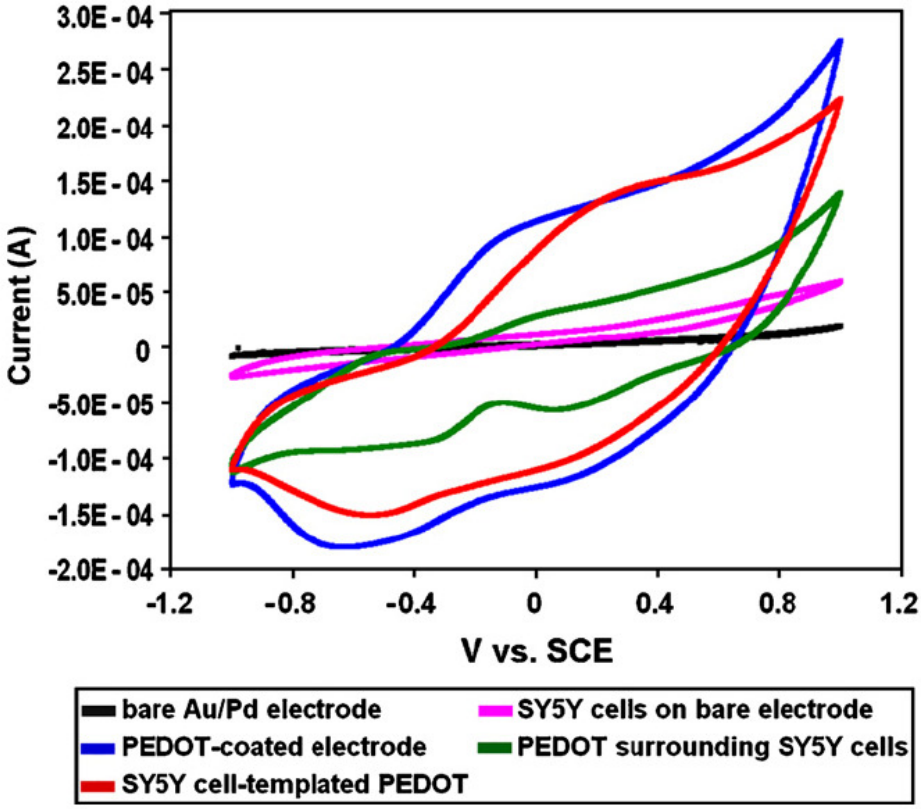


Figure 2-8. Cyclic voltammetry of PEDOT deposited around living SY5Y neuroblastoma on AuPd-sputtered electrodes.

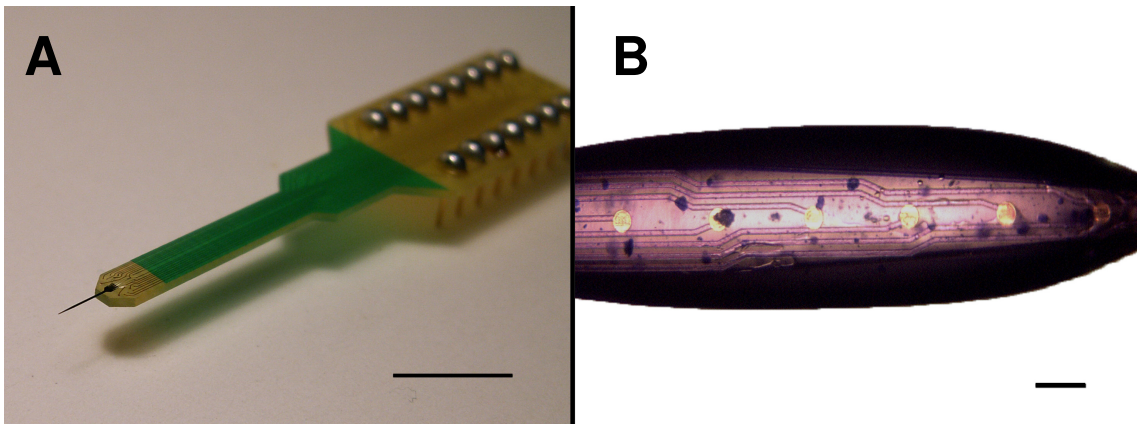


Figure 2-9. (A) Acute neural recording microelectrode formerly made at the University of Michigan Center for Neural Communication Technology (CNCT) (scale bar = 1 cm). (B) Hydrogel coating containing stained neural cells on neural probe (scale bar = 100 µm).

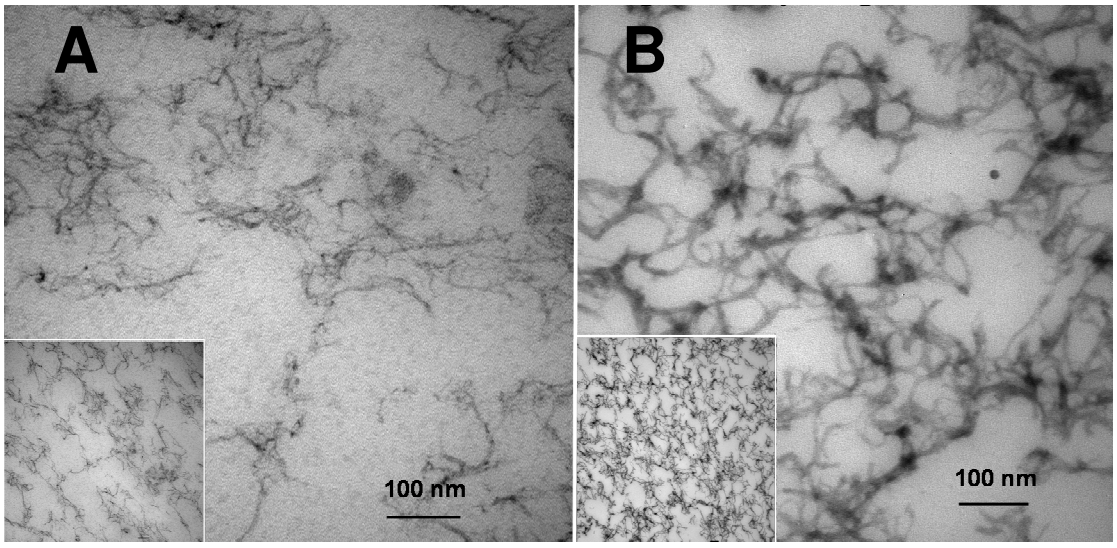


Figure 2-10. Transmission electron micrograph of alginate and PEDOT. (A) Alginate hydrogel network along and (B) alginate hydrogel with PEDOT-PSS deposited within.

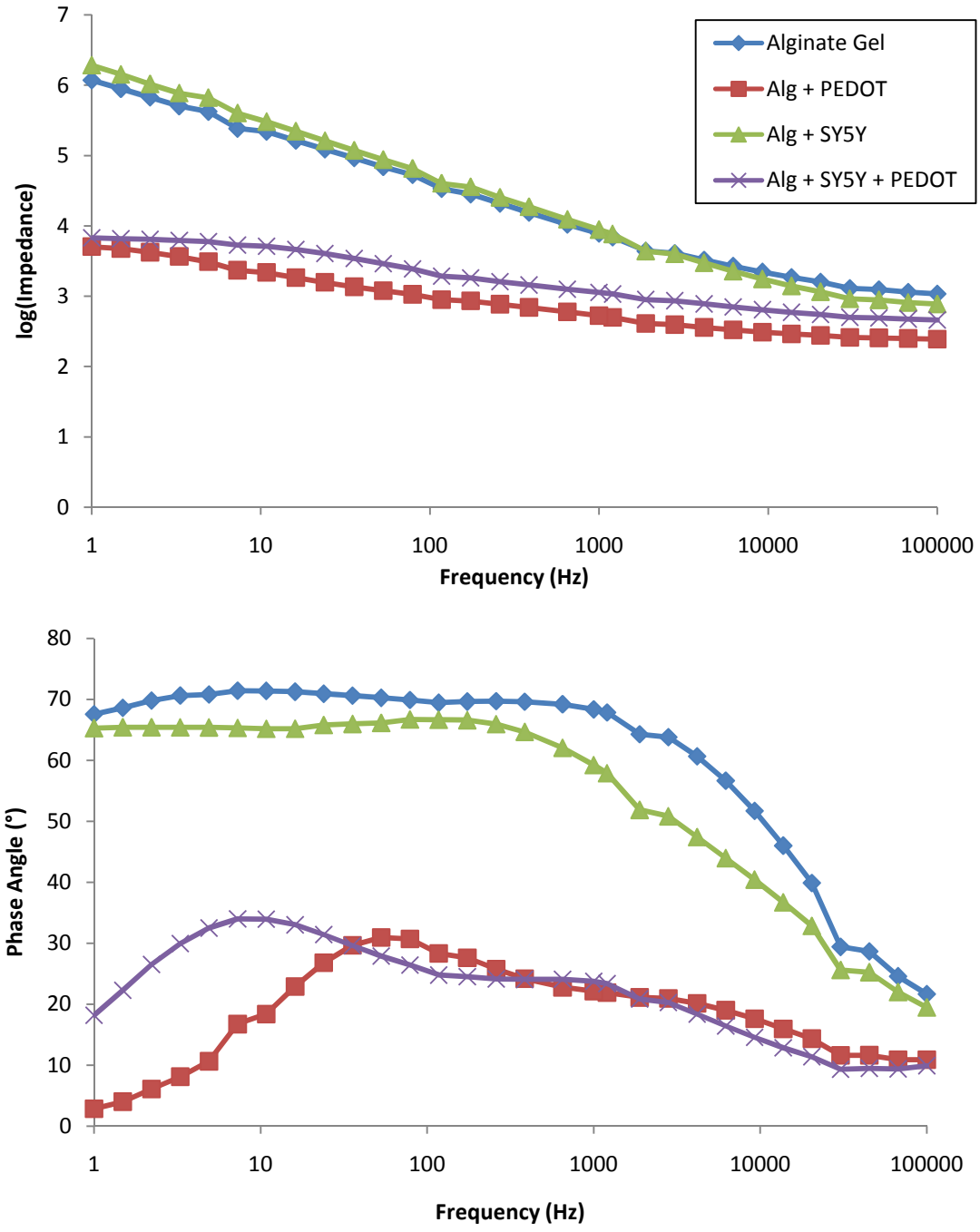


Figure 2-11. Impedance spectroscopy and phase angle of PEDOT grown off of gold wire into alginate hydrogel tissue scaffold seeded with SY5Y neuroblastoma.

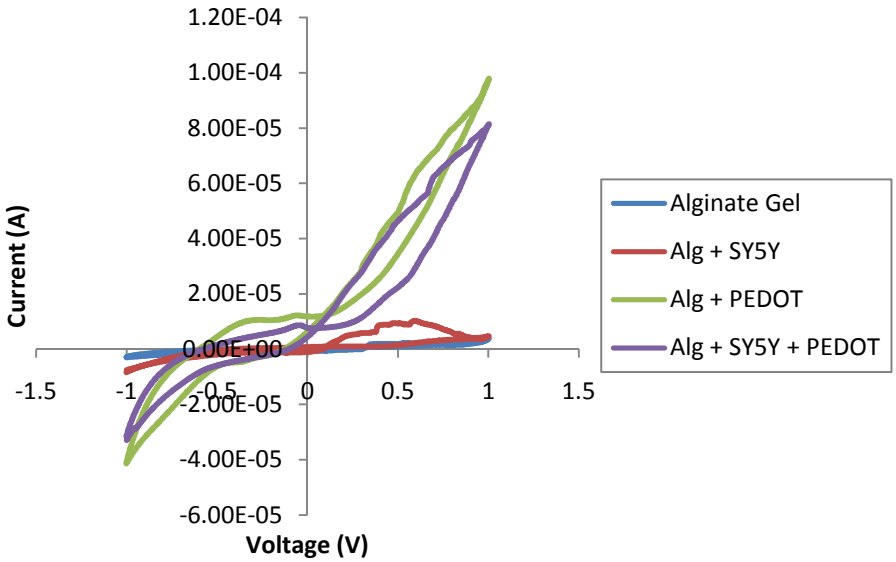


Figure 2-12. Cyclic voltammetry of PEDOT deposited within alginate hydrogel and in an alginate hydrogel seeded with SY5Y neuroblastoma.

# References


1. Sarje, A. and N. Thakor, *Neural interfacing.* Conf Proc IEEE Eng Med Biol Soc, 2004. **7**: p. 5325-8.

2. Lempka, S.F., et al., Optimization of microelectrode design for cortical recording based on thermal noise considerations. Conf Proc IEEE Eng Med Biol Soc, 2006. **1**: p. 3361-4.

3. Polikov, V.S., P.A. Tresco, and W.M. Reichert, *Response of brain tissue to chronically implanted neural electrodes.* Journal of Neuroscience Methods, 2005. **148**(1): p. 1-18.

4. Widge, A.S., et al., Self-assembled monolayers of polythiophene conductive polymers improve biocompatibility and electrical impedance of neural electrodes. Biosensors & Bioelectronics, 2007. **22**(8): p. 1723-1732.

5. Stieglitz, T., Flexible biomedical microdevices with double-sided electrode arrangements for neural applications. Sensors and Actuators a-Physical, 2001. **90**(3): p. 203-211.

6. Kim, D.H., M. Abidian, and D.C. Martin, *Conducting polymers grown in hydrogel scaffolds coated on neural prosthetic devices.* Journal of Biomedical Materials Research Part A, 2004. **71A**(4): p. 577-585.

7. Nyberg, T., O. Inganas, and H. Jerregard, *Polymer hydrogel microelectrodes for neural communication.* Biomedical Microdevices, 2002. **4**(1): p. 43-52.

8. Yang, J.Y. and D.C. Martin, Impedance spectroscopy and nanoindentation of conducting poly(3,4-ethylenedioxythiophene) coatings on microfabricated neural prosthetic devices. Journal of Materials Research, 2006. **21**(5): p. 1124-1132.

9. Rousche, P.J., et al., Flexible polyimide-based intracortical electrode arrays with bioactive capability. IEEE Trans Biomed Eng, 2001. **48**(3): p. 361-71.

10. Kim, D.H. and D.C. Martin, Sustained release of dexamethasone from hydrophilic matrices using PLGA nanoparticles for neural drug delivery. Biomaterials, 2006. **27**(15): p. 3031-3037.

11. Zhong, Y.H. and R.V. Bellamkonda, Dexamethasone-coated neural probes elicit attenuated inflammatory response and neuronal loss compared to uncoated neural probes. Brain Research, 2007. **1148**: p. 15-27.

12. Winter, J.O., S.F. Cogan, and J.F. Rizzo, *Neurotrophin-eluting hydrogel coatings for neural stimulating electrodes.* Journal of Biomedical Materials Research Part B-Applied Biomaterials, 2007. **81B**(2): p. 551-563.

13. Kim, D.H., et al., Effect of immobilized nerve growth factor on conductive polymers: Electrical properties and cellular response. Advanced Functional Materials, 2007. **17**(1): p. 79-86.

14. Kennedy, P.R., The Cone Electrode - a Long-Term Electrode That Records from Neurites Grown onto Its Recording Surface. Journal of Neuroscience Methods, 1989. **29**(3): p. 181-193.

15. Stauffer, W.R. and X.T. Cui, *Polypyrrole doped with 2 peptide sequences from laminin.* Biomaterials, 2006. **27**(11): p. 2405-2413.

16. He, W. and R.V. Bellamkonda, *Nanoscale neuro-integrative coatings for neural implants.* Biomaterials, 2005. **26**(16): p. 2983-2990.

17. Moxon, K.A., et al., Bioactive properties of nanostructured porous silicon for enhancing electrode to neuron interfaces. J Biomater Sci Polym Ed, 2007. **18**(10): p. 1263-81.

18. Raffa, V., et al., Design criteria of neuron/electrode interface. The focused ion beam technology as an analytical method to investigate the effect of electrode surface morphology on neurocompatibility. Biomedical Microdevices, 2007. **9**(3): p. 371-383.

19. Stieglitz, T., Neural prostheses in clinical practice: biomedical microsystems in neurological rehabilitation. Acta Neurochir Suppl, 2007. **97**(Pt 1): p. 411-8.

20. Cui, X.Y. and D.C. Martin, Electrochemical deposition and characterization of poly(3,4-ethylenedioxythiophene) on neural microelectrode arrays. Sensors and Actuators B-Chemical, 2003. **89**(1-2): p. 92-102.

21. Cui, X.Y., et al., *In vivo studies of polypyrrole/peptide coated neural probes.* Biomaterials, 2003. **24**(5): p. 777-787.

22. Xiao, Y.H., et al., Surface modification of neural probes with conducting polymer poly(hydroxymethylated-3,4-ethylenedioxythiophene) and its biocompatibility. Applied Biochemistry and Biotechnology, 2006. **128**(2): p. 117-129.

23. Yang, J.Y., et al., Ordered surfactant-templated poly(3,4-ethylenedioxythiophene) (PEDOT) conducting polymer on microfabricated neural probes. Acta Biomaterialia, 2005. **1**(1): p. 125-136.

24. Abidian, M.R., D.H. Kim, and D.C. Martin, *Conducting-polymer nanotubes for controlled drug release.* Advanced Materials, 2006. **18**(4): p. 405-+.

25. Yang, J., K. Lipkin, and D.C. Martin, Electrochemical fabrication of conducting polymer poly(3,4-ethylenedioxythiophene) (PEDOT) nanofibrils on microfabricated neural prosthetic devices. J Biomater Sci Polym Ed, 2007. **18**(8): p. 1075-89.

26. Vazquez, M., et al., Solution-cast films of poly(3,4-ethylenedioxythiophene) as ion-to-electron transducers in all-solid-state ion-selective electrodes. Sensors and Actuators B-Chemical, 2004. **97**(2-3): p. 182-189.

27. Wang, L.X., X.G. Li, and Y.L. Yang, *Preparation, properties and applications of polypyrroles.* Reactive & Functional Polymers, 2001. **47**(2): p. 125-139.

28. Potter, W., R.E. Kalil, and W.J. Kao, *Biomimetic material systems for neural progenitor cell-based therapy.* Front Biosci, 2008. **13**: p. 806-21.

29. Lakatos, A. and R.J.M. Franklin, *Transplant mediated repair of the central nervous system: an imminent solution?* Current Opinion in Neurology, 2002. **15**(6): p. 701-705.

30. Imitola, J., Prospects for neural stem cell-based therapies for neurological diseases. Neurotherapeutics, 2007. **4**(4): p. 701-14.

31. Kovacs, G.T., *Enabling Technologies for cultured neural networks*. 1st ed. 1994: San Diego, CA: Academic Press.

32. Nisbet, D.R., et al., *Neural tissue engineering of the CNS using hydrogels-A review.* J Biomed Mater Res B Appl Biomater, 2007.

33. Prang, P., et al., The promotion of oriented axonal regrowth in the injured spinal cord by alginate-based anisotropic capillary hydrogels. Biomaterials, 2006. **27**(19): p. 3560-9.

34. Rejali, D., et al., Cochlear implants and ex vivo BDNF gene therapy protect spiral ganglion neurons. Hear Res, 2007. **228**(1-2): p. 180-7.

# Chapter 3

# Laser interference patterning and direct laser writing of PEDOT-PSS for neuronal guidance

## 3.1 Introduction

It has been noted that the chemical composition, biochemical functionality, micro- and nano-structure of biomaterials all play roles in the adhesion, proliferation and differentiation of cells in contact with biomaterials [1]. Thus when selecting materials for implanted devices, tissue engineering applications, or cell culture substrates, the surface chemistry and cell-scale surface structure are crucial factors in determining the biological response. The contact and integration of cells on a biomedical device surface often play key roles in the device function. For example the integration of bone cells on a hip implant surface, the proximity of neurons to recording microelectrodes, and the adhesion of cells in culture assays are requirements for these devices to function. In many cases the tissue response to biomaterials can often have deleterious effects including death of target cells and scarring [2, 3], underscoring the need for materials capable of influencing these responses.

Conducting polymers including polypyrrole (PPy), poly(3,4-ethylene dioxythiophene) (PEDOT) and their derivatives have been increasingly used in biomedical electrode applications due to their desirable electrical, mechanical,

and chemical properties [4]. When applied to biomedical electrodes, they reduce the electrochemical impedance, increase the charge injection densities, and provide a soft surface that can be functionalized with pharmacological agents or cell adhesion molecules to direct cellular adhesion, proliferation, and differentiation [5-7]. Controlled delivery of anti-inflammatory agents, growth factors and other molecules can be achieved with conducting polymer electrodes [8-11]. The microstructure of conducting polymer electrodes can also be controlled to produce extremely fuzzy, soft, and porous surfaces [12-14]. In contrast to the traditional inert metals that are used for biomedical electrodes, conducting polymers offer many properties similar to those of living tissue which makes then well-suited for use at the interface between the engineered device and the living organism. These properties include: ionic conductivity, bioactivity, structural features on the nano-micro scales, and similar mechanical stiffnesses. By promoting a transition of mechanical and electrical properties and by directing the tissue response at the interface, a more robust and functional interface may be possible that will provide long-term, reliable communication. The improvements in electrical properties and bioactive capabilities are of interest not only of implantable biomedical devices but for biosensors, drug delivery, cell culture assays, fundamental electrophysiology, bioMEMS, and tissue engineering. The microscale surface structure of the device is one of the key tools for directing the cell and tissue response to the biomaterials with which they are in contact.

A number of methods have been used to pattern biomaterials surface topography and biochemical functionality with controlled dimensions in the nano and microscales for biomedical applications [15, 16]. Methods such as soft lithography, photolithography [17], block copolymers, and photo-polymerization have been used to create topographical structures including microfluidic channels, cages, wells, textures and biomimetic patterns. These patterned surfaces are capable of directing cell viability, fate, proliferation, differentiation, adhesion, orientation, morphology [18-20]. Among these methods, patterning with nanosecond and femtosecond lasers has emerged as a flexible method to

reproducibly pattern large areas with miscoscale features. Patterning of the electrically conducting polymer poly(3,4-ethylene dioxythiophene)-poly(styrenesulfonate) (PEDOT-PSS) has been achieved using direct laser writing (DLW) in which a pulsed femto-second laser was used to ablate portions of the film to produce lines and holes in PEDOT/PSS with lateral resolution of 2 µm [21]. Lines and spots are written one-at-a-time by focusing the laser into a small spot on the samples surface while the sample is moved by an electrically-controlled stage. Another laser patterning method which has recently been used to pattern conducting polymers and other materials is direct laser interference patterning (DLIP) [22-24]. When multiple lasers spots are directed onto the sample, interference of the laser beams produces periodic variations in laser intensity leading to ablation at the interference maxima. Using this method, large areas can be patterned with periodic features in a single step. Laser patterning offers an extremely flexible method for incorporating microscale topographical features onto biomaterials. Our goal is to investigate and compare the use of laser patterning methods for introducing controlled surface features onto PEDOT-PSS electrodes.

In the current study we demonstrate that the growth and orientation of electrically active cells can be directed on conducting polymer surfaces with controlled morphologies. The micron-scale channels used to guide cells were created using direct laser interference patterning as well as direct laser writing. Linear structures of PEDOT-PSS on a metallic substrate were produced and the resulting morphologies were investigated using optical and scanning electron microscopy. Electrically active neuroblastoma cells were then cultured on the patterned substrates and analyzed using fluorescent and scanning electron microscopy. Impedance spectroscopy and cyclic voltammetry of the laser-patterned films were also performed, to investigate the electrical properties of the conducting polymer electrodes.

## 3.2 Experimental

### 3.2.1. Electrochemical deposition of PEDOT-PSS

Gold-palladium (AuPd) thin films were sputtered on indium-tin oxide (ITO) substrates (70 $mm^2$) to facilitate electrochemical deposition and to improve adhesion of conducting polymer films. Subsequently, PEDOT-PSS conducting polymers were electrochemically deposited from a solution of PSS (0.2% w/v) and ethylene dioxythiophene (EDOT) (0.1% w/v) in deionized water. The polymerization was carried out galvanostatically by applying a current density of 0.75 $mA/cm^2$ using a potentiostat/galvanostat (AutoLab PGStat 12, Eco Chemie, Netherlands). By varying the deposition time, and thus the total deposition charge, PEDOT-PSS films of three different average thicknesses (70 nm, 825 nm, and 2220 nm) were fabricated.

### 3.2.2. Direct laser writing of PEDOT-PSS

Machining was performed using a Clark MXR CPA-2001 Ti:sapphire femtosecond laser. The laser produces 150 fs pulses with a Gaussian spatial profile at 780 nm wavelength. During machining, pulses were delivered to the target with a repetition rate of 1000 Hz after power had been modulated using neutral density filers and a waveplate/polarizer combination (Figure 1). Different focusing conditions were used to produce varied focal spot sizes on the sample surfaces.

### 3.2.3. Laser interference patterning of PEDOT-PSS

A commercial Nd:YAG laser (Quanta-Ray PRO 290, Spectra Physics) was used. The fundamental wavelength of the Nd:YAG laser is 1064 nm from which shorter wavelengths (532, 355 and 266 nm) can be obtained by harmonic generation. Samples were irradiated at 355 nm with pulses lasting 10 ns at normal incidence. The primary laser beam (355 nm) was split into two beams that were then recombined on the sample surface to create an interference

pattern on the sample surface (Figure 1). To reduce influences from the optical elements, high flatness of the optical components is needed to construct the optical system. The angle between the laser beams was changed in order to produce different periodic spacing. All samples were irradiated at ambient temperature and pressure conditions.

### 3.2.4. Cell culture

SH-SY5Y neuroblastoma-derived cells between passages of 50 and 70 were seeded onto samples at a density of 100 cells/mm$^2$ and cultured in Dulbecco's Modified-Eagle's Media (Invitrogen) supplemented with 10 % (v/v) calf serum (Invitrogen). Cell cultures were maintained in humidified incubators at 37 ℃ and 5 % $CO_2$.

For fluorescence microscopy, cells were fixed in 4 % formaldehyde/PBS at RT for 30 min. The F-actin cytoskeleton was labeled by Oregon Green Phalloidin (Invitrogen) (1:50 in PBS) overnight at 4 ℃. Prolong, an anti-fade agent with DAPI (Invitrogen) was used to mount samples. For SEM imaging, cells were fixed using 1% glutaraldehyde in PBS, washed in deionized water, then dehydrated in ascending ethanol washes (50%, 75%, 95%, 100%; 10 min each), and finally dried overnight in hexamethyldisilazane (HMDS) (Ted Pella, Inc.). The SEM samples were sputter coated with 20 Å of gold prior to imaging.

### 3.2.5. Microscopy

The patterned samples were imaged using an optical microscope (Nikon OptiPhot POL-2) with attached CCD camera (Spot RT) and high-resolution scanning electron microscopes (SEM) with an operating voltage of 10 kV (LEO 1530 Thermally-Assisted Field Emission and FEI Nova Field Emission Gun microscopes). Fluorescently-labeled samples were imaged with a fluorescent microscope (Nikon Diaphot) and captured with CCD camera (Hamamatsu).

### 3.2.6. Electrochemical characterization

Electrochemical impedance spectroscopy (EIS) was performed using the AutoLab PGstat 12. A three electrode setup was used in which the coated electrode served as the working electrode, a 6 x 6 mm platinum foil as the counter electrode, and a saturated calomel electrode (SCE) as the reference electrode. The electrolyte used was room temperature PBS (pH = 7.4)(HyClone). The impedance was measured at frequencies from 1-1,000,000 Hz upon application of a 5 mV RMS sine wave between the working and counter electrode. Cyclic voltammetry was performed to measure the charge storage and transfer properties of the electrodes. The equipment and three-electrode setup described above were used. The current was measured as the voltage was cycled from +0.8 to -0.6 V versus the SCE at a rate of 0.1 V/s.

### 3.2.7. Neurite quantification

Images of cells on patterned substrates were analyzed using ImageJ (version 1.41b, by Wayne Rasband). Three parameters were measured: the orientation of each neurite from the point it leaves the cell body to its tip, the length of each neurite, and the number of neurites for a given area. The orientation of neurites was then divided into nine groups based on their deviation from the pattern orientation. The first group contained neurites with orientation within 10° (either to the right or left) of the pattern orientation; the second group contained those neurites with orientation 10-20° (either right or left) from the pattern direction; the third group contained those 20-30° from the pattern orientation, and so on.

## 3.3 Results and discussion

### 3.3.1. Fabrication and characterization of direct laser written PEDOT-PSS channels

The machining of 825 nm thick PEDOT-PSS films with direct laser writing produced channels of various widths in the conducting polymer film (Figure 3-2). Due to the higher ablation threshold of the underlying AuPd and ITO layers, PEDOT-PSS could be removed without damaging the substrates below. By tuning the focal spot size of the fs-pulsed laser, it was possible to create channels of various widths, from 2 µm to 60 µm. Using the stage controller, the inter-line spacing can easily be varied to create PEDOT ridge of varying width. The stage controller also much flexibility in channel geometry, as rectangles, rounded shapes and any grayscale bitmap image can easily be patterned onto the film. In order for this method to work reliably, it is crucial that the substrate be very well aligned, perpendicular to the incident laser. Small misorientations led to large regions that did not get patterned. The channels created by fs-pulsed direct laser writing had rough edges with some peeling back of the PEDOT-PSS layer. Subsequent cell culture assays with SH-SY5Y neuroblastoma indicated that cells aligned in the pattern direction when they were near the channels (Figure 3-2C). Cell bodies tended to prefer to lay within the channels. Neurites tended to prefer the edges of the channels, where the PEDOT is cracked and peeled back (Figure 3-2D). Direct laser writing of PEDOT-PSS is a very powerful method for creating microscale patterns on the film surface, but due to difficulties with the setup, we focused on the use of laser interference patterning in subsequent studies.

### 3.3.2. Fabrication and morphology of laser interference patterned PEDOT-PSS channels

Figure 3-3 shows scanning electron microscopy images of the laser interference patterning of PEDOT-PSS films on gold-palladium-sputtered ITO.

The laser fluences (energy/unit area) required to ablate the PEDOT-PSS films increases with film thickness for films of approximately 825 nm or less, as has been previously measured for this system by single shot experiments [25]. For 70 nm films, a laser fluence of 43 mJ/cm$^2$ was sufficient to remove the PEDOT-PSS film without harming the underlying AuPd or ITO layers (Figure 2A). At fluences above 128 mJ/cm$^2$ the AuPd layer is damaged as well (Figure 2B). In many cases it is possible to see the re-solidified droplets of gold-palladium on top of the ITO or at the PEDOT-PSS/substrate interface (Figures 2C) and at higher fluencies, the ITO itself becomes cracked, porous and eventually removed (Figure 2D). The minimum laser fluencies required for complete ablation of PEDOT-PSS films 825 and 2220 nm thick are 252 and 255 mJ/cm$^2$, respectively. In these cases, the underlying AuPd and ITO films are intact, but at increasing laser fluences the underlying films can be removed. For thicker PEDOT-PSS films, it is possible to ablate the PEDOT-PSS film by using either increased laser fluence or multiple shots to the same area. At laser fluences below the threshold for PEDOT-PSS ablation, the conducting polymer becomes extremely porous and fuzzy in the ablated regions (Figure 2E). Multiple layers of the PEDOT film are also exposed (Figure 2F). Scanning electron microscopy and AFM imaging confirm that the height of PEDOT-PSS at the interface of ablated/non-ablated regions is taller than the original PEDOT-PSS films, likely due to folding back of the polymer layers or deposition of ablated material as has been seen in similar systems (data not shown) [21, 25]. By altering the angle of the incoming laser beams, lines were ablated into the PEDOT-PSS films with two different periods, 7.82 and 13.5 µm.

### 3.3.3. Electrical properties of laser interference-patterned PEDOT-PSS

For bio-electrical recording and stimulating applications, low electrical impedance and high charge storage and delivery densities are desirable for safe and effective device operation. Past studies have shown that coatings of PEDOT-PSS on metallic biomedical electrodes can provide significant improvements to electrode impedance and charge delivery capabilities [12, 26,

27]. In the present study, PEDOT-PSS coatings reduced the average impedance of 1 $mm^2$ AuPd/ITO electrodes at frequencies below 10 kHz (Figure 6A). At 1 kHz, the average impedance decreased from 883 Ω to 562 Ω for the unpatterned 825 nm thick PEDOT-PSS film. The thickest (2220 nm) PEDOT-PSS film had an average impedance of 520 Ω at 1 kHz. Cyclic voltammetry (CV) studies, shown in Figure 6B, reveal that the average charge storage capacity, proportional to the integral of the CV curve, increases with PEDOT film thickness. The initial charge storage capacity of AuPd/ITO electrodes was 6.37 $mC/cm^2$. As more PEDOT-PSS was grown on the electrode, the charge storage capacity grew to 65.3, and 256 $mC/cm^2$ for the 825 and 2220 nm films of unmodified PEDOT-PSS respectively.

In order to investigate the effects of laser interference patterning on the electrical properties of the films, impedance spectroscopy and cyclic voltammetry were performed before and after patterning for a group of 825 nm thick PEDOT-PSS films. Despite the removal of material from the samples the average impedance of the electrodes remained the same (Figure 5A). It is possible that the increased surface area from the laser patterning helped to offset the loss of conducting polymer. The charge storage capacity of 825 nm thick PEDOT-PSS coated electrodes decreased slightly from 65.3 $mC/cm^2$ for the unpatterned film, to 62.3 $mC/cm^2$ after patterning. Given that the charge storage capacity of the laser interference patterned film is still ten times greater than the value for the uncoated AuPd/ITO electrode, this patterning method offers the ability to introduce topographical control of the conducting polymer electrode surface while maintaining the vastly improved electrical properties of the coated electrode.

### 3.3.4. Neurite orientation on PEDOT-PSS channels

Following morphological characterization of the laser-interference patterned PEDOT-PSS films, SH-SY5Y neuroblastoma were cultured on the samples to investigate the effects of patterned conducting polymer structures on the orientation of neuronal-like cells. SY5Y cells adhered and sent out processes on all substrates: patterned PEDOT-PSS, unpatterned PEDOT-PSS and

unpatterned ITO. Representative images of SY5Y orientation on laser interference patterned PEDOT-PSS and controls are shown in Figure 3-3. The ability of the patterned structures to direct neurite elongation and orientation was measured (Figure 4). On the unpatterned PEDOT-PSS of various thicknesses and unpatterned ITO neurites extended in all directions in roughly equal proportions. No difference in preferred orientation could be seen based on the thickness of the PEDOT-PSS layer or on the bare ITO. On the 70 nm PEDOT-PSS with laser interference patterned channels that extend to the underlying AuPd layer, a fraction of the neurites were oriented along the pattern direction. 35 % of neurites were aligned within 10° of the pattern direction for 7.82 µm period, and 28 % on 13.5 µm period patterns. The distribution of remaining neurite orientations is shown in Figure 4. The channels in 825 nm thick PEDOT-PSS provided the highest degree of neurite alignment, with 87 % of neurites on 7.82 µm period patterns and 78 % of neurites on 13.5 µm period patterns oriented within 10° of the pattern direction. The deepest channels, those on 2220 nm thick PEDOT-PSS films had 83 % and 66 % of neurites within 10° of the pattern direction for 7.8 um and 13.5 um period patterns respectively. The underlying AuPd layer helps to limit the laser radiation and produce a flat bottom to the channels. However, it is possible to pattern channels which do not extend through the PEDOT layer using lower laser fluences.

The thinnest laser-patterned PEDOT-PSS films produced the least orientation of neurites. This could be due to the fact that the channels are much shorter, and thus it is easier for neurites to escape the shallow trenches. Alternatively, we have found that when laser-patterned, the 825 and 2220 nm thick PEDOT-PSS films produce an extremely fuzzy surface with many exposed sub-layers of the film exposed while the 70 nm PEDOT-PSS films are less fuzzy and contain only a single sub-layer. The fuzziness and roughness of the thicker PEDOT-PSS films may account for the increased orientation of neurites.

To investigate whether or not the exposed AuPd layer helps to direct neurite orientation, we patterned channels into 2220 nm thick PEDOT that did not extend through the entire layer. These are referred to as “all PEDOT” since the

bottom of the channel is still PEDOT as opposed to AuPd in the other cases. The “all PEDOT” channels are also shorter than their counterparts since they do not extend through the entire layer. These “all PEDOT” channels successfully oriented 54 % and 27 % of neurites within 10 ° of the pattern direction for 7.82 and 13.5 µm period patterns, respectively. Although we can clearly see that there is an orientational effect of these channels, the ability to direct neurite growth is far lower than the PEDOT/AuPd counterpart, indicating that the presence of the AuPd layer at the channel bottom has an influence on directing neurite orientation. This could be due to the chemical composition of the AuPd layer, the surface roughness of the AuPd layer, or perhaps the presence of a PEDOT-PSS/AuPd/ITO interface. These results suggest that the smaller period pattern (7.82 µm) is able to direct neurite orientation more than the larger period pattern (13.5 µm) in all cases. On samples with both 7.82 and 13.5 µm pattern periods, SY5Y cell bodies tended to grow on the taller PEDOT-PSS structures found between ablated channels while their processes predominantly grew within the ablated trenches (Figure 6). Scanning electron microscopy studies indicate that neurites preferentially adhere along the edges of the channels, that has the PEDOT-PSS/AuPd/ITO interface (Figure 6-inset).

Neurite lengths were measured to investigate the effects of substrate patterning on neurite growth and are presented in Table 1. The longest average neurites, 48.8 ± 28.0 µm, were seen on substrates with the highest amount of neurite alignment, the 825 nm thick PEDOT with 7.82 µm period channels. On unpatterned PEDOT of the same thickness, neurites had an average length of 29.2 ± 17.3 µm. In general, average neurite length correlated with the amount of neurite orientation, although these comparisons lack statistical significance due to large distributions of neurite length.

## 3.4 Conclusions

Laser patterning techniques offer extremely flexible methods for patterning a variety of microscale structures onto biomaterials substrates. Direct laser writing can be used to machine nearly any 2-dimensional shape and to rapidly test many pattern geometries. Laser interference patterning represents a fast and reproducible technique for patterning large areas with microscale structures and texture. When used to pattern conducting polymers, it is possible to produce electrically active substrates and scaffolds capable of directing cell growth. These biomaterials can be used for neural regeneration, tissue engineering, implantable devices, biosensors and cell culture assays.

Laser interference patterning of conductive PEDOT-PSS films was accomplished in order to produce linear topographical structures on the electrode surface with periods of 7.82 and 13.5 µm. This novel method is highly scalable and can be in used in conjunction with organic electronic processing to rapidly pattern large areas with periodic structures in a single step while preserving electrical functionality. These features were used to direct the elongation of SY5Y neuroblastoma cells on conducting polymer electrodes. Laser interference patterned channels with 7.82 µm periodicity on 825 and 2220 nm thick PEDOT-PSS provided the highest degree of alignment of any substrates, with 83 – 87 % of neurites aligned within 10° of the pattern direction. The average neurite length was also greatest for this condition. Overall, neurite alignment was higher on substrates with 7.82 µm period channels than on 13.5 µm period channels. Additionally, results suggest that the presence of the ITO/AuPd/PEDOT interface is an important factor in promoting the extension of cell processes along the channel and thus facilitates neurite orientation.

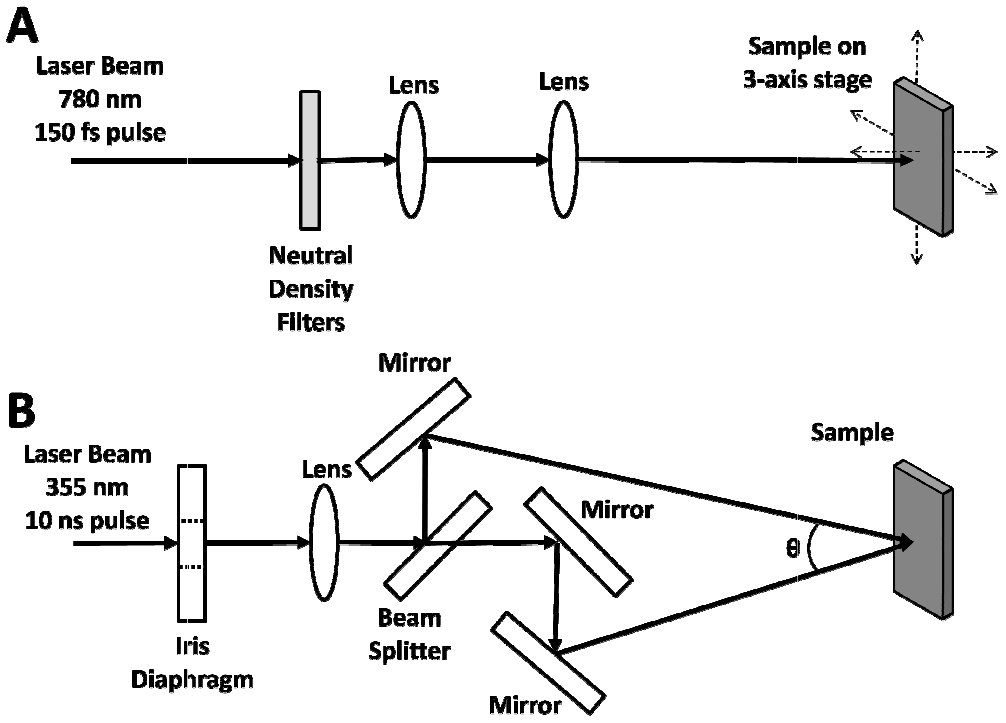


Figure 3-1. Laser patterning setups. (A) Schematic of direct laser writing setup for patterning of PEDOT-PSS cell substrates.(B) Schematic of laser interference patterning setup with two laser beams.

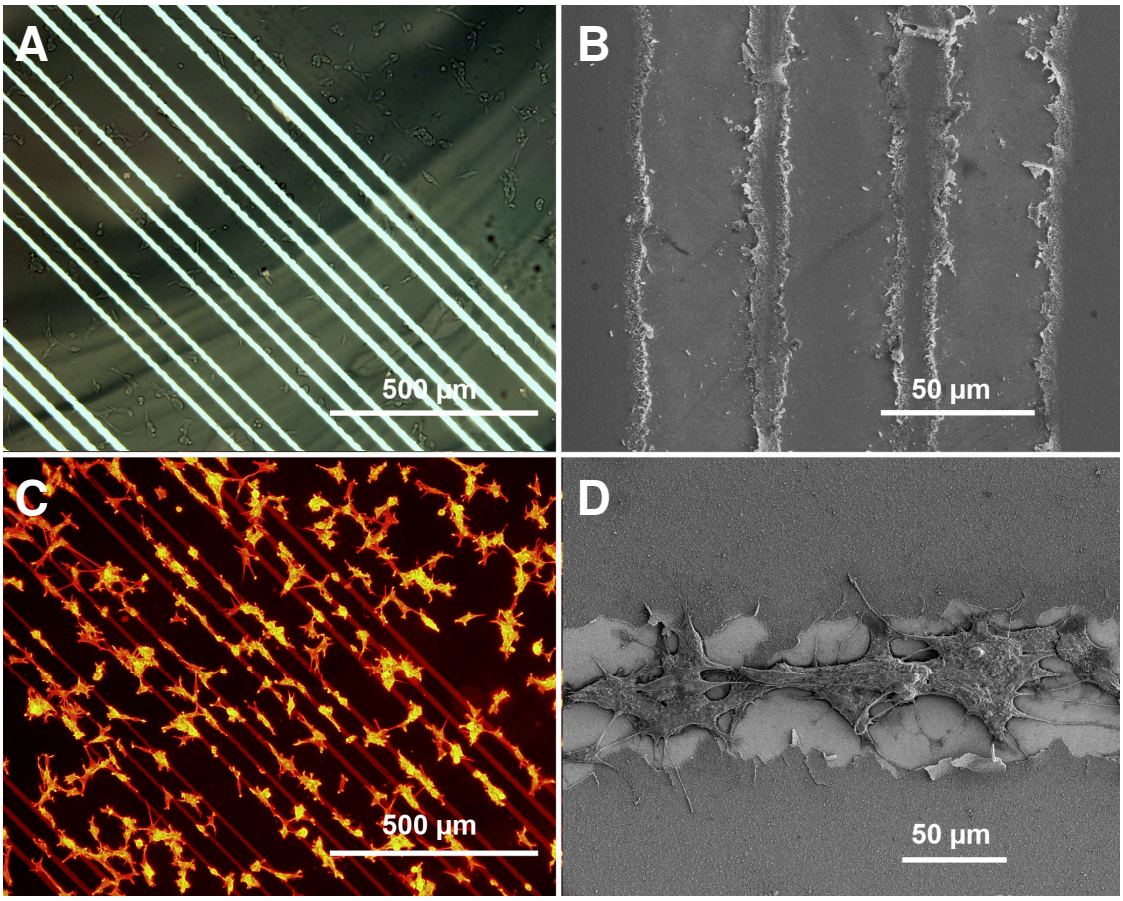


Figure 3-2. Direct laser written patterns in PEDOT-PSS on AuPd/ITO. (A) Optical micrograph of direct laser written lines of widths 32 µm in 200 nm thick PEDOT-PSS. (B) Electron micrograph of direct laser written channels in PEDOT-PSS films on AuPd/ITO showing limited horizontal damage from ablated areas. (C) SH-SY5Y cultured on samples shown in (A) and stained with Phalloidin-AlexaFluor594 (Red). (D) Electron micrograph of SH-SY5Y cultured on direct laser written PEDOT-PSS films, showing neurite attachment at the materials interface.

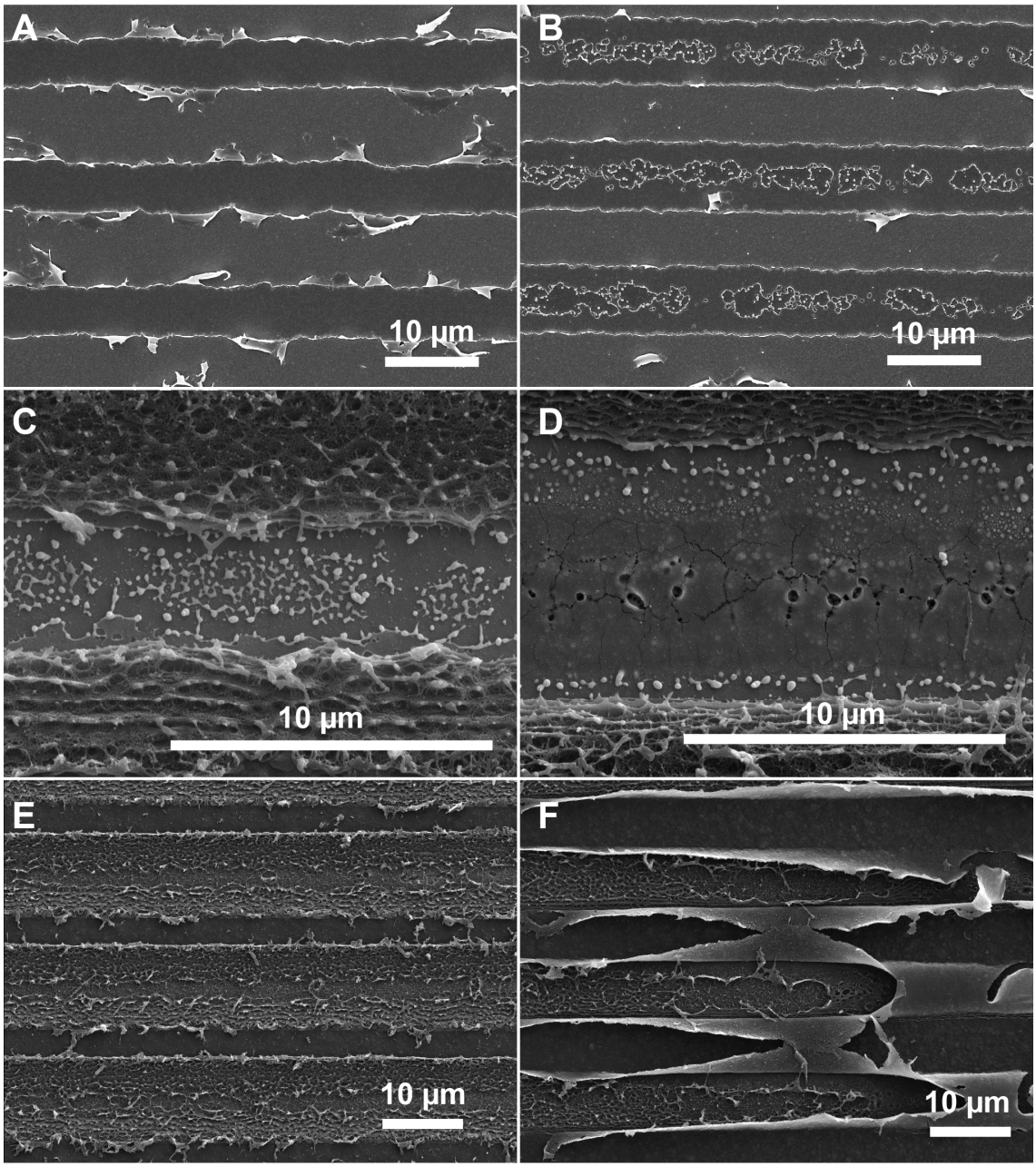


Figure 3-3. Morphology of PEDOT-PSS films on AuPd/ITO with laser interference patterning. (A) 70 nm PEDOT-PSS film with underlying substrate intact. (B) 70 nm PEDOT-PSS film with damage to the AuPd layer. (C) 825 nm thick PEDOT-PSS film showing damage to AuPd layer and fuzziness of PEDOT-PSS film after patterning. (D) At higher fluences, the AuPd is completely removed and the underlying ITO is damaged. (E) 2220 nm thick PEDOT-PSS film roughened by laser interference patterning. (F) At the edge of the laser spot, it is clear that layers of the 2220 nm PEDOT-PSS film are being peeled back.

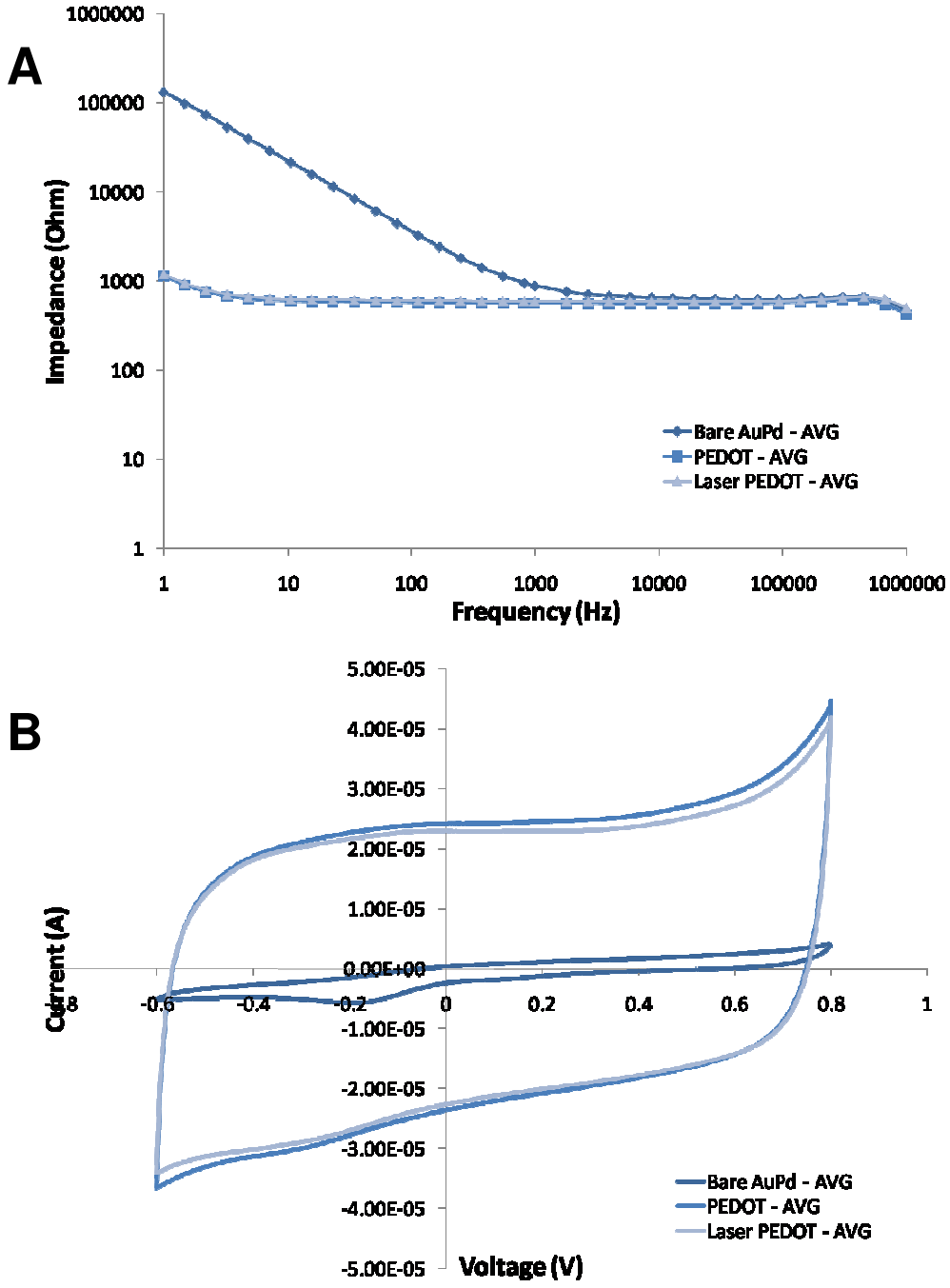


Figure 3-4. Electrochemical characterization of 825 nm laser interference patterned PEDOT-PSS films. (A) Electrochemical impedance spectroscopy and (B) cyclic voltammetry of bare AuPd electrode, PEDOT-PSS coated electrode, and laser-interference patterned PEDOT-PSS.

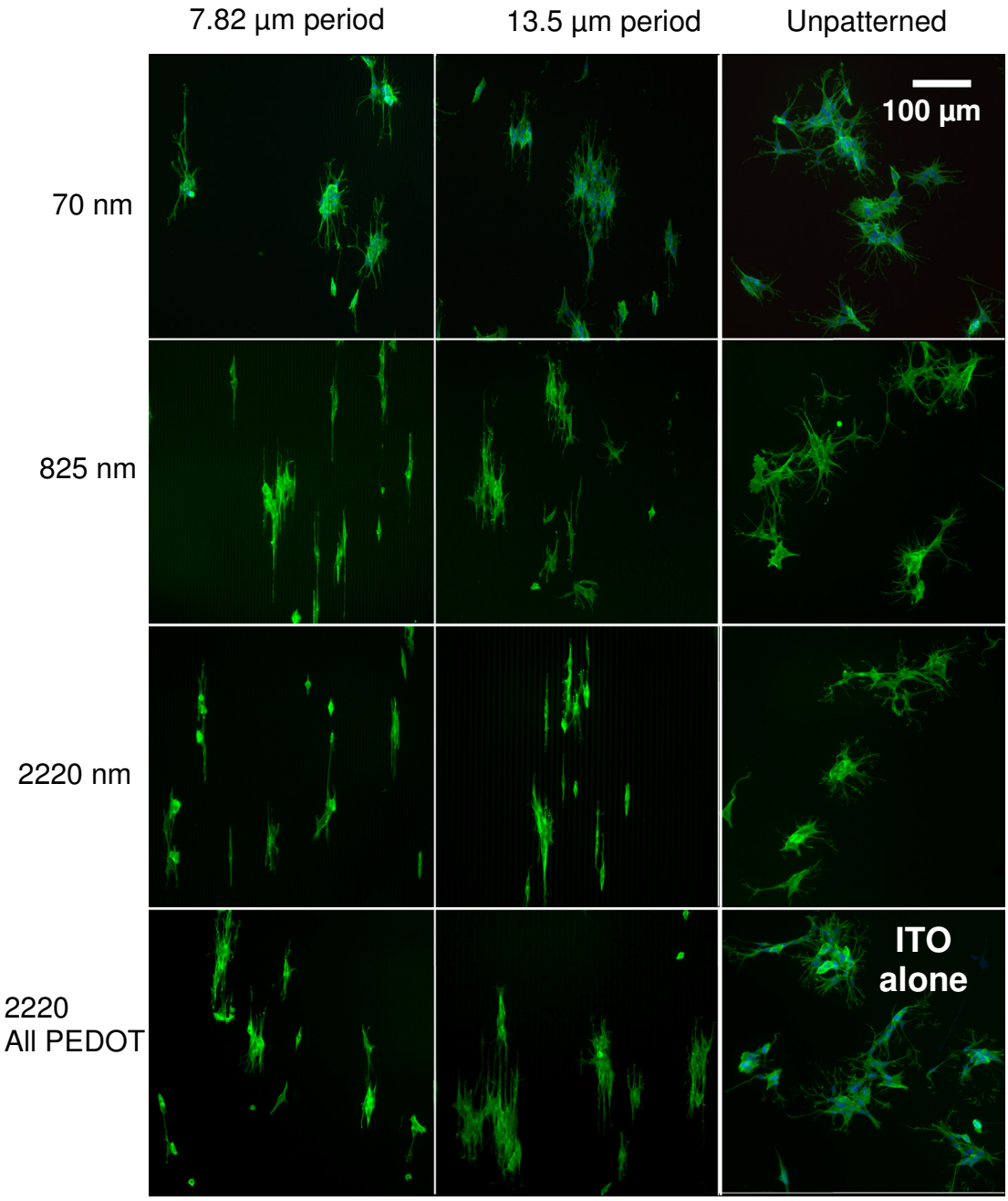


Figure 3-5. Alignment and proliferation of SH-SY5Y neuroblastoma on PEDOT-PSS films patterned with DLIP. Three thicknesses of PEDOT-PSS were patterened with channels: 70nm, 825 nm, and 2220 nm. Laser-patterning removed the PEDOT-PSS film to the underlying AUPd/ITO layer in all cases except “2000 nm All PEDOT”, where PEDOT was only partially removed leaving PEDOT at the bottom of the channels. Channels with periodicity of 7.82 and 13.5 µm were created. Cell orientation on ITO and three thicknesses of unpatterned PEDOT was used for control. Scale bare applies to all images.

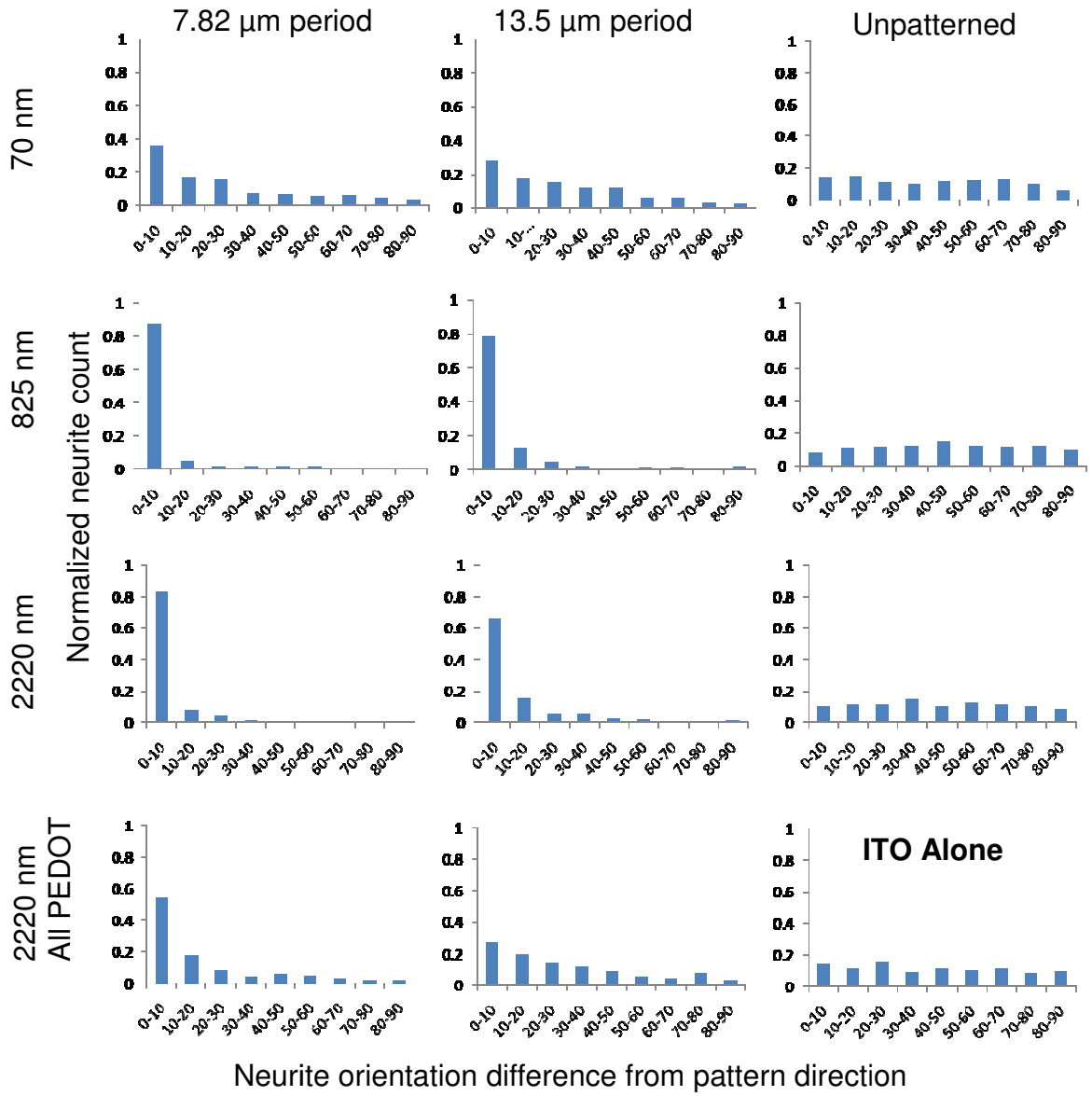


Figure 3-6. Histogram of neurite orientation difference from the direction of the pattern. Number of neurites is normalized by the total number of neurites for each condition. The periodicity of patterned features is given at the top: 7.82 µm, 13.5 µm and unpatterned. Channels were ablated through three thicknesses of PEDOT, 70, 825, and 2220 nm, to the underlying metallic substrate. "All PEDOT" channels were created in the 2220 nm PEDOT that did not reach the underlying metal and only contained PEDOT.

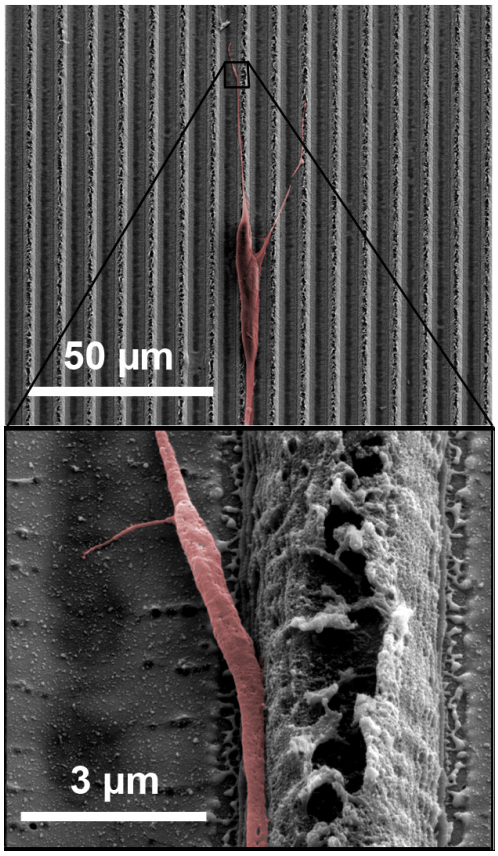


Figure 3-7. SY5Y (pseudo-colored red) on 7.82 µm period patterned 2220 nm thick PEDOT-PSS. The cell bodies tend to favor growing on top of the PEDOT stripes while the neurites tend to favor the flat channel bottoms and in particular the corners with PEDOT/AuPd/ITO interface.

| | 7.8 um period pattern | | | | 13.2 um period pattern | | | | No Pattern (Control) | | | |
|---|---|---|---|---|---|---|---|---|---|---|---|---|
| PEDOT height (nm) | 70 | 825 | 2220 | 2220-All PEDOT | 70 | 825 | 2220 | 2220-All PEDOT | 70 | 825 | 2220 | ITO |
| **Avg. neurite length (μm)** | 40.4 | 48.8 | 41.4 | 34.9 | 36.7 | 39.4 | 41.6 | 31.9 | 33.7 | 29.2 | 32.6 | 33.8 |
| **Standard deviation (μm)** | 20.0 | 28.0 | 22.9 | 22.9 | 16.9 | 16.9 | 24.3 | 17.9 | 16.0 | 17.3 | 18.6 | 15.7 |

Table 3-1. Average neurite length on laser interference patterned PEDOT-PSS on AuPd/ITO, on unpatterned PEDOT-PSS, and on ITO alone.

# References


1. Jandt, K.D., *Evolutions, revolutions and trends in biomaterials science - A perspective.* Advanced Engineering Materials, 2007. **9**(12): p. 1035-1050.

2. Szarowski, D.H., et al., *Brain responses to micro-machined silicon devices.* Brain Res, 2003. **983**(1-2): p. 23-35.

3. Biran, R., D.C. Martin, and P.A. Tresco, *Neuronal cell loss accompanies the brain tissue response to chronically implanted silicon microelectrode arrays.* Exp Neurol, 2005. **195**(1): p. 115-26.

4. Guimard, N.K., N. Gomez, and C.E. Schmidt, *Conducting polymers in biomedical engineering.* Progress in Polymer Science, 2007. **32**(8-9): p. 876-921.

5. De Giglio, E., et al., *Synthesis, analytical characterization, and osteoblast adhesion properties on RGD-grafted polypyrrole coatings on titanium substrates.* J Biomater Sci Polym Ed, 2000. **11**(10): p. 1073-83.

6. D.-H. Kim, S.M.R.-B.J.L.H.C.S.D.C.M., *Effect of Immobilized Nerve Growth Factor on Conductive Polymers: Electrical Properties and Cellular Response.* Advanced Functional Materials, 2007. **17**(1): p. 79-86.

7. Lee, J.W., et al., *Carboxylic acid-functionalized conductive polypyrrole as a bioactive platform for cell adhesion.* Biomacromolecules, 2006. **7**(6): p. 1692-5.

8. Pernaut, J.M. and J.R. Reynolds, *Use of conducting electroactive polymers for drug delivery and sensing of bioactive molecules. A redox chemistry approach.* Journal of Physical Chemistry B, 2000. **104**(17): p. 4080-4090.

9. Abidian, M.R., D.H. Kim, and D.C. Martin, *Conducting-polymer nanotubes for controlled drug release.* Advanced Materials, 2006. **18**(4): p. 405-+.

10. Richardson, R.T., et al., *The effect of polypyrrole with incorporated neurotrophin-3 on the promotion of neurite outgrowth from auditory neurons.* Biomaterials, 2007. **28**(3): p. 513-23.

11. Wadhwa, R., C.F. Lagenaur, and X.T. Cui, *Electrochemically controlled release of dexamethasone from conducting polymer polypyrrole coated electrode.* J Control Release, 2006. **110**(3): p. 531-41.

12. Yang, J., et al., *Ordered surfactant-templated poly(3,4-ethylenedioxythiophene) (PEDOT) conducting polymer on microfabricated neural probes.* Acta Biomater, 2005. **1**(1): p. 125-36.

13. Yang, J., K. Lipkin, and D.C. Martin, *Electrochemical fabrication of conducting polymer poly(3,4-ethylenedioxythiophene) (PEDOT) nanofibrils on microfabricated neural prosthetic devices.* J Biomater Sci Polym Ed, 2007. **18**(8): p. 1075-89.

14. Yang, J.Y. and D.C. Martin, *Microporous conducting polymers on neural microelectrode arrays - I - Electrochemical deposition.* Sensors and Actuators B-Chemical, 2004. **101**(1-2): p. 133-142.

15. Falconnet, D., et al., *Surface engineering approaches to micropattern surfaces for cell-based assays.* Biomaterials, 2006. **27**(16): p. 3044-63.

16. Hasirci, V. and H. Kenar, *Novel surface patterning approaches for tissue engineering and their effect on cell behavior.* Nanomed, 2006. **1**(1): p. 73-90.

17. Kaihara, S., et al., *Silicon micromachining to tissue engineer branched vascular channels for liver fabrication.* Tissue Eng, 2000. **6**(2): p. 105-17.

18. Khademhosseini, A., et al., *Interplay of biomaterials and micro-scale technologies for advancing biomedical applications.* J Biomater Sci Polym Ed, 2006. **17**(11): p. 1221-40.

19. Khademhosseini, A., et al., *Microscale technologies for tissue engineering and biology.* Proc Natl Acad Sci U S A, 2006. **103**(8): p. 2480-7.

20. McBeath, R., et al., *Cell shape, cytoskeletal tension, and RhoA regulate stem cell lineage commitment.* Dev Cell, 2004. **6**(4): p. 483-95.

21. McDonald, J.P., et al., *Femtosecond pulsed laser patterning of poly(3,4-ethylene dioxythiophene)-poly(styrenesulfonate) thin films on gold/palladium substrates.* Journal of Applied Physics, 2007. **102**(1): p. -.

22. Lasagni, A., C. Holzapfel, and F. Mucklich, *Production of two-dimensional periodical structures by laser interference irradiation on bi-layered metallic thin films.* Applied Surface Science, 2006. **253**(3): p. 1555-1560.

23. Lasagni, A., A. Manzoni, and F. Mucklich, *Micro/nano fabrication of periodic hierarchical structures by multi-pulsed laser interference structuring.* Advanced Engineering Materials, 2007. **9**(10): p. 872-875.

24. Lasagni, A.F., et al., *One-step production of organized surface architectures on polymeric materials by direct laser interference patterning.* Advanced Engineering Materials, 2007. **9**(1-2): p. 99-103.

25. Lasagni, A., et al., *Direct laser interference patterning of poly(3,4-ethylene dioxythiophene)-poly(styrene sulfonate) (PEDOT-PSS) thin films.* Organic Electronics, Submitted.

26. Cui, X., et al., *Surface modification of neural recording electrodes with conducting polymer/biomolecule blends.* J Biomed Mater Res, 2001. **56**(2): p. 261-72.

27. Cui, X.Y. and D.C. Martin, *Electrochemical deposition and characterization of poly(3,4-ethylenedioxythiophene) on neural microelectrode arrays.* Sensors and Actuators B-Chemical, 2003. **89**(1-2): p. 92-102.

# Chapter 4

# Bioactive, conducting polymer coatings for cochlear stimulating electrodes

## 4.1 Introduction

Cochlear implants help many adults and children with profound deafness regain the ability to hear. They are one of the most successful clinical neural prosthetic devices [1, 2]. Cochlear implants are used specifically in patients with a loss of inner ear sensory hair cells, whose job is to transduce vibrations in the basilar membrane into neuro-electrical signals which are sent via the cochlear nerve to the brain. Cochlear implants replace this lost pathway by digitally converting sounds captured by a microphone into electrical signals which are sent via electrodes implanted in the cochlea to the remaining cochlear nerve processes. The location of each electrode in the cochlea dictates which tones it activates as the cochlea is arranged tonotopically with highest frequencies near the base and lowest frequencies at the apex. Thus, high density electrode arrays capable of precise and localized stimulation provide the highest tonal resolution.

Since the introduction of the first FDA-approved cochlear implant in 1984, advances in the electronics, speech processing, and fabrication of the devices have improved their safety, reliability and tonal range [3]. Recent advances have produced clinical devices with up to 22 metallic electrode sites and with

positioning systems to conform to the shape of the cochlea to reduce the distance between electrodes and spiral ganglia (Figure 4-1) [4-6]. Progress has also been made to reduce the trauma to cochlear structures during surgical implantation [7, 8]. Meanwhile, improvements in the materials and bioactivity of cochlear implants remain modest and the incidence of meningitis associated with implantation is on the rise [3]. While cochlear implants work well to help patients regain the ability to perceive speech, they have had limited success representing music or sounds with broad tonal ranges, and function poorly in atmospheres with loud background noise [3, 9, 10]. Studies on the tissue reaction have increasingly shown the detrimental effects of the cochlear tissue reaction to implanted electrode arrays. Implantation trauma includes mechanical damage to the basilar membrane, spiral ligament, modiolar wall, osseous spiral lamina, Reisner's membrane and breach of the scala vestibuli [4, 6, 7, 11]. This damage can cause a chronic response that includes inflammation, fibrous and bony encapsulation in the scala tympani and degeneration of target neurons [12-15]. Strategies to preserve the neuronal processes and more directly couple them with electrodes sized similar to cell dimensions may permit increased tonal specificity while reducing the overall power consumption of the device.

Currently, the size of the electrodes must be large enough so that sufficient charge is delivered to elicit a response without producing irreversible electrochemical reactions such as hydrolysis. The reversible charge injection limit of a material dictates the total amount of charge that can be stored reversibly by a given surface area [16]. Materials used for neural stimulation are chosen for their large reversible charge injection limit as well as biocompatibility, stability and other desirable electrochemical properties. These materials include platinum, platinum-iridium, gold, iridium, titanium, stainless steel, nickel-chromium, nickel-titanium and ceramic wires [17, 18]. For neural stimulation in the central nervous system and *in vitro* applications, surface coatings including platinum black, titanium nitride, iridium oxide and more recently carbon nanotubes have been used to increase the charge injection limit of an electrode

[19-24]. Typically these coatings promote the roughening of the electrode surfaces thereby increasing the total area of charge transfer.

Conducting polymer coatings have been studied for neural recording applications due to their extremely low impedance and biocompatibility [25-31]. They offer extremely fuzzy surfaces and both ionic and electronic conductivity which make them ideal for interfacing metallic and biological systems. They can be used as actuators to direct the placement of arrays in the cochlea [32]. Conducting polymer coatings can also be modified with biological components and pharmacological agents to help direct the tissue response [30, 33-37]. These properties make conducting polymers a very attractive material for cochlea electrodes. Other promising materials developed for neural recording and regeneration applications include hydrogels which are spongy, water-filled polymer networks. Hydrogels have been used in the cochlea and central nervous system for the delivery of pharmaceutical agents [38-41], as scaffolds for cell delivery and differentiation [42-44], and to make soft, porous electrodes [45-48]. The use of hydrogels functionalized with adhesion ligands, including the RGD tripeptide, has also been used to direct cell growth and attachment [49-52].

In order to improve the function of cochlear implants, we proposed a series of coatings to reduce the distance between the stimulating electrode and the spiral ganglion (Figure 4-1), to promote the health and viability of the remaining neural processes, reduce the trauma of insertion of cochlear electrodes and improve the charge injection density at the electrode/electrolyte interface. In this chapter, we will examine the coating of cochlear electrode with conducting polymers and hydrogels. We will assess their electrochemical and morphological properties along with their ability to be sterilized using traditional hospital sterilization methods.

## 4.2 Experimental

### 4.2.1. Cochlear implant fabrication

Monopolar cochlear electrodes were manufactured using polytetrafluoroethylene (PTFE)-coated 75 µm diameter platinum-iridium alloy (Pt-Ir; 90 % / 10 %) wire (A-M Systems). The wire was melted using a propane /oxygen flame to produce a ball electrode of diameter 450 µm. A portion of Pt-Ir wire under the ball exposed by the flame was re-insulated with Sylgard 184 silicone (Dow Corning) up to the base of the ball electrode.

### 4.2.2. Cochlear implant coating

Cochlear electrodes were first electrochemically coated with poly(3,4-ethylene dioxythiophene)-poly(styrenesulfonate) (PEDOT-PSS). Some implants subsequently received RGD-functionalized alginate hydrogel coatings in addition to PEDOT-PSS. PEDOT-PSS was deposited from a solution containing 0.1 % (w/v) ethylene dioxythiophene (EDOT; H.C. Starck) and 0.2 % (w/v) poly(styrenesulfonate sodium salt) (PSS; Acros Organics) in deoinized water. The cochlear electrode was immersed into the monomer solution and served as the working electrode (anode). A 6 x 6 mm platinum foil served as the counter electrode (cathode). Galvanostatic currents of 1-5 µA were applied using an AutoLab PGStat12 Potentiostat/Galvanostat (EcoChemie). The deposition length was varied from 30 seconds to 930 seconds.

Hydrogel coating of the cochlear electrodes was performed using an alginate hydrogel covalently modified with the adhesion ligand arginine-glycine-aspartic acid (RGD). The hydrogel was generously provided by Dr. David Mooney, Harvard University and its preparation has been described elsewhere [49-51]. The cochlear electrodes were dip-coated in a solution of 1 % (w/v) RGD-alginate in PBS and then dipped into a solution of 2 % (w/v) calcium chloride (CaCl2; Sigma-Aldrich) in PBS. The dipping was repeated to achieve a uniform coating 150-200 µm thick.

### 4.2.3. Coating of microfabricated silicon neural probe

For biphasic stimulation studies, PEDOT-PSS was deposited onto 8-channel microfabricated silicon neural probes (NeuroNexus Technologies). The neural probes are used to facilitate acute neural recording and stimulation using an array of 8 – 40 µm diameter gold electrode sites. As described above, PEDOT-PSS was deposited from a solution containing 0.1 % (w/v) EDOT and 0.2 % (w/v) PSS in deionized water. The neural probe was immersed into the monomer solution and an individual electrode site served as the working electrode (anode). A 6 mm x 6 mm platinum foil served as the counter electrode (cathode). A galvanostatic current of 6 nA was applied using an AutoLab PGStat12 Potentiostat/Galvanostat (EcoChemie). The deposition length was varied from 30 seconds to 3600 seconds.

### 4.2.4. Electrochemical characterization

Electrochemical impedance spectroscopy (EIS) was performed using the AutoLab PGstat 12. A three electrode setup was used in which the coated electrode served as the working electrode, a 6 mm x 6 mm platinum foil as the counter electrode, and a saturated calomel electrode (SCE) as the reference electrode. The electrolyte used was room temperature PBS (pH = 7.4). The impedance was measured at frequencies from 1 – 100,000 Hz upon application of a 5 mV root mean square (RMS) sine wave between the working and counter electrode. Cyclic voltammetry was performed to measure the charge storage and transfer properties of the electrodes. The equipment and three-electrode setup described above were used. The current was measured as the voltage was cycled from +1.0 to -1.0 V versus the SCE at a rate of 0.1 V/s. The CV data was filtered using a built-in smoothing function in General Purpose Electrochemical System software (EcoChemie) to remove noise at 19 ± 0.5 Hz.

### 4.2.5. Biphasic stimulation

Biphasic current stimulation was performed by Aditi Ray and James Weiland at USC Doheney Eye Institute. Cathodic-first biphasic charge-balanced

current pulses were sourced from a STG 2008 stimulus generator (Multichannel Systems) while the voltage response was monitored with a TDS 5043B oscilloscope (Tecktronix). The current amplitude was varied from 10 – 2000 μA and the pulse duration was varied from 0.1 – 1 ms. 15 pulses were sourced in each signal train. To measure the maximal charge injection density before failure, a train of pulses with the smallest amplitude were given first, and then gradually increased until mechanical delamination of the coating occurred.

### 4.2.6. Cell culture

SH-SY5Y neuroblastoma cell lines (SY5Y) were obtained from Dr. Joseph Corey and Dr. Eva Feldman at the University of Michigan and used at passages between 30 and 60. SY5Y were maintained at 37℃ in a humid incubator with 5 % CO2 in media consisting of Dulbecco's Modified Eagle's Media (DMEM with glucose, L-glutamine; Gibco/Invitrogen) supplemented with 10 % (v/v) fetal bovine serum (FBS; Gibco/Invitrogen) and 1 % (v/v) antibiotic-antimicotic solution (Gibco/Invitrogen). Cell media was replaced every four days, and cells were passaged every 7 days. SY5Y were passaged using a solution of 0.25 % trypsin and 1 mM EDTA in PBS. Cells were fixed in 4 % paraformaldehyde in PBS for 1 hour at room temperature. The f-actin cytoskeleton was stained by incubating samples in Phallodin-Oregon Green (Molecular Probes/Invitrogen), diluted 1:300 in PBS with 0.1 % (w/V) Triton X (PBSX) for 1 hour at 4℃.

### 4.2.7. Microscopy

Samples were imaged optically using a Nikon OptiPhot POL microscope with SPOT RT digital camera with transmitted and/or reflected light. Fluorescent and phase contrast images were captured using an Olympus BX-51 upright microscope with Olympus CCD camera and Olympus imaging software (University of Michigan Morphology and Imaging Analysis Core Laboratory). Scanning electron microscopy (SEM) was performed using a FEI Nova 200 Nanolab Dualbeam FIB (University of Michigan Electron Microbeam Analysis

Laboratory(EMAL)). Samples were first sputtered with approximately 10 Å of gold prior to SEM imaging.

#### 4.2.8. Gas sterilization

Ethylene oxide gas sterilization was performed by the University of Michigan Hospital Central Sterile Supply (CSS).

## 4.3 Results and discussion

#### 4.3.1. PEDOT-PSS and hydrogel coating of implants

Electrochemical deposition of PEDOT-PSS onto Pt-Ir ball electrodes resulted in thin films of conducting polymer coating the surface of the electrode. The color of the electrode changes from metallic grey (Figure 4-2 (A)) to bluish-black (Figure 4-2 (B)) as the thickness of the PEDOT-PSS increases. After 30 s of deposition at a current of 1 μA the electrode still appears metallic grey. After 90 s, the electrode is a muted dull grey. The electrode takes on a light blue-green hue after 210 s, and then darkens to dark blue at 450 s. Finally, after 930 s of PEDOT-PSS deposition the electrode appears bluish-black. We hypothesize that the color change is due to the roughening of the surface and the reflection of light off this roughened surface.

After deposition of PEDOT-PSS onto the electrode surface, some electrodes receive a second coating with hydrogel in order to provide a soft buffer layer around the implant to reduce insertion trauma and to help center the electrode in the scala tympani after insertion. The hydrogel layer can also be used as a scaffold for the deposition of conducting polymer electrode extensions, or for the delivery of cells or pharmaceuticals from the cochlear electrode. Hydrogels are made almost entirely from water held together in a loosely crosslinked polymer matrix. Their high water content contributes to the hydrogel's high hydrophilicity, a property which has been shown to prevent cell adhesion [53-56]. Alginate hydrogel functionalized with the polypeptide

containing arginine-glycine-aspartic acid (RGD) have been shown to promote cell adhesion and proliferation on or within the hydrogel [50-52, 57].

The electrodes are dipped 4-5 times in both the alginate solution and the calcium chloride solution in order to produce coatings that are ~150 μm thick as shown in Figure 4-2 (C). Upon dehydration the thickness of the hydrogel coatings is reduced to roughly 10-20 μm, as shown in Figure 4-2 (D).

### 4.3.2. Electrochemical impedance spectroscopy

Deposition of PEDOT-PSS onto cochlear electrodes resulted in a reduction of impedance at 1 – 100,000 Hz as shown in Figure 4-3 (A). As the thickness of PEDOT-PSS increased with longer deposition times, the impedance of the electrode decreased at frequencies below 400 Hz. For the thickest coating, polymerized for 930s at 1 μA, the impedance at these low frequencies was reduced by 2 – 2.5 orders of magnitude from the original values of the Pt-Ir electrode. In general, the phase angles of the coated electrodes, which are related to the nature of charge transfer at the electrode/electrolyte interface, decreased with PEDOT-PSS coatings for all but the lowest frequencies (Figure 4-3 (B)). For the thinnest PEDOT-PSS coating, the phase angle drops below 5 degrees, indicating that charge is transferred in an almost entirely resistive method which is not time dependent. The phase angle for the thinnest PEDOT-PSS coated electrode is less than the phase angle for the bare Pt-Ir electrode at all frequencies above 100 Hz. As the thickness of PEDOT-PSS on the electrode increases, the phase angle is decreased across all frequencies, is closer to zero across a broader frequency range, and is less than the phase angle of the bare electrode across a broader frequency range.

### 4.3.3. Cylic voltammetry

Figure 4-4 (A) shows the response of a bare Pt-Ir cochlear electrode and PEDOT-PSS coated cochlear electrodes to cyclic voltammetry. The deposition of PEDOT-PSS on Pt-Ir cochlear electrodes reduces the presence of Pt-Ir's oxidation and reduction peaks. PEDOT-PSS has a small reduction peak at

approximately - 0.2 V, but overall the PEDOT-PSS coatings tend to be fairly non-reactive over the voltage range tested: + 0.8 to - 0.6 V. The charge storage capacity (CSC) is used to measure the amount of charge capable of being delivered through an electrode. The CSC is proportional to the area within the CV path and is shown in Figure 4-4 (B). As the PEDOT-PSS coatings grow increasingly thick, the current levels and total amount of charge passed through the electrode within the same voltage range and timespan increase. The CSC of the bare Pt-Ir electrode is 20.4 μC for these CV parameters. The relationship of the *CSC* (in μC) of PEDOT-PSS coated electrodes to the deposition charge, *x*, (in μC) of the coating follows the second-order polynomial: $CSC(x) = 8.34*10^{-5} x^2 + 2.31*10^{-4}x + 20.4$. For this fit the $R^2$ is 0.99. The CSC for a PEDOT-PSS coating deposited with 930 μC of charge is 93.0 μC, an increase of 356 % over the bare Pt-Ir electrode. It has been speculated that the increase in CSC and aforementioned decrease in impedance of PEDOT-coated electrodes are due to the rough and fuzzy morphology seen in Figure 4-5 which imparts more surface area for charge transfer and its ability to conduct both electrons and ions [27-29].

### 4.3.4. Biphasic stimulation and charge injection limits of PEDOT-PSS coatings

The effects of PEDOT-PSS coatings on biphasic current pulses were examined in collaboration with Aditi Ray and James Weiland at the Doheney Eye Institute at the University of Southern California. For the stimulation of nervous tissue, biphasic, cathodic-first, charge-balanced current pulses are typically used [17]. In some cases asymmetric pulses with slower recovery are used in order to inject larger quantities of charge without exceeding the water window, the voltages beyond which the hydrolysis of water occurs to form gaseous $O_2$ and $H_2$ [58]. Electrodes capable of delivering higher current and charge densities are desirable in order to deliver sufficient charge for neural activation without producing high voltages which result in bubble formation and tissue damage. Electrode materials with higher charge injection densities than traditional materials can also deliver the required amount of charge from a smaller surface

area, thus making room for increased number of electrode sites for better tonal resolution.

PEDOT-PSS coatings were applied to gold sites on multichannel, microfabricated, silicon neural probes in order to test a variety of coating thicknesses using a single device. The voltage response of electrodes to a 1.6 $mC/cm^2$ biphasic, cathodic first current pulse in PBS is shown in Figure 4-6. The total voltage excursion for the bare iridium site is 3.0 V. For the PEDOT-PSS coated site the voltage excursion is 1.6 V. The uncoated iridium electrode has a much larger voltage response than does the site coated with 480 $mC/cm^2$ of PEDOT-PSS indicating that higher charge densities can be delivered with PEDOT-coated sites before reaching harmful conditions. When the coated sites are stimulated with higher charge densities eventually they fail, usually due to mechanical delamination or cracking. The sites coated with 480 $mC/cm^2$ of PEDOT-PSS experienced failure at a charge density of 3.2 $mC/cm^2$. This value is much higher than the charge injection limit of Pt-It which is 0.30 $mC/cm^2$, and slightly lower than the value of iridium oxide ($IrO_x$), 3.9 $mC/cm^2$ [20]. However, thicker coatings of PEDOT-PSS can achieve higher charge injection densities than $IrO_x$, the current state of the art electrode surface for neural and cardiac stimulation. The charge density of PEDOT-coated electrodes at failure is given in Figure 4-7. As the thickness of the PEDOT-PSS coating increases, the charge injection limit increases. This relation can be fit with the polynomial $y = 6.62*10^{-6}x^2 - 0.00323x + 1.92$. The value of $R^2$ for this fit is 0.994. For the thickest coating tested of 1800 $mC/cm^2$, the charge injection limit is 16 $mC/cm^2$, 410 % higher than that of $IrO_x$.

### 4.3.5. Sterilization

The effects of ethylene oxide (EtO) gas sterilization on the electrochemical properties of PEDOT-PSS electrode coatings were examined. EtO is an extremely basic, flammable gas which is widely used for medical sterilization because of its low cost, low temperature, and effectiveness at neutralizing bacteria, spores and viruses. Currently, EtO is the most widely used method for

sterilizing medical devices [59]. Both PEDOT-PSS coated and bare Pt-Ir cochlear electrodes were packaged in gas permeable packaging and submitted to EtO sterilization at the University of Michigan Hospital. After sterilization, both PEDOT-PSS coated implants and bare Pt-Ir implants visually appeared identical to unsterilized implants. Electrochemical impedance spectroscopy of implants before and after sterilization revealed no change for the PEDOT-PSS coated implants. For the bare Pt-Ir electrode, the impedance increased slightly, most notably below 10 Hz. In separate animal studies using EtO sterilized PEDOT-PSS coated implants, there have been no incidence of infection (Chapter 5). According to these studies, EtO is an effective method for sterilizing PEDOT-PSS coated implants which does not affect the electrochemical properties of the electrode coating.

### 4.3.6. Electrochemical characterization of PEDOT-PSS and hydrogel coatings

Part of the strategy for improving stimulation with cochlear electrodes is to place the electrode closer to the spiral ganglion neurons, to promote the viability of these target cells and to reduce the trauma of electrode insertion. In addition to PEDOT-PSS electrode coatings which improve charge transfer between the electrode and electrolyte and can be used to deliver bioactive molecules, we have also investigated the use of soft hydrogel coatings which can buffer the metallic implant during insertion, can be loaded with pharmaceutical agents or cells, can aid in mechanical fixation, can serve as a scaffold for neuronal growth towards the electrode, and can swell inside the scala tympani in order to push the electrode away from the lateral wall (Figure 4-1 (A)) and towards the modiolus where the spiral ganglion cell bodies are found (Figure 4-1 (B)). Once implanted, the hydrogel may also serve as a reservoir for water-soluble electrolytes at the electrode's surface.

The electrochemical properties of PEDOT-PSS coated electrodes with an additional layer of RGD-functionalized Alginate hydrogel were studied using impedance spectroscopy and cyclic voltammetry. As shown in Figure 4-9 (A),

the impedance in PBS of a cochlear electrode coated with PEDOT-PSS is significantly lower than that of a bare Pt-Ir electrode at frequencies under 10 kHz. After a layer of 150 μm thick RGD-Alginate hydrogel is coated around the PEDOT-PSS, the impedance in PBS remains unchanged from that of the PEDOT-PSS coated electrode. Cyclic voltammetry of the PEDOT-PSS coated cochlear electrode and RGD-alginate + PEDOT-PSS coated electrode show nearly identical behavior as seen in Figure 4-9B. There is a slight decrease in the amplitude of the reduction peak at -0.2V. It seems as though the high water content (99 % w/v) of the hydrogel responds similarly to the PBS in which the electrode is submerged. According to our impedance spectroscopy and cyclic voltammetry studies, the electrochemical properties of a PEDOT-PSS coated cochlear electrode and a PEDOT-PSS + RGD-alginate hydrogel coated cochlear electrode are the same.

### 4.3.7. Cell adhesion to RGD-alginate

The adhesion and morphology of SH-SY5Y neuroblastoma on alginate functionalized with the RGD-adhesion polypeptide was examined in order to verify the hydrogel's use as a scaffold within the cochlea for neuronal attachment and anchoring. SY5Y were cultured on RGD-functionalized alginate hydrogel surfaces and unmodified alginate surfaces for 24 hours. The results of this assay are shown in Figure 4-10. SY5Y adhere to unmodified alginate, but are small and do not send out processes. Instead they remain ball-shaped, indicating limited focal adhesion. On the RGD-modified surface, SY5Y appear larger, due to their elongated morphology. They are triangular or star-shaped as they attach to the hydrogel surface at many points. RGD-modified alginate appears to be a useful scaffold material for neuronal attachment and elongation. RGD-modified alginate hydrogels may be very useful for reducing the distance between cochlear electrodes and target neurons, especially in the case where neuronal processes can be directed towards the electrode.

## 4.4 Conclusions

Platinum-iridium cochlear electrodes were successfully coated with the conducting polymer PEDOT-PSS and a form of alginate hydrogel functionalized with the RGD adhesion ligand. SEM revealed the nodular texture of PEDOT-PSS on the surface of the electrode which corresponds to increased surface area. Electrochemical impedance spectroscopy showed reduced electrode impedance as PEDOT coatings grew thicker, also indicating increased effective surface area. EIS also indicated that charge transfer became increasingly dominated by faradaic mechanisms, especially at frequencies above 1 kHz. Cyclic voltammetry measurements of coated electrodes showed an increase in the reversible charge injection limit of the electrode that grew with the thickness of the PEDOT film. Biphasic current stimulation confirmed the high charge density of the PEDOT-PSS coated electrodes and revealed that the conducting polymer coatings help to deliver the same amount of charge as Pt-Ir electrodes while operating in a much smaller voltage range. The highest charge injection density at failure for PEDOT-PSS coated electrodes was 16 $mC/cm^2$. The addition of an alginate hydrogel layer over the PEDOT-PSS film had little effect on the electrical properties, but provides a soft mechanical buffer between the electrode and the delicate structures of the cochlea, and provides a matrix which can encourage neuronal attachment and proliferation. The electrical properties of PEDOT-PSS coatings were shown to be unaffected by sterilization with ethylene oxide gas. These *in vitro* results are very encouraging and will next be characterized *in vivo* for their ability to efficiently stimulate cochlear neurons without producing harmful effects.

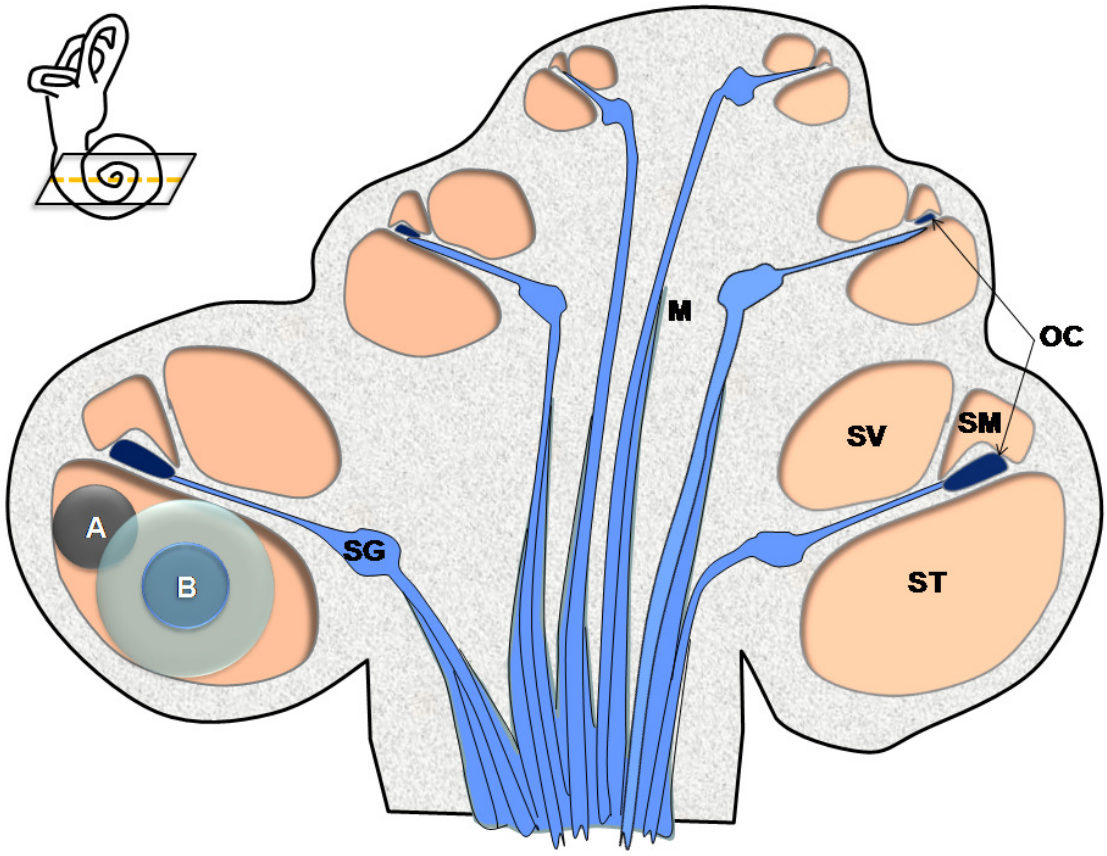


Figure 4-1. Cross-section of the cochlea showing electrode placement. (A) represents the lateral placement of stimulating electrodes placed in the scala tympani, *ST*, and (B) shows the placement of a PEDOT-PSS and hydrogel-coated electrode. *SV* is the scala vestibuli, *SM* is the scala media, *OC* is the Organ of Corti, *M* is the modiolus, and *SG* are the spiral ganglion neurons.

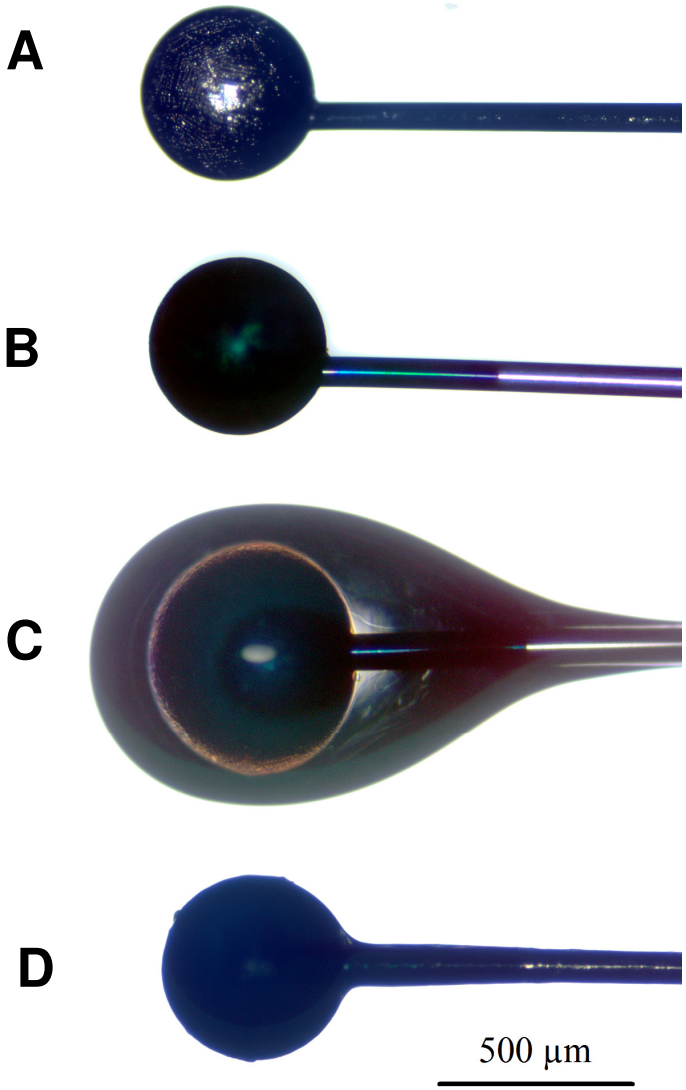


Figure 4-2. Custom-built cochlear implants made from PTFE-coated platinum-iridium (Pt-Ir) wire. (A) Bare Pt-It cochlear electrode. (B) PEDOT-PSS coated cochlear electrode. (C) Alginate hydrogel (Alg HG) and PEDOT-PSS coated cochlear electrode. (D) Dehydrated Alg HG and PEDOT-PSS-coated cochlear electrode.

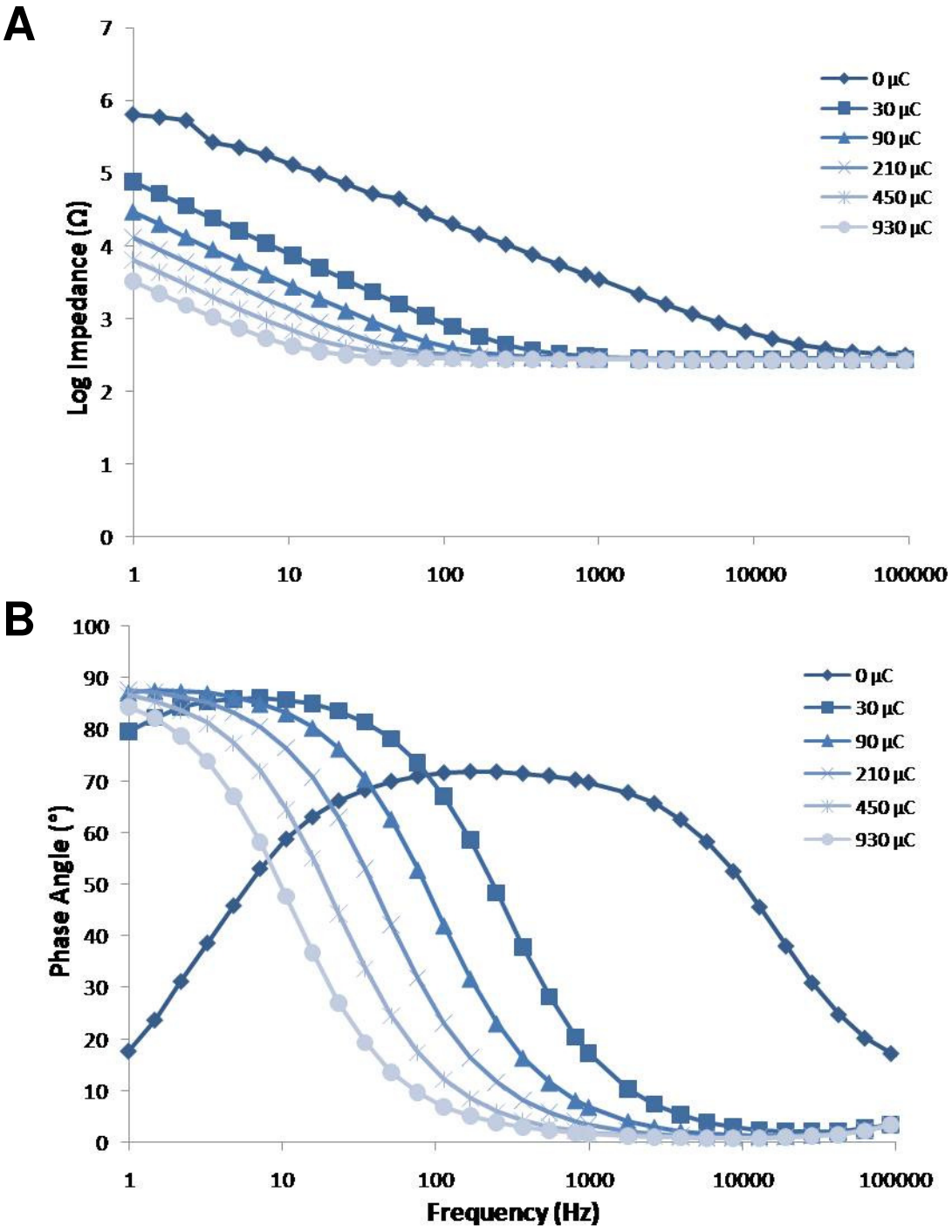


Figure 4-3 (A) Impedance spectroscopy of PEDOT-PSS coatings of increasing thickness on Pt-Ir cochlear electrodes. (B) Phase angle response to impedance spectroscopy.

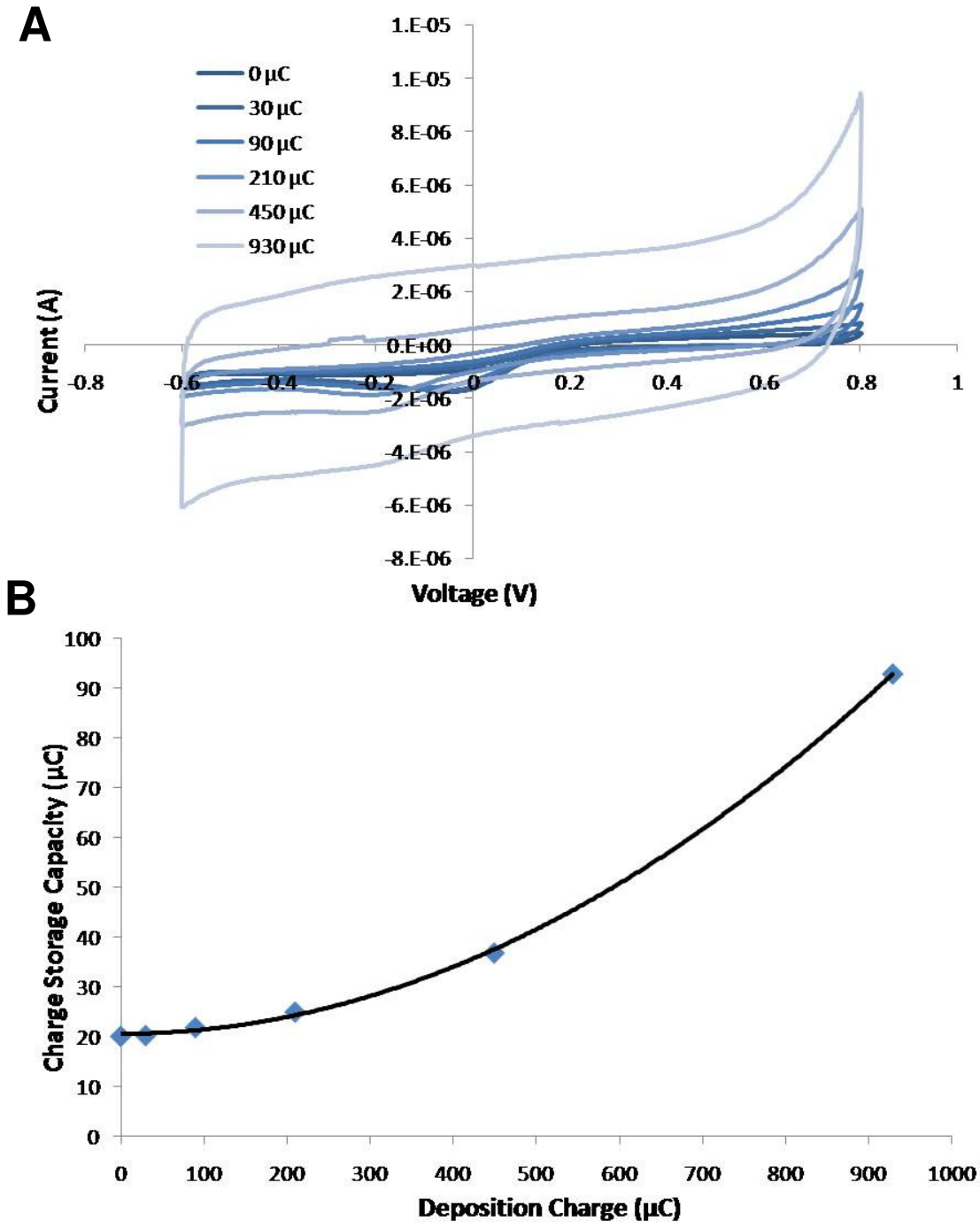


Figure 4-4. (A) Cyclic voltammetry of PEDOT-PSS coatings of increasing thickness on Pt-Ir cochlear electrodes. (B) Charge storage capacity of PEDOT-PSS coatings of increasing thickness on Pt-Ir cochlear electrodes. Polynomial fit: CSC(x) = 8.34*10-5 x2 + 2.31*10-4x + 20.4. $R^2$ = 0.99.

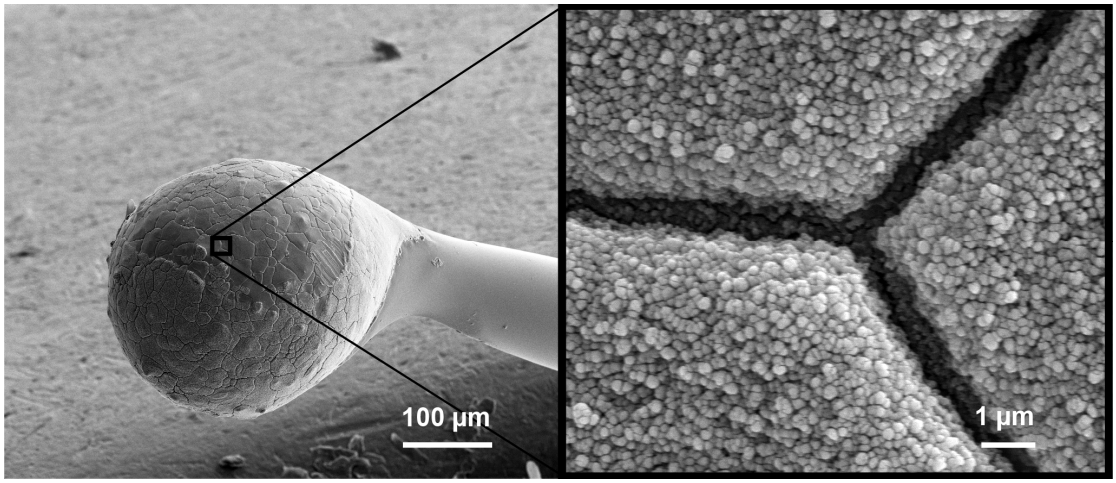


Figure 4-5. Scanning electron micrograph of PEDOT-PSS coated cochlear electrode. Inset shows the fuzzy textured surface of PEDOT-PSS.

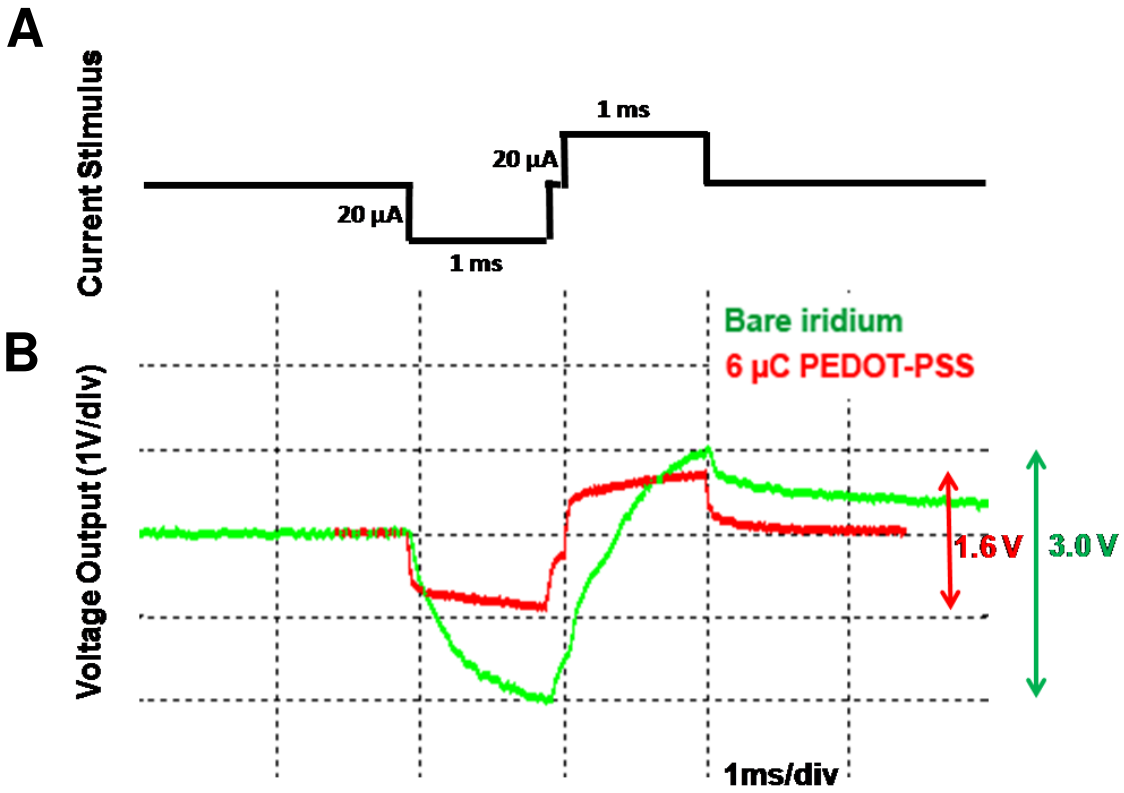


Figure 4-6. (A) A 1.6 mC/cm$^2$ current waveform sourced through PEDOT-PSS coated electrodes and bare iridium electrodes. (B) The resulting voltage response to the current waveform. The green trace is the voltage output from a bare gold site, and red is the voltage response through a PEDOT-PSS coated iridium site deposited with 480 mC/cm$^2$. (In collaboration with Aditi Ray and James Weiland, USC)

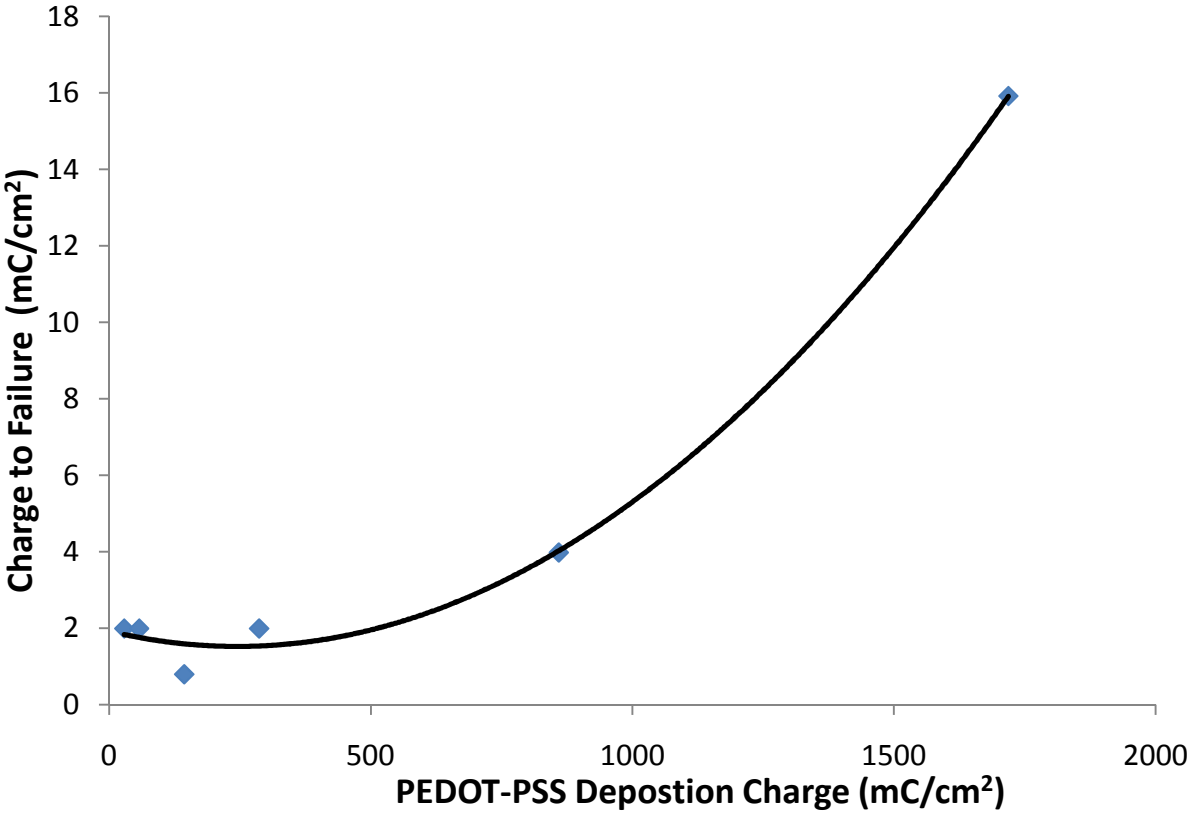


Figure 4-7. Charge injection densities at failure of PEDOT-PSS coatings on neural electrodes. (In collaboration with Aditi Ray and James Weiland, USC)

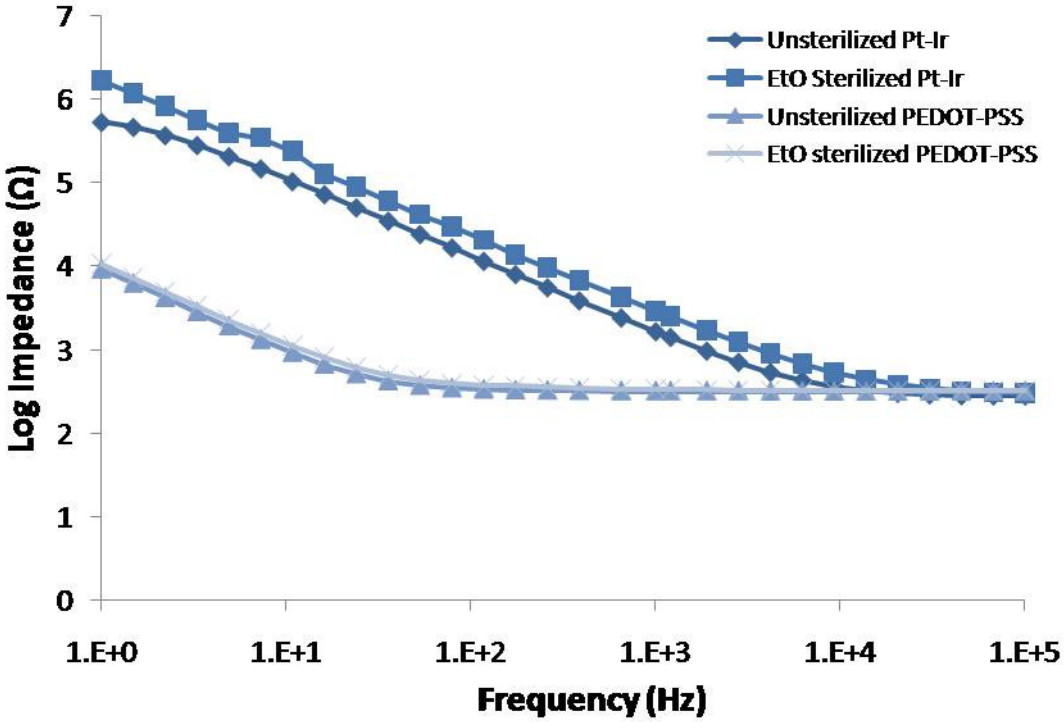


Figure 4-8. Effects of ethylene oxide (EtO) gas sterilization on electrochemical impedance of PEDOT-PSS coated cochlear electrodes.

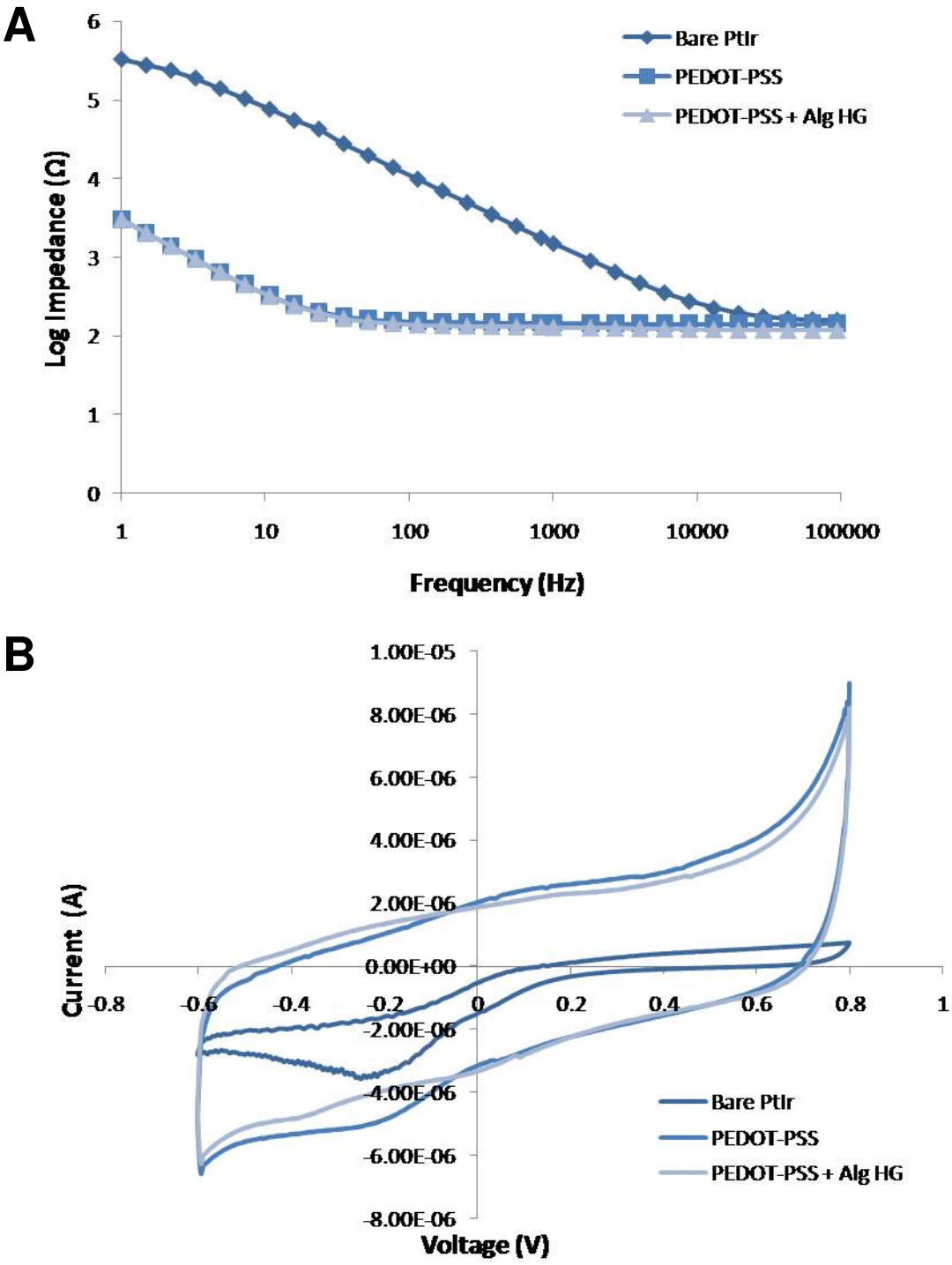


Figure 4-9. Electrochemical characterization of cochlear electrodes coated with PEDOT-PSS and alginate hydrogel. (A) Electrochemical impedance spectroscopy and (B) cyclic voltammetry of custom-built cochlear implants with conducting polymer and hydrogel coatings.
Q(+/-) for bare Pt-Ir: 3.73 mC/cm$^2$; PEDOT-PSS: 8.81 mC/cm$^2$; PEDOT-PSS + RGDAlg: 8.18 mC/cm$^2$.

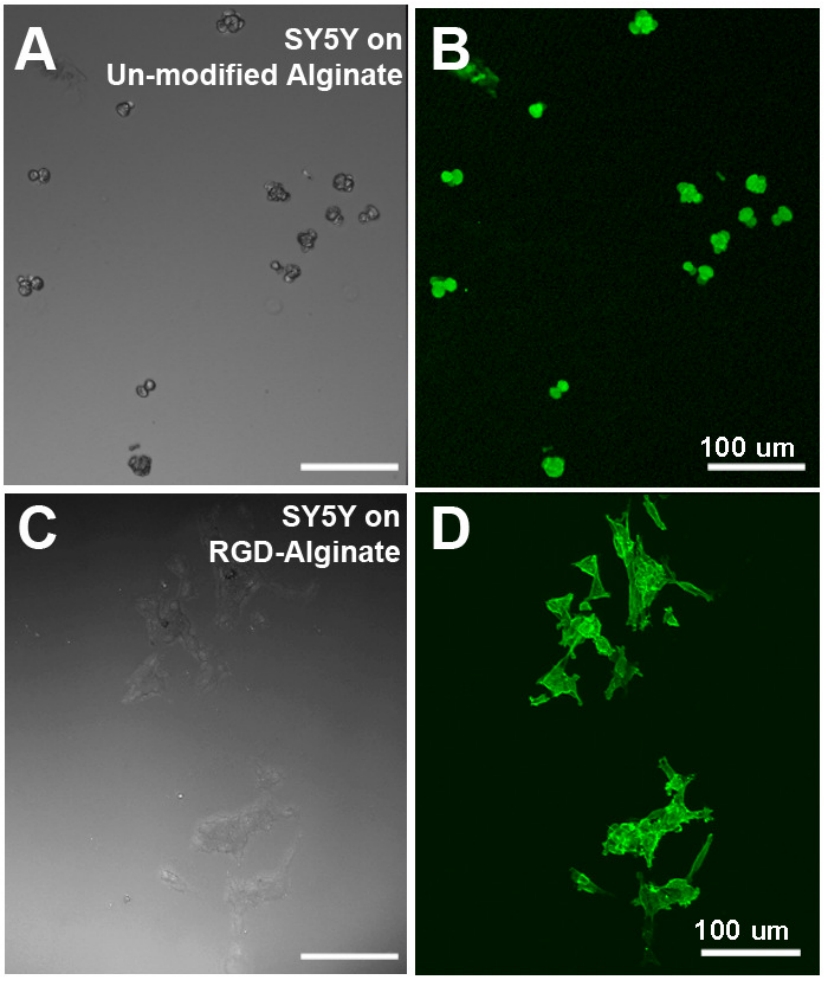


Figure 4-10. SH-SY5Y neuroblastoma cultured on alginate hydrogel. (A) Phase contrast image of SY5Y cultured directly onto unmodified alginate. (B) Fluorescent image of SY5Y stained with Phalloidin-Oregon Green which labels f-actin filaments found in the cytoskeleton. (C) Phase contrast image of SY5Y cultured on alginate hydrogel modified with covalently-bound RGD adhesion polypeptides. (D) Fluorescent image of SY5Y on RGD-modified alginate labeled with Phalloidin-Oregon Green to show the extended morphology of the cells due to the presence of biochemical adhesion cues on the hydrogel surface.

# References


1. Rauschecker, J.P. and R.V. Shannon, *Sending sound to the brain.* Science, 2002. **295**(5557): p. 1025-9.

2. Middlebrooks, J.C., J.A. Bierer, and R.L. Snyder, *Cochlear implants: the view from the brain.* Curr Opin Neurobiol, 2005. **15**(4): p. 488-93.

3. Zeng, F.G., *Trends in cochlear implants.* Trends Amplif, 2004. **8**(1): p. 1-34.

4. Wardrop, P., et al., A temporal bone study of insertion trauma and intracochlear position of cochlear implant electrodes. II: Comparison of Spiral Clarion and HiFocus II electrodes. Hear Res, 2005. **203**(1-2): p. 68-79.

5. van der Beek, F.B., et al., Clinical evaluation of the Clarion CII HiFocus 1 with and without positioner. Ear Hear, 2005. **26**(6): p. 577-92.

6. Adunka, O.F., H.C. Pillsbury, and J. Kiefer, Combining perimodiolar electrode placement and atraumatic insertion properties in cochlear implantation -- fact or fantasy? Acta Otolaryngol, 2006. **126**(5): p. 475-82.

7. Eshraghi, A.A., N.W. Yang, and T.J. Balkany, *Comparative study of cochlear damage with three perimodiolar electrode designs.* Laryngoscope, 2003. **113**(3): p. 415-9.

8. Zhang, J., et al., *A pilot study of robot-assisted cochlear implant surgery using steerable electrode arrays.* Med Image Comput Comput Assist Interv Int Conf Med Image Comput Comput Assist Interv, 2006. **9**(Pt 1): p. 33-40.

9. Middlebrooks, J.C. and R.L. Snyder, *Auditory prosthesis with a penetrating nerve array.* Jaro-Journal of the Association for Research in Otolaryngology, 2007. **8**(2): p. 258-279.

10. McDermott, H.J., *Music perception with cochlear implants: a review.* Trends Amplif, 2004. **8**(2): p. 49-82.

11. Adunka, O. and J. Kiefer, *Impact of electrode insertion depth on intracochlear trauma.* Otolaryngol Head Neck Surg, 2006. **135**(3): p. 374-82.

12. Leake, P.A., G.T. Hradek, and R.L. Snyder, Chronic electrical stimulation by a cochlear implant promotes survival of spiral ganglion neurons after neonatal deafness. J Comp Neurol, 1999. **412**(4): p. 543-62.

13. Rebscher, S.J., R.L. Snyder, and P.A. Leake, The effect of electrode configuration and duration of deafness on threshold and selectivity of responses to intracochlear electrical stimulation. J Acoust Soc Am, 2001. **109**(5 Pt 1): p. 2035-48.

14. Shepherd, R.K., et al., Cochlear pathology following reimplantation of a multichannel scala tympani electrode array in the macaque. Am J Otol, 1995. **16**(2): p. 186-99.

15. Hanekom, T., Modelling encapsulation tissue around cochlear implant electrodes. Med Biol Eng Comput, 2005. **43**(1): p. 47-55.

16. Rose, T.L. and L.S. Robblee, Electrical stimulation with Pt electrodes. VIII. Electrochemically safe charge injection limits with 0.2 ms pulses. IEEE Trans Biomed Eng, 1990. **37**(11): p. 1118-20.

17. Merrill, D.R., M. Bikson, and J.G. Jefferys, *Electrical stimulation of excitable tissue: design of efficacious and safe protocols.* J Neurosci Methods, 2005. **141**(2): p. 171-98.

18. Shepherd, R.K. and G.M. Clark, Scanning electron microscopy of platinum scala tympani electrodes following chronic stimulation in patients. Biomaterials, 1991. **12**(4): p. 417-23.

19. Patan, M., T. Shah, and M. Sahin, *Charge Injection Capacity of TiN Electrodes for an Extended Voltage Range.* Conf Proc IEEE Eng Med Biol Soc, 2006. **1**: p. 890-2.

20. Cogan, S.F., et al., In vitro comparison of the charge-injection limits of activated iridium oxide (AIROF) and platinum-iridium microelectrodes. IEEE Trans Biomed Eng, 2005. **52**(9): p. 1612-4.

21. Meyer, R.D., et al., *Electrodeposited iridium oxide for neural stimulation and recording electrodes.* IEEE Trans Neural Syst Rehabil Eng, 2001. **9**(1): p. 2-11.

22. Troyk, P.R., et al., *"Safe" charge-injection waveforms for iridium oxide (AIROF) microelectrodes.* Conf Proc IEEE Eng Med Biol Soc, 2004. **6**: p. 4141-4.

23. Gabay, T., et al., Electro-chemical and biological properties of carbon nanotube based multi-electrode arrays. Nanotechnology, 2007. **18**(3): p. -.

24. Weiland, J.D., D.J. Anderson, and M.S. Humayun, *In vitro electrical properties for iridium oxide versus titanium nitride stimulating electrodes.* IEEE Trans Biomed Eng, 2002. **49**(12 Pt 2): p. 1574-9.

25. Cui, X.Y. and D.C. Martin, Electrochemical deposition and characterization of poly(3,4-ethylenedioxythiophene) on neural microelectrode arrays. Sensors and Actuators B-Chemical, 2003. **89**(1-2): p. 92-102.

26. Cui, X.Y., et al., *In vivo studies of polypyrrole/peptide coated neural probes.* Biomaterials, 2003. **24**(5): p. 777-787.

27. Yang, J., K. Lipkin, and D.C. Martin, Electrochemical fabrication of conducting polymer poly(3,4-ethylenedioxythiophene) (PEDOT) nanofibrils on microfabricated neural prosthetic devices. J Biomater Sci Polym Ed, 2007. **18**(8): p. 1075-89.

28. Yang, J.Y., et al., Ordered surfactant-templated poly(3,4-ethylenedioxythiophene) (PEDOT) conducting polymer on microfabricated neural probes. Acta Biomaterialia, 2005. **1**(1): p. 125-136.

29. Yang, J.Y. and D.C. Martin, Impedance spectroscopy and nanoindentation of conducting poly(3,4-ethylenedioxythiophene) coatings on microfabricated neural prosthetic devices. Journal of Materials Research, 2006. **21**(5): p. 1124-1132.

30. Schmidt, C.E., et al., *Stimulation of neurite outgrowth using an electrically conducting polymer.* Proc Natl Acad Sci U S A, 1997. **94**(17): p. 8948-53.

31. Xiao, Y.H., et al., Surface modification of neural probes with conducting polymer poly(hydroxymethylated-3,4-ethylenedioxythiophene) and its biocompatibility. Applied Biochemistry and Biotechnology, 2006. **128**(2): p. 117-129.

32. Zhou, D., et al., *Actuators for the cochlear implant.* Synthetic Metals, 2003. **135**(1-3): p. 39-40.

33. Kim, D.H., et al., Effect of immobilized nerve growth factor on conductive polymers: Electrical properties and cellular response. Advanced Functional Materials, 2007. **17**(1): p. 79-86.

34. Richardson-Burns, S.M., et al., Polymerization of the conducting polymer poly(3,4-ethylenedioxythiophene) (PEDOT) around living neural cells. Biomaterials, 2007. **28**(8): p. 1539-52.

35. Richardson, R.T., et al., The effect of polypyrrole with incorporated neurotrophin-3 on the promotion of neurite outgrowth from auditory neurons. Biomaterials, 2007. **28**(3): p. 513-23.

36. Thompson, B.C., et al., Optimising the incorporation and release of a neurotrophic factor using conducting polypyrrole. J Control Release, 2006. **116**(3): p. 285-94.

37. Abidian, M.R., D.H. Kim, and D.C. Martin, *Conducting-polymer nanotubes for controlled drug release.* Advanced Materials, 2006. **18**(4): p. 405-409.

38. Ito, J., et al., *A new method for drug application to the inner ear.* ORL J Otorhinolaryngol Relat Spec, 2005. **67**(5): p. 272-5.

39. Iwai, K., et al., Cochlear protection by local insulin-like growth factor-1 application using biodegradable hydrogel. Laryngoscope, 2006. **116**(4): p. 529-33.

40. Noushi, F., et al., *Delivery of neurotrophin-3 to the cochlea using alginate beads.* Otol Neurotol, 2005. **26**(3): p. 528-33.

41. Balough, B.J., et al., Kinetics of gentamicin uptake in the inner ear of Chinchilla langier after middle-ear administration in a sustained-release vehicle. Otolaryngol Head Neck Surg, 1998. **119**(5): p. 427-31.

42. Bellamkonda, R., et al., *Hydrogel-Based 3-Dimensional Matrix for Neural Cells.* Journal of Biomedical Materials Research, 1995. **29**(5): p. 663-671.

43. Nisbet, D.R., et al., *Neural tissue engineering of the CNS using hydrogels-A review.* J Biomed Mater Res B Appl Biomater, 2007.

44. Rejali, D., et al., Cochlear implants and ex vivo BDNF gene therapy protect spiral ganglion neurons. Hear Res, 2007. **228**(1-2): p. 180-7.

45. Kim, D.H., M. Abidian, and D.C. Martin, *Conducting polymers grown in hydrogel scaffolds coated on neural prosthetic devices.* Journal of Biomedical Materials Research Part A, 2004. **71A**(4): p. 577-585.

46. Asberg, D.P. and O. Inganas, *PEDOT/PSS hydrogel networks as 3-D enzyme electrodes.* Synthetic Metals, 2003. **137**(1-3): p. 1403-1404.

47. Asberg, P. and O. Inganas, *Hydrogels of a conducting conjugated polymer as 3-D enzyme electrode.* Biosens Bioelectron, 2003. **19**(3): p. 199-207.

48. Nyberg, T., O. Inganas, and H. Jerregard, *Polymer hydrogel microelectrodes for neural communication.* Biomedical Microdevices, 2002. **4**(1): p. 43-52.

49. Alsberg, E., et al., Cell-interactive alginate hydrogels for bone tissue engineering. J Dent Res, 2001. **80**(11): p. 2025-9.

50. Comisar, W.A., et al., Engineering RGD nanopatterned hydrogels to control preosteoblast behavior: a combined computational and experimental approach. Biomaterials, 2007. **28**(30): p. 4409-17.

51. Rowley, J.A. and D.J. Mooney, *Alginate type and RGD density control myoblast phenotype.* J Biomed Mater Res, 2002. **60**(2): p. 217-23.

52. Woerly, S., et al., Spinal cord repair with PHPMA hydrogel containing RGD peptides (NeuroGel (TM)). Biomaterials, 2001. **22**(10): p. 1095-1111.

53. Bergstrom, K., et al., Effects of branching and molecular weight of surface-bound poly(ethylene oxide) on protein rejection. J Biomater Sci Polym Ed, 1994. **6**(2): p. 123-32.

54. Holmberg, M., et al., Competitive protein adsorption to polymer surfaces from human serum. J Mater Sci Mater Med, 2007.

55. Nath, N., et al., Surface engineering strategies for control of protein and cell interactions. Surface Science, 2004. **570**(1-2): p. 98-110.

56. Osterberg, E., et al., Protein-rejecting ability of surface-bound dextran in end-on and side-on configurations: comparison to PEG. J Biomed Mater Res, 1995. **29**(6): p. 741-7.

57. Musoke-Zawedde, P. and M.S. Shoichet, Anisotropic three-dimensional peptide channels guide neurite outgrowth within a biodegradable hydrogel matrix. Biomedical Materials, 2006. **1**(3): p. 162-169.

58. Cogan, S.F., et al., Potential-biased, asymmetric waveforms for charge-injection with activated iridium oxide (AIROF) neural stimulation electrodes. IEEE Trans Biomed Eng, 2006. **53**(2): p. 327-32.

59. Mendes, G.C.C., T.R.S. Brandao, and C.L.M. Silva, *Ethylene oxide sterilization of medical devices: A review.* American Journal of Infection Control, 2007. **35**(9): p. 574-581.

# Chapter 5

# Performance of BDNF-secreting, PEDOT-coated cochlear implants *in vivo*

## 5.1 Introduction

Cochlear implants are widely-used clinical auditory prosthetic devices that provide hearing sensation and function for a large patient group by electrically stimulating the spiral ganglion neurons (SGN) in the cochlea. The long-term reliability and utility of these devices depends on the stability of the neuron-electrode interface. Ideally, the interface should be permanent and provide highly localized electrical interactions. In order to avoid broad, non-specific auditory activation, the electrodes should be small and in close proximity to functional SGN that correspond to distinct auditory frequencies. Unfortunately, sensory hair cell loss, the most common cellular cause of sensorineural hearing loss, often leads to the retraction of neuronal processes and degeneration of auditory nervous structures [1-5]. Additionally, surgical implantation of the electrode array into the cochlea can damage many cochlear structures. This trauma has been associated with the later development of fibrous and bony tissue growth around the electrode, thus limiting current flow between the electrode and SGN [6, 7].

Many techniques have been explored to promote the health and function of tissue necessary for cochlear implant function. Specifically, methods to reduce surgical trauma and to promote the survival of SGN and support cells in the inner ear are of interest. Pharmacological strategies have employed many compounds including neurotrophic factors, antioxidants, anti-inflammatory steroids, antibiotics, cytokine inhibitors, neurotransmitters and anti-apoptotic agents for preserving spiral ganglion cells [8, 9]. Various methods including microfluidic delivery using osmotic pumps with microcatheters [10, 11], iontopheresis [12, 13], degradable particles and gels [14-17], transtympanic injections [18-20], the Silverstein microwick [21, 22], and drug-soaked materials placed in the middle ear [23, 24] can provide localized drug delivery of these compounds into the inner ear. Cell delivery [25-28] and gene therapy [29-31] have also been explored as methods to increase the survival and function of SGN in the inner ear. Electrical stimulation of auditory neurons has also been shown to promote their viability [32-34] although it has also been shown to promote tissue inflammation in the inner ear [35].

Hydrogels are one of the materials that have studied for their ability to provide sustained drug delivery to the inner ear. In previous studies, BDNF-soaked biodegradable collagen hydrogels placed in the middle ear over the round window increased perilymph BDNF levels from 3 pg/µl to 884 pg/µl after one week. Alginate, a type of hydrogel derived from algae, has also been used to deliver neurotrophins to the inner ear. Alginate beads loaded with NT-3 were shown to be biocompatible and able to promote the survival of SGN in deafened guinea pigs when placed over the round window membrane [23]. Hydrogels have also been used as biomedical coatings to control tissue adhesion and fixation elsewhere in the body. Due to their high water content, hydrogels naturally resist non-specific protein adsorption. They can be functionalized with extracellular matrix components in order to promote stable tissue fixation while minimizing fibrous encapsulation around neural implants [36].

In the previous chapter, we presented coatings for cochlear electrodes that improve charge transfer and integration at the neuron-electrode interface

(Figure 5-1). These coatings, composed of the conducting polymer poly(3,4-ethylene dioxythiophene) (PEDOT) and a soft hydrogel layer functionalized with the RGD adhesion peptide sequence, are able to deliver higher current densities at the same voltage as uncoated platinum-iridium electrodes. The PEDOT layer increases the surface area of the electrode to facilitate charge transfer, while the hydrogel layer provides a soft exterior to reduce insertion trauma and provides a scaffold for conducting fibers extending from the electrode as well as for neuronal processes growing towards the implant. The hydrogel layer also provides a spongy matrix for loading with biological factors, such as BDNF, to improve SGN survival near the electrode site. Once implanted, the hydrogel layer re-swells and provides a layer of electrolyte surrounding the electrode which is required for rapid charge transfer [37], particularly when the electrode is encapsulated in fibrous or bony tissue.

Electrochemical impedance spectroscopy (EIS) of implanted neural electrodes has been used as a method to evaluate the tissue response and degree of encapsulation in real-time in order to adjust cochlear electrode parameters or to implement pharmacological treatment. In contrast, histological evaluation of tissue can only be performed postmortem to evaluate the tissue reaction to implanted electrodes. EIS provides a method for monitoring the tissue reaction as it occurs, which could enable new treatment modalities to counteract fibrous encapsulation. By probing the impedance of the tissue-electrode complex across a wide range of frequencies, information can be gained about the tissue composition near the electrode. Duan et al. used EIS to monitor the chronic tissue response to platinum cochlear electrodes. The study correlated increases in impedance with poor conduction at the electrode-tissue interface and diffusional blocking of charge carriers, as well as an elevated contact resistance possibly due to a reduction in perilymph fluid near the electrode and an increase in adsorbed tissue on the electrode [37]. Other studies employing EIS to monitor the local environment surrounding implanted electrodes found a correlation between the extent of tissue reaction and increased impedance at 1 kHz and above [38].

In this study, we investigated the ability of coatings made of PEDOT, hydrogel, and BDNF to modify the tissue-electrode interface of cochlear implants in an animal model of hearing loss. The release of BDNF was measured *in vivo* by sampling perilymph from guinea pigs that received coated implants. We then used impedance spectroscopy and equivalent circuit models of the electrode-tissue interface to determine if changes in the interface composition and conductivity could be produced with the novel cochlear electrode coatings over the course of 6 months.

## 5.2 Experimental

### 5.2.1 Cochlear implant electrode fabrication

For the BDNF release study and chronic impedance measurements, monopolar platinum-iridium (Pt-Ir, 90 %/10 %) ball electrodes were used. Cochlear electrodes were manufactured using polytetrafluoroethylene (PTFE)-coated 75 µm diameter platinum-iridium alloy (Pt-Ir; 90 % / 10 %) wire (A-M Systems). The wire was melted using a propane /oxygen flame to produce a ball electrode of nominal diameter 400 µm. A portion of Pt-Ir wire under the ball exposed by the flame was re-insulated with Sylgard 184 silicone (Dow Corning) up to the base of the ball electrode. The distal end of the electrode was connected to a dip-socket connector which was mounted on the skull during surgery.

### 5.2.2 Cochlear implant coating and BDNF loading

Cochlear electrodes were first electrochemically coated with poly(3,4-ethylene dioxythiophene)-poly(styrenesulfonate) (PEDOT-PSS) and subsequently coated in RGD-functionalized alginate hydrogel which covered the electrode and 2-3 mm of the wire below. PEDOT-PSS was deposited from a solution containing 0.1 % (w/v) ethylene dioxythiophene (EDOT; H.C. Starck) and 0.2 % (w/v) poly(styrenesulfonate sodium salt) (PSS; Acros Organics) in

deoinized water. The cochlear electrode was immersed into the monomer solution and served as the working electrode (anode). A 6 x 6 mm platinum foil served as the counter electrode (cathode). Galvanostatic charges of 600 µC were applied using an AutoLab PGStat12 Potentiostat/Galvanostat (EcoChemie). In order to equalize any effects of the electrical charge on the metal substrate, bare implants were exposed to the same voltages as coated electrodes while submerged in deionized water.

Hydrogel coating of the cochlear electrodes was performed using an alginate hydrogel covalently modified with the peptide sequence GGGG**RGD**Y that contains the adhesion ligand arginine-glycine-aspartic acid (RGD). The hydrogel was generously provided by Dr. David Mooney, Harvard University and its preparation has been described elsewhere [39-41]. The cochlear electrodes were dip-coated in a solution of 1 % (w/v) RGD-alginate in PBS and then dipped into a solution of 2 % (w/v) calcium chloride ($CaCl_2$; Sigma-Aldrich) in PBS. The dipping was repeated to achieve a uniform coating 150 - 200 µm thick (Figure 1B).

For BDNF loading, implants were soaked in BDNF prior to surgical implantation. The sterilized implants were immersed in 1 µl of PBS solution containing 500 ng of BDNF (Chemicon) for 15 minutes and then dried for 15 minutes before insertion into the cochlea.

### 5.2.3 Animal subjects

Two groups of adult pigmented guinea pigs were used in these studies. For impedance modeling of the neural interface with coated cochlear implants, 4 animals received functional monopolar cochlear implants and were monitored for 6 months. For assessing BDNF release from cochlear implant coatings *in vivo*, 12 animals were implanted with monopolar cochlear implants that were not electrically functional. These animals were sacrificed at one or two weeks post-implantation and their perilymph collected in order to measure BDNF concentration.

### 5.2.4 Surgical procedures

Guinea pigs were systematically deafened via a subcutaneous injection of kanamycin (400mg/kg) followed 2 hours later by an intravenous injection of ethacrynic acid (40mg/kg). Deafness was confirmed using an auditory brainstem response to pure tone sinusoids.

For implantation of cochlear electrodes, the animals were anesthetized with a mix of ketamine (40 mg/kg) and xylazine (10 mg/kg) (IM). Core temperature was maintained by a heating pad and measured by an anal thermometer. Lidocaine was used as a local anesthetic. An incision was made in an arc caudal to the pinna of the ear to be implanted and the muscle and underlying tissue was then retracted to expose the bulla. A hole was made in the bulla using the tip of a scalpel blade, and a small cochleostomy was drilled below the lip of the round window to provide access to the scala tympani. The cochlear implant was then inserted approximately 2 -3 mm into the scala tympani. The implant was held in place using a suture threaded through a small hole in the bulla and covered with carboxylate cement (Durelon). The implant was also held in place by a stainless steel restraining bolt that was affixed over bregma using stainless steel screws threaded through small holes drilled and tapped in the skull. The skin flap was then sutured in two layers. The animals were given yohimbe (1 mg/kg), and allowed to recover for four days prior to electrical stimulation.

Impedance spectroscopy of the cochlear electrode-neuron interface was performed on animals that were anesthetized as stated above. The intracochlear electrode was connected to the working electrode of the potentiostat/galvanostat with frequency response analyzer (AutoLab PGStat12, Eco Chemie). The stainless steel restraining bolt was connected to the counter/reference electrode of the potentiostat. After measurements, the animals recovered as stated above.

### 5.2.5 BDNF measurements

Pigmented guinea pigs were anesthetized with 40 mg/kg ketamine, 10 mg/kg xylazine (i.p.) and decapitated. Both temporal bones were removed and

opened to expose the cochlea. For each cochlea, the following procedure was performed: an opening was made into the scala tympani of the basal turn (the opening sometimes extended into scala media); microcapillary tubes (1 µl Drummond Microcaps) were used to extract 2 µl of fluid from the opening in the base (in one case, only 1 µl of fluid was collected) and which was transferred to a gasket-sealed, screw-cap microcentrifuge tube for storage. Due to extension of the basal turn opening into scala media and breeching of the bony roof of scala tympani by the microcapillary tubes, the fluid collected was probably composed of both perilymph and endolymph. The fluid samples were stored at -80° C until further use. BDNF concentration was quantified using an enzyme-linked immuno-sorbent assay (ELISA) kit (Chemicon International) read with a SpectraMax 340 plate reader. For ELISA, the samples were diluted with 100 µl standard/sample diluent, except for the 1ul sample, which was diluted with 101 µl.

### 5.2.6 Impedance measurements

Electrochemical impedance spectroscopy (EIS) was performed on cochlear electrodes in saline after coatings and prior to implantation. A three electrode setup was used in which the cochlear electrode served as the working electrode, a 6 mm x 6 mm platinum foil as the counter electrode, and a saturated calomel electrode (SCE) as the reference electrode. The electrolyte used was room temperature phosphate-buffered saline (HyClone Media, pH = 7.4). The impedance was measured at frequencies from 1 – 1,000,000 Hz upon application of a 5 mV root mean square (RMS) sine wave between the working and counter electrode using a potentiostat with frequency response analysis (FRA) module (AutoLab PGStat 12, Eco Chemie).

Once implanted, EIS was performed using a two electrode setup and the potentiostat with FRA module. The cochlear electrode was connected to the working electrode, and the stainless steel restraining bolt was connected to the counter and reference electrodes. The impedance was measured at 35 frequencies from 10-10,000 Hz upon application of a 2.5 µA RMS sine wave. In

preliminary *in vitro* studies, the impedance of cochlear electrodes was the same using with both 2.5 μA and 5 mV sine waves; constant current measurements were also found to be safer than constant voltage measurements (data not shown).

### 5.2.7 Microscopy

Samples were imaged optically using a Nikon OptiPhot POL microscope with SPOT RT digital camera with transmitted and/or reflected light. Fluorescent and phase contrast images were captured using an Olympus BX-51 upright microscope with Olympus CCD camera and Olympus imaging software (University of Michigan Morphology and Imaging Analysis Core Laboratory). Scanning electron microscopy (SEM) was performed using a FEI Nova 200 Nanolab Dualbeam FIB (University of Michigan Electron Microbeam Analysis Laboratory (EMAL)). Samples were first sputtered with approximately 1 nm of gold prior to SEM imaging.

### 5.2.8 Equivalent circuit modeling

Equivalent circuit modeling of electrodes in both PBS and implanted in guinea pig cochlea was performed to monitor the tissue interface over time for the coated and uncoated electrodes. The electrochemical impedance data for frequencies between 10 and 100,000 Hz was introduced into the program ZSimpWin. The fits were evaluated using a least-squares regression which yields a $\chi^2$ value as an indication of the deviation between measured data and the equivalent circuit model fit. Models with $\chi^2$ values of under 0.002 were considered to be good fits.

The equivalent circuit models used in this study for platinum-iridium electrodes and PEDOT-, hydrogel-, BDNF-coated Pt-Ir electrodes are derived from previous studies of cochlear electrodes and coated neural electrodes. In general, the electrode-electrolyte interface is separated into a component representing the interfacial impedance and the impedance of the electrolyte, sometimes referred to as the solution resistance. In the circuits used by Duan et

al. [37] to model the electrode-electrolyte interface of implanted intracochlear electrodes (Figure 5-2 (A-C)), the electrolyte impedance can be represented by a simple resistor, R, or by diffusive impedance, $Z_D$, which denotes ionic flow at the surface through a finite medium. The interface impedance can be represented by a constant phase element (CPE) which denotes dissipative double-layer capacitance that is typically present with rough surfaces, or by a CPE in parallel with the adsorption resistance, $R_{AD}$, as material adsorbs to the electrode surface.

Models for neural electrodes with conducting polymer coatings take a similar form. Cui et al. [42] modeled the electrical characteristics of PEDOT-coated neural electrodes using a model composed of the solution resistance, $R_S$, in series with a diffusive impedance element, $Z_D$, and the bulk capacitance, $C_d$ (Figure 5-2 (D)). Richardson-Burns et al. [43] found that PEDOT-coated neural electrodes could be modeled with a modified Randles' Circuit which includes a CPE in series with the interface resistance (Figure 5-2 (E)). More elaborate circuits can be used which provide more physiochemical relevance to the model. Abidian and Martin [44] implemented such a model to describe the properties of conducting polymer nanotubes (Figure 5-2 (F)).

Our model consists of the solution resistance, Rs, in series with a diffusional impedance element, $Z_D$, and then by the interface impedance, a resistor, $R_I$, and constant phase element, $Q_I$, in parallel (Figure 5-2 (G)).

## 5.3 Results and discussion

### 5.3.1 BDNF delivery *in vivo*

In order to promote the survival and growth of spiral ganglion processes towards the cochlear electrode, BDNF was incorporated into implants with PEDOT and hydrogel coatings (Figure 5-1) and released by passive diffusion once implanted within the cochlea. Release from hydrogels typically occurred quickly due to the porosity and high-water content of the hydrogel matrix.

Test subjects each received a coated cochlear implant in their left ear. Half of the implants were loaded with BDNF prior to implantation and half were not. Subjects that received coated cochlear implants with no BDNF had baseline perilymph BDNF concentrations of 1.7 ng/ml in both ears after 1 week as shown in Figure 5-3. When the implants were loaded with BDNF, the BDNF concentration of perilymph at 1 week was 30.3 ng/ml for the ear that received the implant. The concentration of BDNF in the contralateral ear was also elevated to 3.8 ng/ml. This is likely due to the connection between the scala tympani and the cerebrospinal fluid (CSF) of the subarachnoid space which provides a fluid path between both ears. Two weeks after implantation, the baseline levels of BDNF for the non-loaded BDNF subjects were slightly higher, 2.6 ng/ml in the implanted ear, and 2.4 ng/ml in the unimplanted ear. For subjects that received BDNF-loaded implants, concentrations were increased to 13.9 ng/ml in the implanted ear and 1.6 ng/ml in the unimplanted ear. The decreased BDNF concentrations seen from week one to week two suggests that the majority of growth factor release from the hydrogel occurs within the first week.

Perilymph sampling can be problematic due to the possibility of introducing CSF into the perilymph during collection. Contamination with CSF leads to inaccurate representation of cochlear BDNF levels due to mixing. Thus, care was taken to remove only 2 µl of fluid from each guinea pig cochlea. Our method using glass microcapillary tubes provides a reliable way to collect a specific volume of perilymph and reduces the risk of CSF contamination.

### 5.3.2 Evaluation of coatings on explanted electrodes

As part of another study investigating the use of PEDOT-PSS coatings for cochlear electrodes, animals were sacrificed after 1 month and the cochlear electrodes were removed. The PEDOT-PSS layers of the coated cochlear implant were intact around the entire ball. There were not any visible cells or tissue attached to the electrode, although there was a film of biological residue which coated the surface of the electrode, as shown in Figure 5-4 (B). It is possible that this is protein adsorption from the perilymph fluids. The biological

residue on the electrode surface may restrict current flow from the coated electrodes which have a fuzzy surface with extremely large effective surface area prior to implantation, as shown in Figure 5-4 (A). There was no fibrous tissue observed in the scala tympani when the electrodes were removed (data not shown).

### 5.3.3 Cochlear electrode impedance *in vivo*

Impedance spectroscopy was performed on both coated and uncoated cochlear electrodes in PBS prior to surgical implantation. The average impedance at 3 different frequencies, 10.7 Hz, 1 kHz, and 93.5 kHz, of the coated electrodes was significantly lower than the uncoated electrodes when compared statistically (1-tail, T-test, p=0.05), as shown in Figure 5-5. At 10.7 Hz, the average impedance and standard deviation of uncoated platinum-iridium electrodes was 35000 ± 1700 Ω, while electrodes with PEDOT and hydrogel coatings had an impedance of 340 ± 30 Ω, a decrease of 99 %. At 1 kHz, the coated electrodes also had much lower impedance than the bare electrodes, 130 ± 1.7 Ω versus 660 ± 52 Ω. At 93.5 kHz, the coated electrodes had an impedance of 120 ± 0.3 Ω while the uncoated electrodes had an impedance of 160 ± 1.3 Ω.

When implanted into the perilymph-filled scala tympani of the cochlea, the impedance of all electrodes increased (Figure 5-6). The average 1 kHz impedance for uncoated electrodes in PBS prior to implantation was 660 Ω. Immediately after implantation the average 1 kHz impedance was 3800 Ω, an increase of 3200 Ω. The coated implants had an average 1 kHz impedance of 120 Ω before implantation. After implantation, their average impedance was 2100 Ω, an increase of 1980 Ω. The immediate increase in impedance for both bare and coated implants is due primarily to changes in the electrolyte surrounding the electrode, changes in the ground electrode used, and the resistance of the path between the working and counter electrodes; over time the tissue reaction can also lead to increased impedance. When tested in PBS *in vitro*, the electrode is immersed in an aqueous solution with abundant ionic

charge carriers. The path to the counter electrode, a large piece of platinum, is fairly direct. *In vivo*, the electrode is placed in the scala tympani, a fluid filled chamber, but in order for current to reach the counter electrode, a stainless steel screw, it must pass through dense and poorly conductive tissue including bone, muscle, and fat.

As time since implantation increased, the impedance of both coated and bare implants increased. The implants were scheduled to last for six months, but the impedance of the uncoated cochlear implant in animal A reached such high levels that useful information could no longer be measured. This animal was thus sacrificed after 81 days; the final 1 kHz impedance was 2.01 MΩ. The other bare cochlear implant lasted for the entire duration of the study and had a final 1 kHz impedance of 200 kΩ, an increase of over 68 times the initial post-implantation impedance of 2900 Ω.

After six months, the final average 1 kHz impedance for coated implants was 5870 Ω, an increase of almost 4 times the average original post-implantation impedance of 1180 Ω. Compared with uncoated electrodes the presence of the coating composed of PEDOT, hydrogel, and BDNF leads to lower impedance *in vitro* and *in vivo* throughout the lifetime of the implant. The overall increase during implantation of coated electrodes is less in terms of both magnitude and fraction of original impedance. In addition, both of the uncoated implants experienced large increases in impedance during the first 3 months, as seen in Figures 5-6 and 5-7. Figure 5-6 shows the 10 Hz, 1 kHz, and 100 kHz impedances of the four implants over the course of time, while Figure 5-7, a Bode plot, shows the increase in impedance across the entire measured frequency spectrum at selected times after implantation. The impedances of coated implants tended to increase more during the first month and remain fairly stable afterwards.

### 5.3.4 Cochlear electrode impedance spectroscopy *in vivo*

Impedance spectroscopy across a range of frequencies provides useful information about charge mobility and the tissue reaction to implanted cochlear

electrodes. It has been noted that the absence of mobile charge carriers and the presence of tissue encapsulation can produce a distorted or incomplete arc in the high frequency data of neural electrodes [37, 38] when the impedance data is viewed in a Nyquist plot. The Nyquist plots show the real (Z') and imaginary (-Z") components of impedance in the complex plane. In Figure 5-8 (A), we see such shifts in the impedance of uncoated electrodes in animals A and B. It is particularly noticeable in the final impedance of animal B, at day 171 after implantation. The close-up of the high frequency data from animals A and B, shown in Figure 5-8 (B), also shows an increase in the real impedance component (Z') of both electrodes, likely due to the increased resistance of the tissue compared to the studies in PBS. The failure of the uncoated electrode in animal A produced a much larger arc, which can be seen in Figure 5-11 (C), which suggests that the failure was due not only to fibrous encapsulation. Preliminary histological evaluation suggests that the electrode and connectors are still intact.

In Figure 5-9 (A), we see that the overall magnitude of the impedance of coated cochlear electrodes was much smaller than their uncoated counterparts. The electrodes implanted in animals C and D also showed similar shifts in high frequency data which have been correlated with fibrous tissue encapsulation near the electrode. As seen in the close-up in Figure 5-9 (B), the shifts occurred over a larger frequency range than for the uncoated electrodes, indicating that charge transfer was still able to occur through faradaic mechanisms at the surface rather than by capacitive methods. This could be related to the large increase in electrode surface area produced by coating the electrode with PEDOT.

Figure 5-10 shows the electrode impedances in PBS prior to implantation and within the first week after implantation. The initial impedance of the uncoated electrodes had a much larger variation with frequency than for coated electrodes, which were clustered near the origin. For the uncoated electrodes in PBS, only frequencies above 77 Hz could fit onto the graph at this scale. During the first week, the variation of impedance with frequency for the uncoated

electrode increased. For PEDOT-hydrogel-BDNF-coated electrodes, the spread of electrode impedance across all frequencies measured also increased with time, although their overall impedance is much lower than for uncoated electrodes. The impedance shifts seen during the first week for both coated and uncoated electrodes showed increased real impedance (resistance) and increased variation between frequencies, indicating that time-dependant charge transfer mechanisms were also affected.

### 5.3.5 Equivalent circuit modeling of interface

The impedance data for both coated and uncoated electrodes were fit using the equivalent circuit model $R_S T_S(R_{AD}Q_I)$. The fit parameters are provided in Table 1. $R_s$ is used to denote the solution or electrolyte resistance, of either PBS or of perilymph, and $T_s$ is the diffusive impedance which occurs when there is a diffusion limited availability of ionic carriers near the surface, especially *in vivo*. $T_s$ represents a transmission line model which is used for impedance due to diffusive processes. The parallel circuit of $R_{AD}Q_I$ relates to charge transfer at the electrode-electrolyte interface. At this interface, charge can be moved through material adsorbed onto the electrode, modeled by $R_{AD}$, the adsorption resistance, or by the double-layer impedance, $Q_I$.

The experimental data and fits for the uncoated electrode in animal A are shown in Figures 5-11 (A). The model was able to fit both *in vitro* and *in vivo* well (Figure 5-11 (B)), although when the electrode ultimately fails, the model provided a poor fit (Figure 5-11 (C)). From past experience, our potentiostat and frequency response module is known to provide poor data above 1 MΩ, thus it is possible that the impedance data for animal A at day 81 was the result not only of biological factors, but also due to the limits of the electrical equipment.

Experimental data and fits for the coated electrode in animal C are shown in Figure 5-12. The solution resistance, $R_S$, for coated electrodes in PBS was lower than for the uncoated electrodes. $R_S$ was calculated using the surface area of the electrode. In this case, the same surface area was used for both coated and uncoated electrodes, using their measured diameters. However,

from electron microscopy and previous studies it is known that the effective surface area is much larger for PEDOT-coated electrodes and depends on the frequency of the measurement [42]. The solution resistance in PBS is independent of frequency and thus corresponds to extremely low frequency conditions. It is also independent of the resistance of the electrode, but depends on the area of the electrode exposed to the electrolyte and the distance between electrodes. In order for the solution resistance of the PEDOT-hydrogel coated electrodes to match the solution resistance of the uncoated platinum-iridium cochlear electrodes, the effective surface area of the coated electrode must be scaled by roughly 1.5 times, yielding an estimated 50 % increased area of interaction between PEDOT-hydrogel coated electrodes in PBS at low frequencies. With the increase in effective surface area from these PEDOT-coatings, it may be possible to reduce the overall electrode size by at least 35 % while still providing enough current for stimulation and without reaching harmful interfacial voltages. For increasingly higher frequency signals, the electrode size could be further reduced, as impedance decreases more at higher frequencies (Figure 5-7). The parameters for fitting the PEDOT-hydrogel-BDNF-coated electrodes have smaller deviations throughout the implantation process, indicating that portions of the electrode-electrolyte interface are more stable when compared to uncoated electrodes (Table 5-1). The fit parameters have the largest deviations for the uncoated electrodes, particularly for their final impedance values, suggesting that the model may not fully correspond to the encapsulated state or that other modes of failure may also be present.

## 5.4 Conclusions and future work

The improvements in electrical properties seen for PEDOT-, hydrogel-, BDNF- coated electrodes *in vitro* were confirmed *in vivo*. The impedance of coated electrodes was significantly lower than for uncoated electrodes across a large frequency range over the course of 6 months. Animals that received

uncoated cochlear implants had large increases in impedance over time, possibly due to the tissue reaction around the electrodes. One of the uncoated electrodes had such high impedance after 3 months that useful electrical information could no longer be collected. In contrast, animals with coated electrodes had small increases in impedance over the first month and then remained fairly stable afterwards. Their impedance was also nearly independent of frequency. Postmortem evaluation of the coated electrodes revealed that the coatings were intact, but covered with thin layers of biological residue.

The ability of these coated electrodes to release significant quantities of BDNF *in vivo* was confirmed. Perilymph levels of BDNF were increased from 1.7 ng/ml to 30.3 ng/ml after 1 week. Histological evaluation of the cochlear tissue for SGN density is underway and will provide further information about the effectiveness of BDNF release. In the future, correlation with electrophysiological measurements can ultimately verify the utility of neurotrophin delivery from cochlear electrodes.

Electrochemical impedance spectroscopy of implanted electrodes provides useful information about the tissue-electrode interface over time. This information is useful for optimizing cochlear implant electrode stimulation parameters as well as when designing strategies to reduce or circumvent fibrous encapsulation. Using conducting polymer coatings, it is possible to deliver pharmacological compounds on demand. These could be used to delivery enzymes to degrade fibrous tissue when its presence is revealed with EIS. Furthermore, equivalent circuit modeling suggests that the size of cochlear electrodes can be reduced by 35 % by coating the metal electrodes with conducting polymer-based coatings. These coatings provide increased current density at a given voltage and can thus be used to improve the tonal resolution of cochlear implants while preserving their safety.

Further studies will use multichannel electrodes with both coated and uncoated sites in the same animal. This should improve the direct comparison of the two. Additionally, application of electrical stimulation through the coated

electrodes while monitoring EIS will provide more clinically relevant results for these novel electrode coatings.

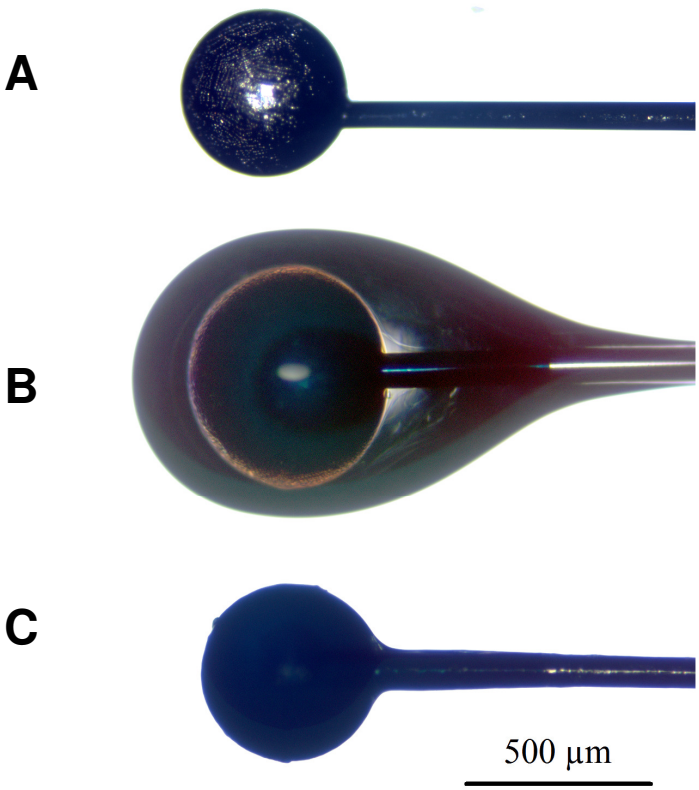


Figure 5-1. Custom-built monopolar cochlear implants made from PTFE-coated platinum-iridium (Pt-Ir) wire. (A) Bare Pt-It cochlear electrode. (B) Alginate hydrogel (Alg HG) and PEDOT-PSS coated cochlear electrode. (C) Dehydrated Alg HG and PEDOT-PSS-coated cochlear electrode that is first sterilized and then submerged into 500 ng of BDNF prior to implantation.

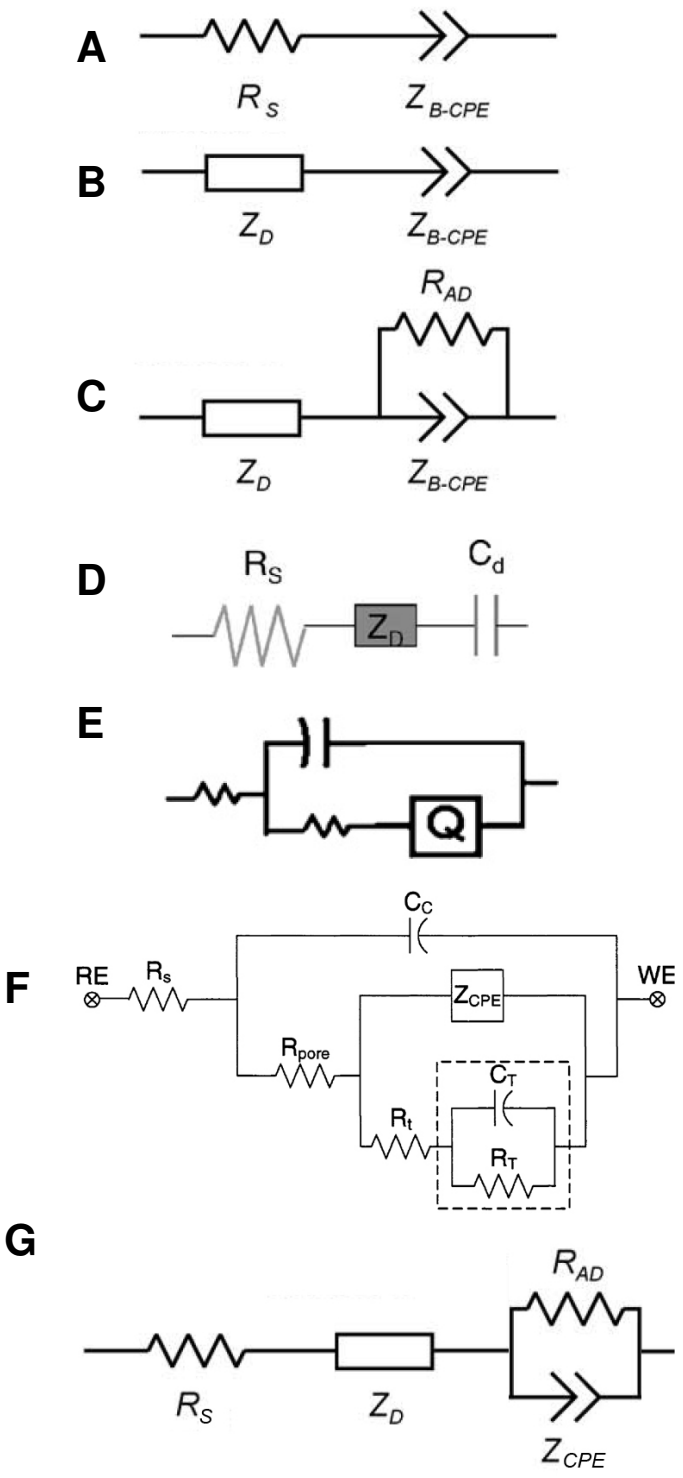


Figure 5-2. Equivalent circuit models for tissue-electrode interface. Models A-C are used to model Pt-Ir intracochlear electrodes *in vivo* [37], both models D and E have been used to model PEDOT-PSS on metallic electrodes in saline [42, 43], Model F is for PEDOT nanotubes [44], Model G is the model used in this chapter for coated and uncoated cochlear electrodes *in vivo*.

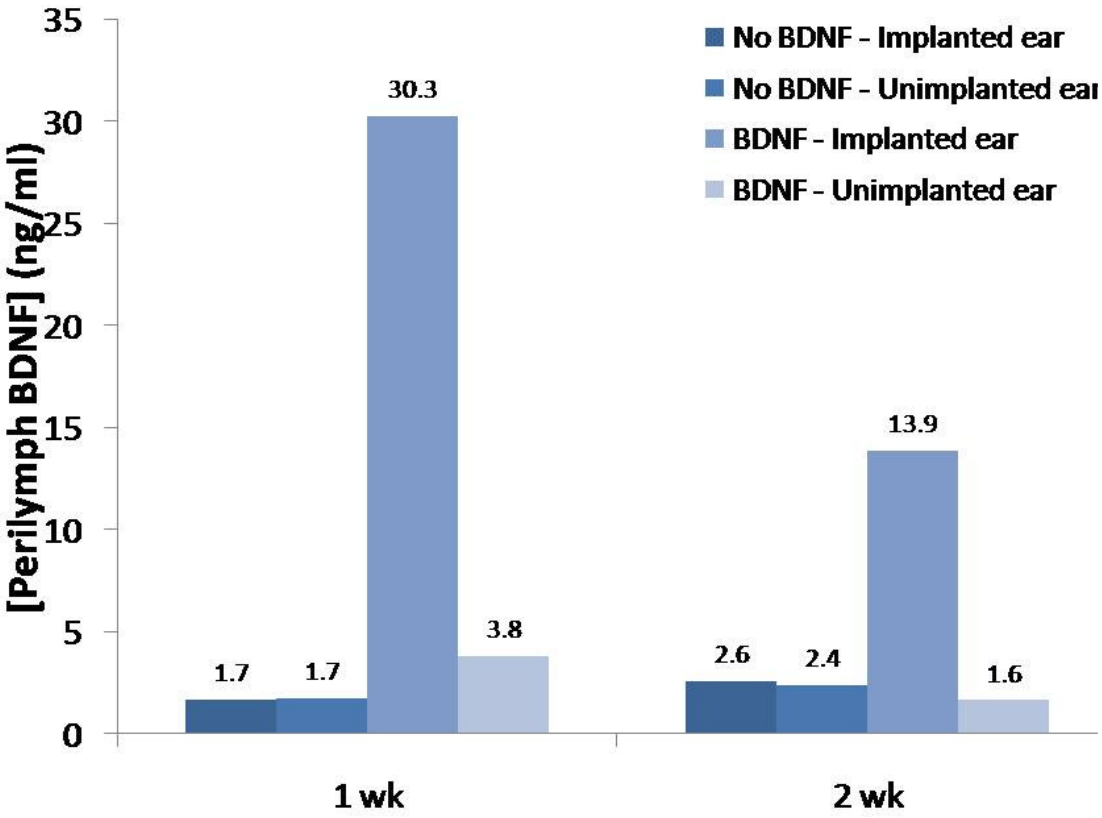


Figure 5-3. Perilymph BDNF concentrations (ng/ml) in the cochleae of animals implanted with coated cochlear electrodes. All implants were coated with PEDOT-PSS and RGD-alginate hydrogel. The implants in the BDNF group were soaked in 500 ng of BDNF prior to implantation. Samples of perilymph were taken from both cochleae, the one with a cochlear implant and the unimplanted ear.

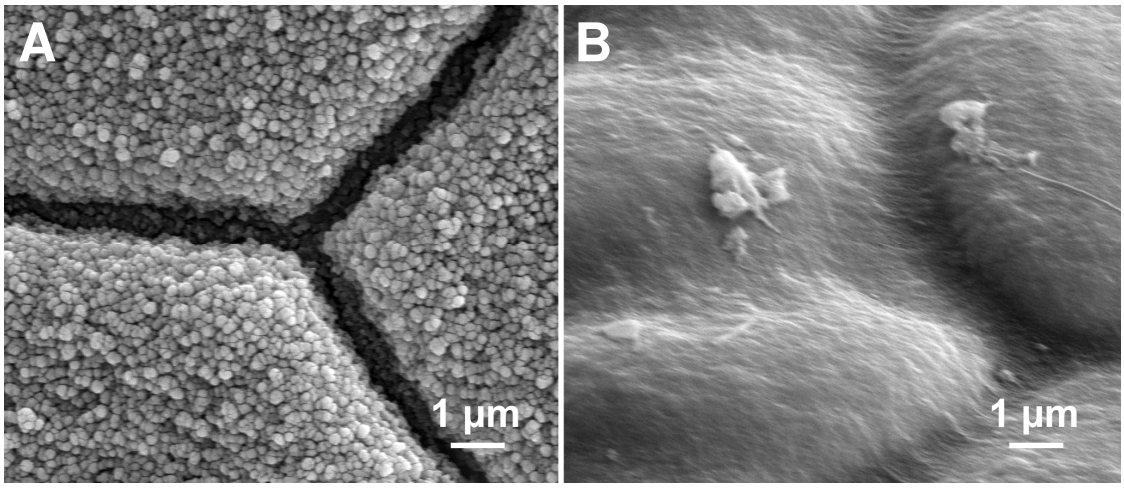


Figure 5-4. (A) Micrograph of PEDOT-PSS coating on cochlear implant before implantation. (B) After implantation, the PEDOT-PSS layer is intact, but covered by a thin layer of biological residue.

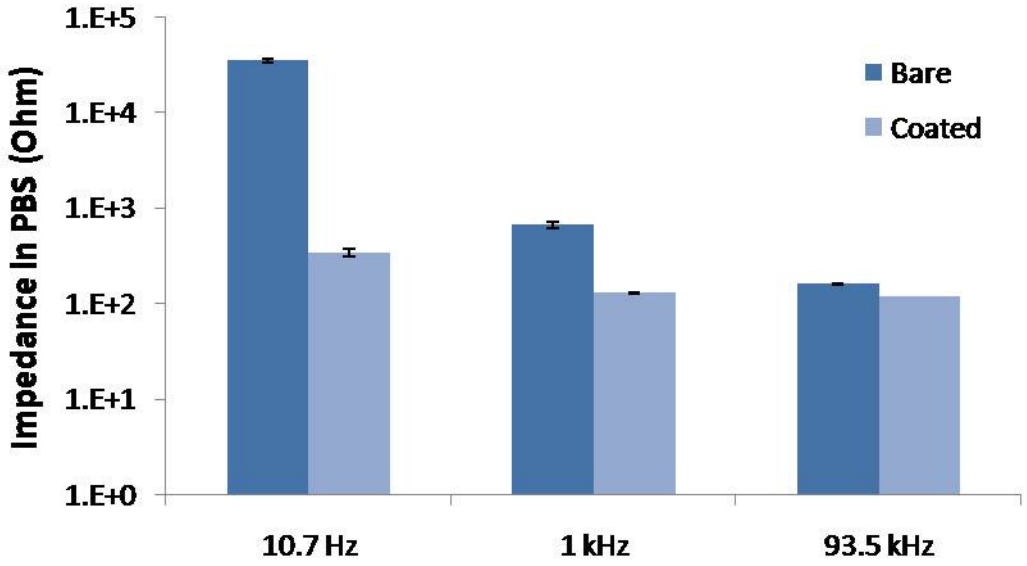


Figure 5-5. Average initial impedance values in saline of PEDOT-hydrogel-BDNF-coated cochlear electrodes compared to uncoated platinum-iridium electrodes. For all frequencies shown, the impedance decrease of coated electrodes compared to uncoated electrodes was statistically significant ($p = .05$).

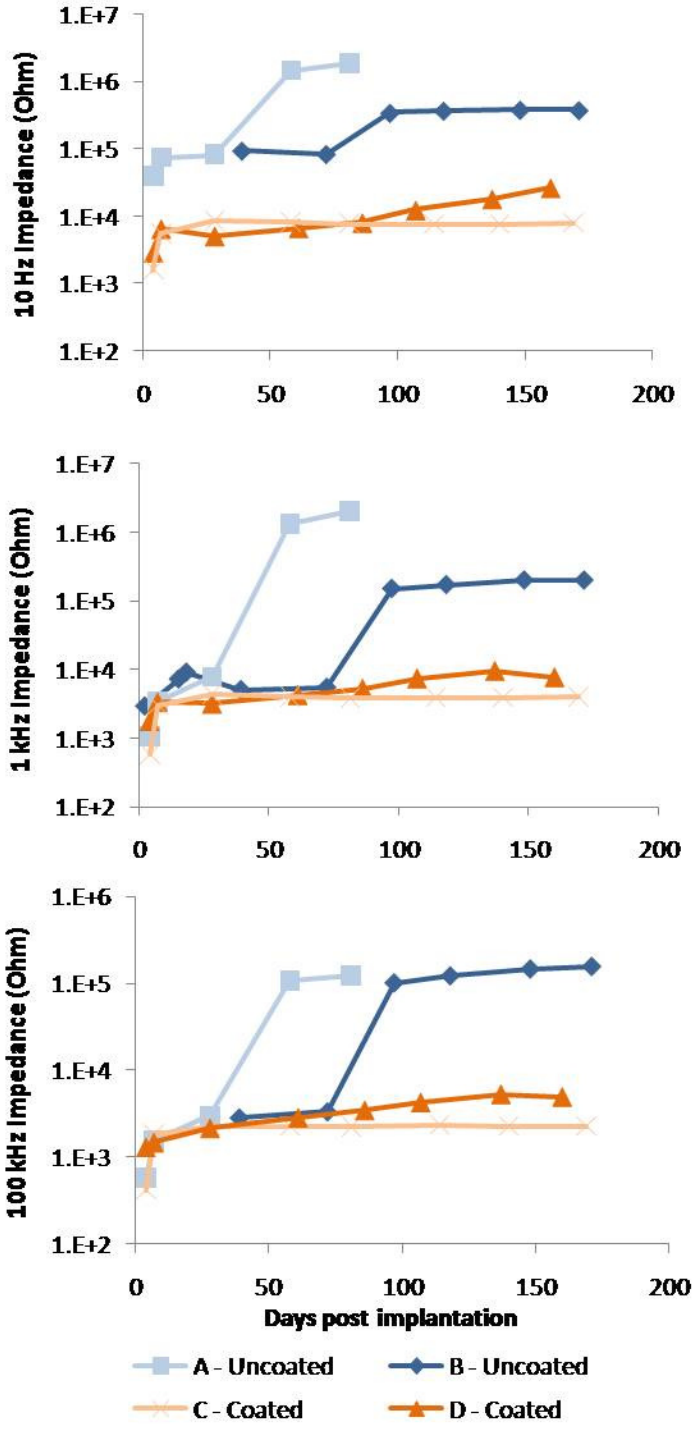


Figure 5-6. Impedances of implanted cochlear electrodes over time. Impedances measured at various frequencies (10 Hz, 1 kHz, 100 kHz) for animals A and B with uncoated platinum-iridium electrodes (blue) and animals C and D with PEDOT-hydrogel -BDNF–coated electrodes (orange).

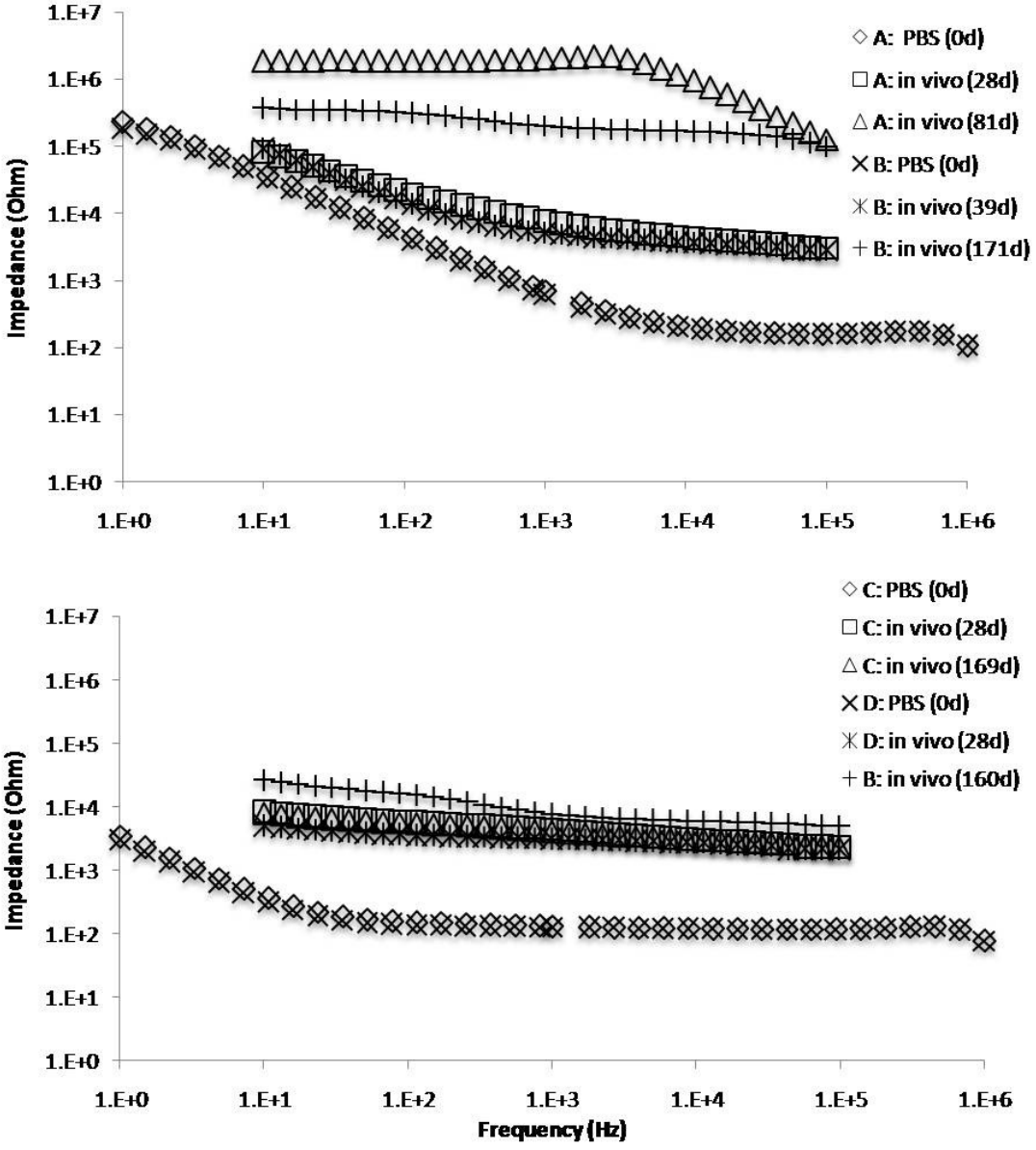


Figure 5-7. (Top) *In vivo* electrochemical impedance spectroscopy of uncoated platinum-iridium cochlear electrodes in animals A and B. (Bottom) PEDOT-hydrogel-BDNF coated cochlear electrodes in animals C and D.

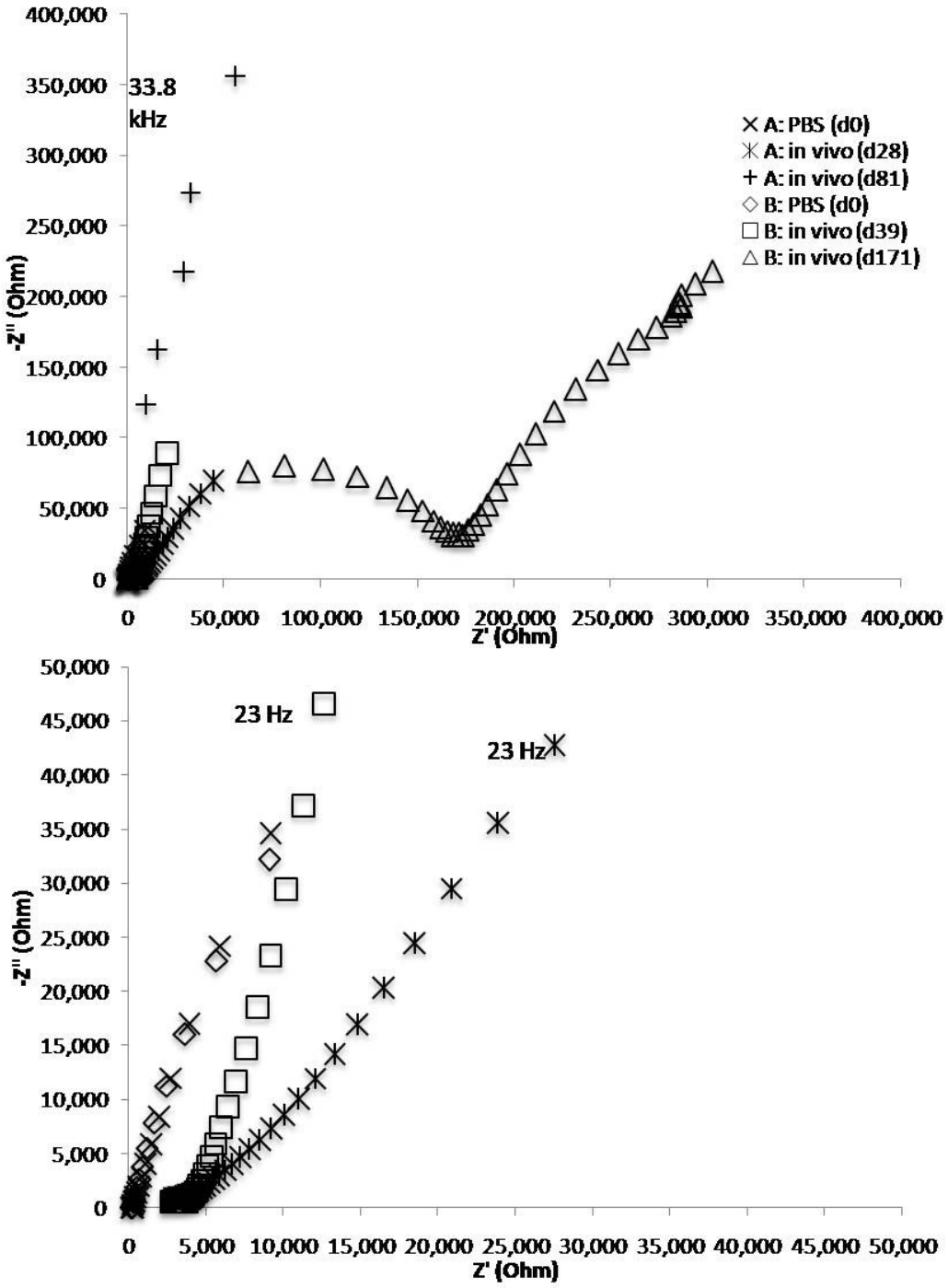


Figure 5-8. (Top) Nyquist plot of impedance of uncoated cochlear implants in PBS and in vivo in animals A and B. (Bottom) Close-up of the high frequency portion of top image. The frequencies listed correspond to the lowest frequency shown for that condition.

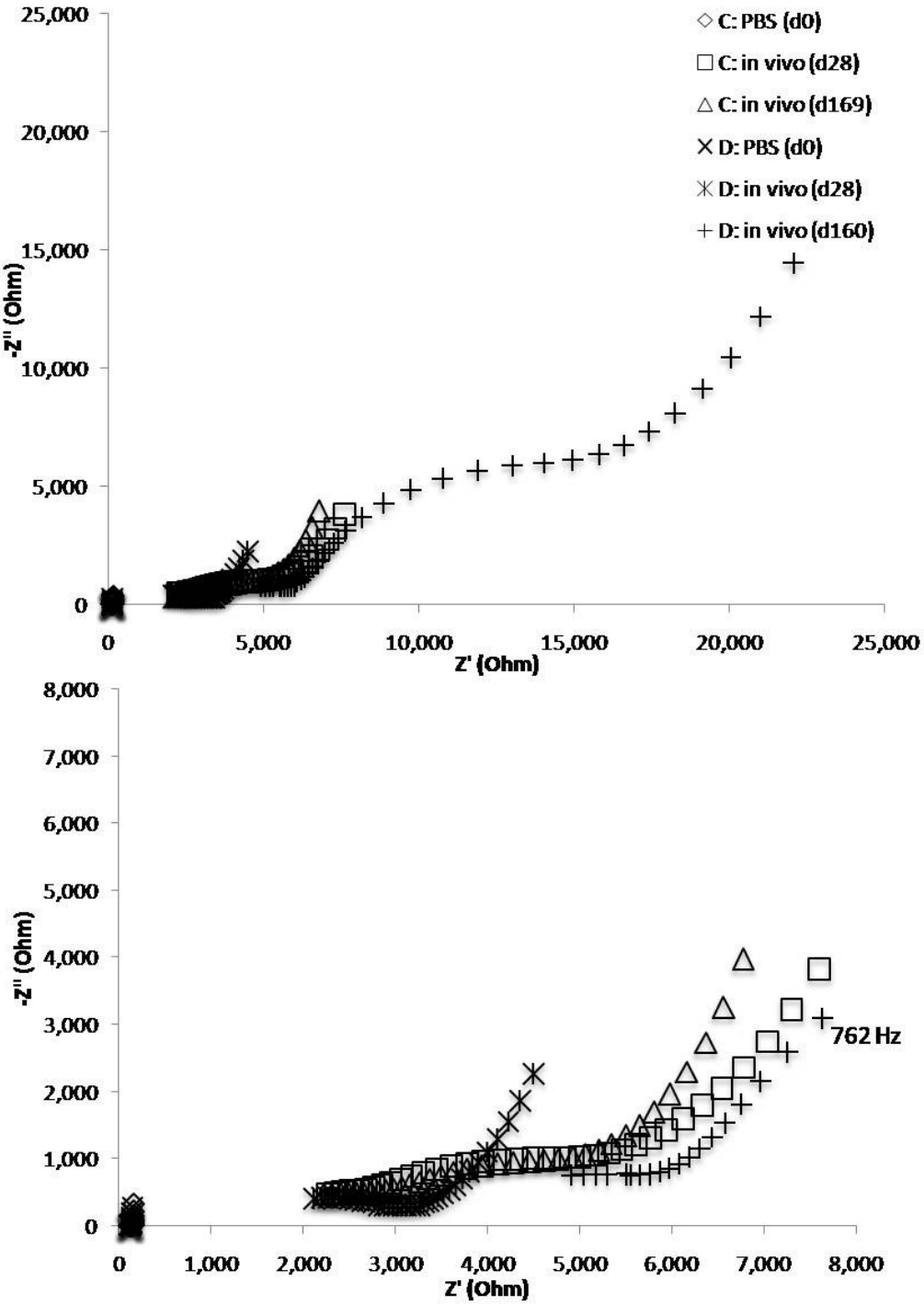


Figure 5-9. Nyquist plot of impedance of PEDOT-hydrogel-BDNF-coated cochlear implants in PBS and in vivo in animals C and D. Bottom image is a close-up of upper image.

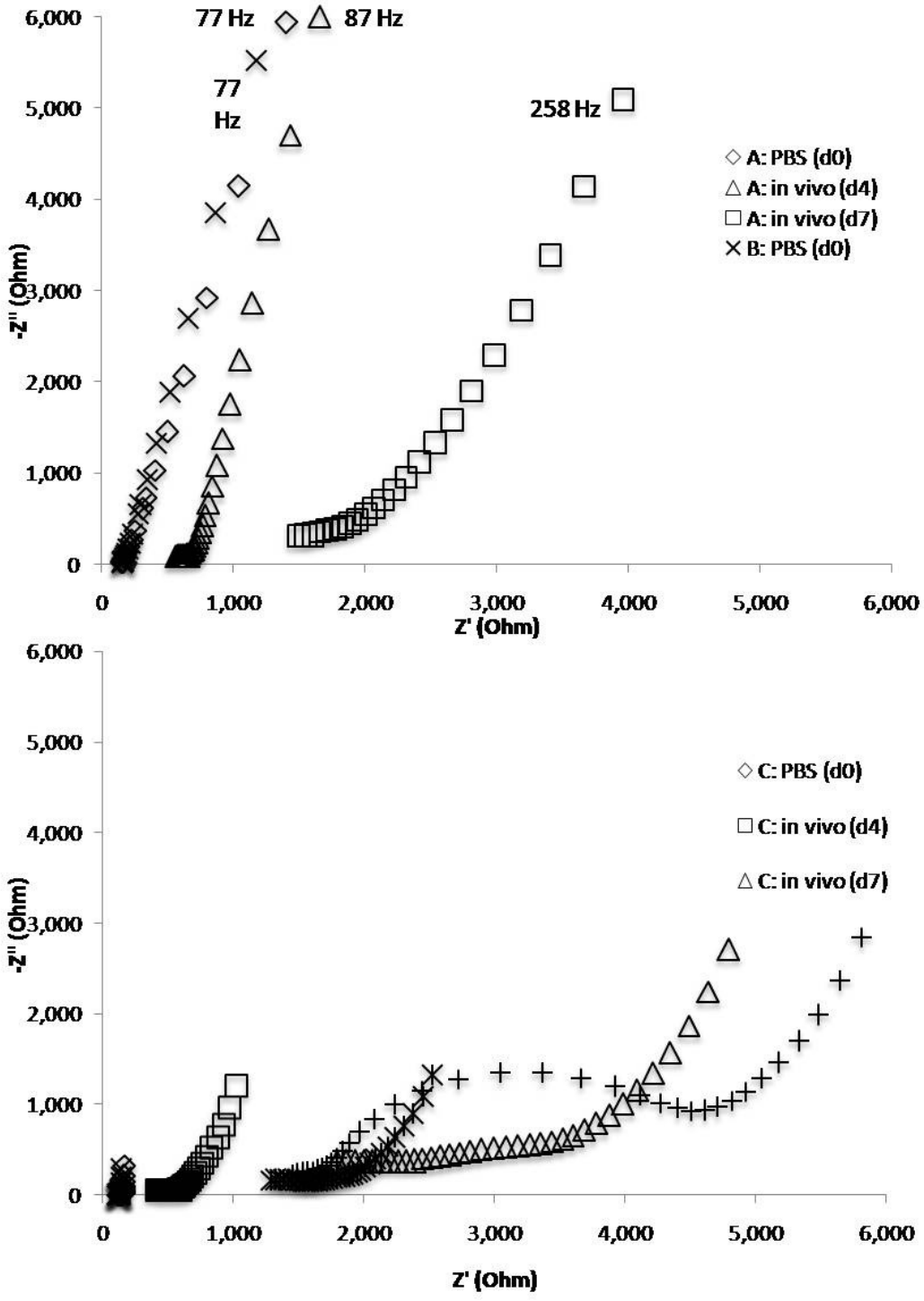


Figure 5-10. Close-up Nyquist plot of cochlear electrode impedances including data in saline and for the first week in vivo. (Top) Uncoated electrodes. (Bottom) Coated electrodes.

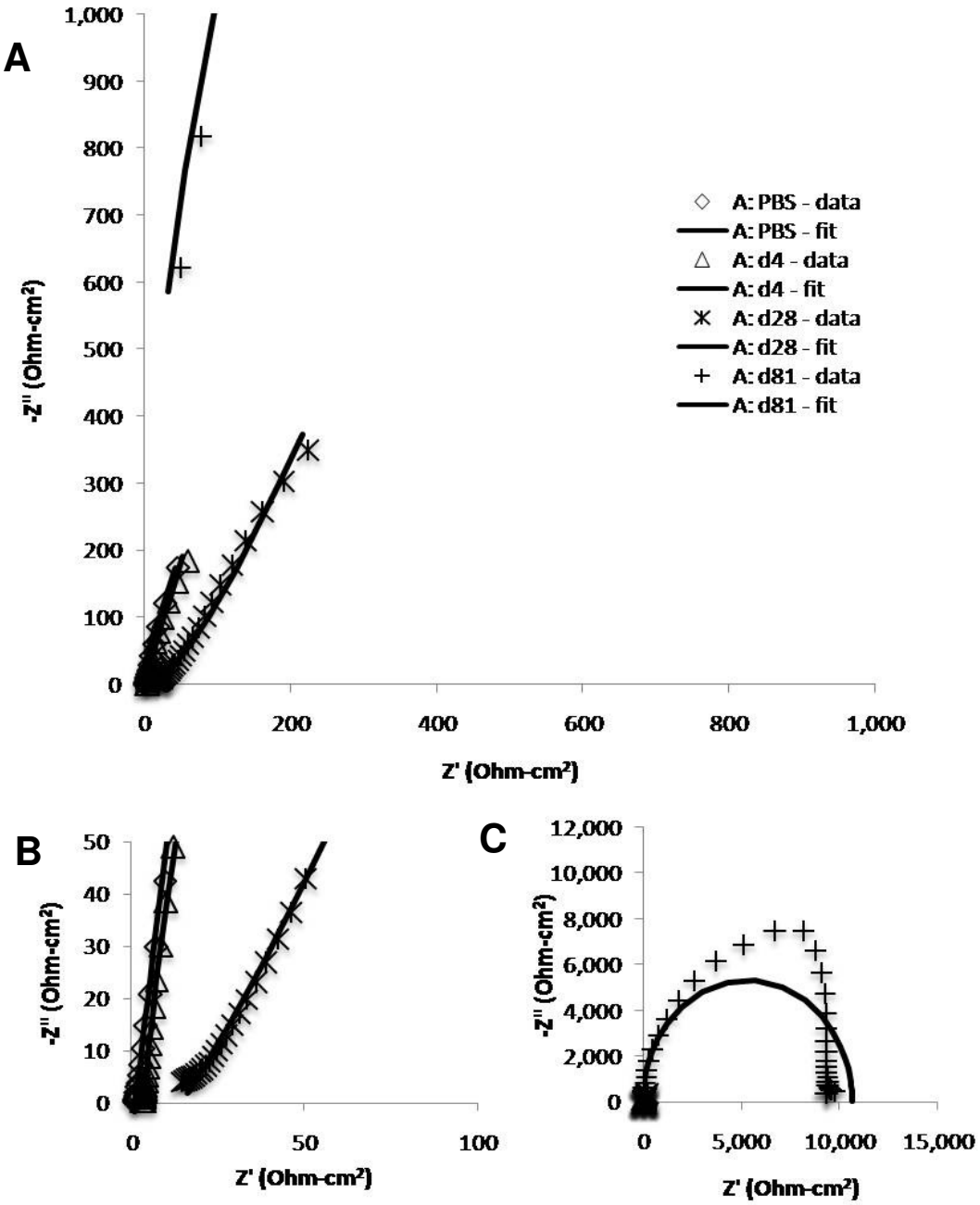


Figure 5-11. (A) Nyquist plot of impedances normalized by surface area from animal A, implanted with an uncoated cochlear electrode. Data fit with RT(RQ) equivalent circuit model. (B) Close-up of high frequency data and fits. (C) Complete field of view including extremely high final impedances.

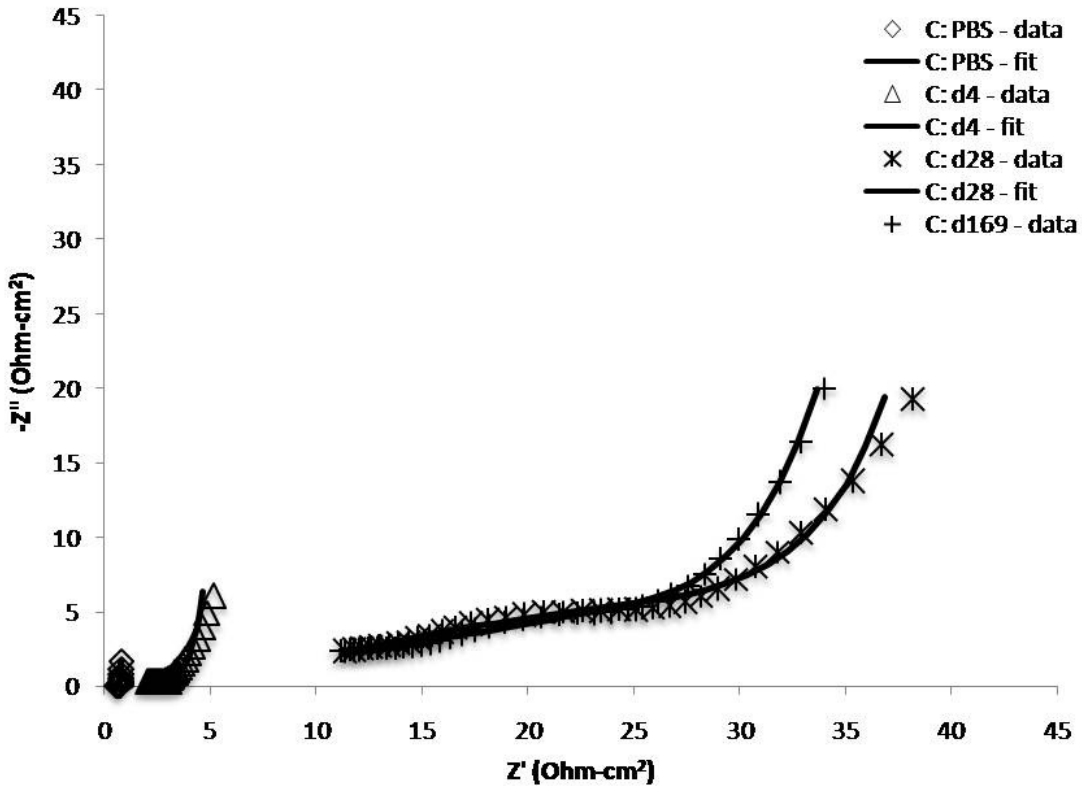


Figure 5-12. Nyquist plot of impedances normalized by surface area from animal C, implanted with a PEDOT-hydrogel-BDNF-coated cochlear electrode. Data fit with RT(RQ) equivalent circuit model.

| | | $R_S$ | $T_S$-Yo | $T_S$-B | $R_{AD}$ | $Q_I$-Yo | $Q_I$-n |
|---|---|---|---|---|---|---|---|
| | | Ω-cm² | S-√sec/cm² | √sec | Ω-cm² | S-sec$^n$/cm² | 0<n<1 |
| **Uncoated** | | | | | | | |
| Animal A | 0d-PBS | 0.71 | 0.0159 | 1.4180 | 1663 | 0.00011 | 0.93 |
| | 4d | 2.84 | 0.0063 | 0.0171 | 104.8 | 0.00029 | 0.87 |
| | 28d | 14.29 | 0.0005 | 994300 | 2472 | 0.00009 | 1.00 |
| | 81d | 9.99E-08 | 21.48 | 9.95E+19 | 10670 | 2.75E-09 | 1.00 |
| Animal B | 0d-PBS | 0.74 | 0.0198 | 1.71E+15 | 1168 | 0.00012 | 0.94 |
| | 39d | 12.96 | 0.0028 | 0.0123 | 2.11E+13 | 0.00275 | 0.40 |
| | 171d | 0.0000001 | 0.00005 | 0.1747 | 772.2 | 3.81E-09 | 0.97 |
| **Coated** | | | | | | | |
| Animal C | 0d-PBS | 0.57 | 0.1913 | 0.0498 | 6.55E+11 | 1.90 | 0.27 |
| | 4d | 1.42 | 0.2954 | 0.0099 | 1.54E+09 | 0.15140 | 0.16 |
| | 28d | 5.52 | 0.0264 | 0.0419 | 50.64 | 0.00438 | 0.26 |
| | 169d | 2.09 | 0.0154 | 0.0702 | 98.56 | 0.01189 | 0.16 |
| Animal D | 0d-PBS | 0.34 | 1.8300 | 0.0058 | 9.01E+08 | 2.16 | 0.05 |
| | 4d | 0.67 | 0.3534 | 0.0081 | 4.45E+15 | 0.06434 | 0.07 |
| | 28d | 7.38 | 0.0090 | 0.1694 | 7.90 | 0.00007 | 0.59 |
| | 160d | 25.66 | 0.0027 | 0.1032 | 84.95 | 0.00028 | 0.62 |

Table 5-1. Equivalent circuit model fit parameters for animals with uncoated cochlear implants and PEDOT-hydrogel-BDNF-coated implants. The experimental data was fit using the model $R_S T_S(R_{AD} Q_I)$.

# References


1. Dodson, H.C. and A. Mohuiddin, *Response of spiral ganglion neurones to cochlear hair cell destruction in the guinea pig.* J Neurocytol, 2000. **29**(7): p. 525-37.

2. Shepherd, R.K. and N.A. Hardie, *Deafness-induced changes in the auditory pathway: implications for cochlear implants.* Audiol Neurootol, 2002. **6**(6): p. 305-18.

3. Spoendlin, H., *Retrograde degeneration of the cochlear nerve.* Acta Otolaryngol, 1975. **79**(3-4): p. 266-75.

4. Nadol, J.B., Jr., *Degeneration of cochlear neurons as seen in the spiral ganglion of man.* Hear Res, 1990. **49**(1-3): p. 141-54.

5. Nadol, J.B., Jr., *Patterns of neural degeneration in the human cochlea and auditory nerve: implications for cochlear implantation.* Otolaryngol Head Neck Surg, 1997. **117**(3 Pt 1): p. 220-8.

6. Li, P.M.M.C., et al., *Analysis of intracochlear new bone and fibrous tissue formation in human subjects with cochlear implants.* Annals of Otology Rhinology and Laryngology, 2007. **116**(10): p. 731-738.

7. Leake-Jones, P.A. and S.J. Rebscher, *Cochlear pathology with chronically implanted scala tympani electrodes.* Ann N Y Acad Sci, 1983. **405**: p. 203-23.

8. Raphael, Y., *Cochlear pathology, sensory cell death and regeneration.* Br Med Bull, 2002. **63**: p. 25-38.

9. Richardson, R.T., F. Noushi, and S. O'Leary, *Inner ear therapy for neural preservation.* Audiol Neurootol, 2006. **11**(6): p. 343-56.

10. Brown, J.N., et al., *Osmotic pump implant for chronic infusion of drugs into the inner ear.* Hear Res, 1993. **70**(2): p. 167-72.

11. Kingma, G.G., J.M. Miller, and M.W. Myers, *Chronic drug infusion into the scala tympani of the guinea pig cochlea.* J Neurosci Methods, 1992. **45**(1-2): p. 127-34.

12. Arnold, A., et al., *Experimental erbium laser surgery in the guinea pig cochlea: its use in the study of afferent cochlear neurotransmitters.* Eur Arch Otorhinolaryngol, 1996. **253**(8): p. 460-3.

13. Ebert, U. and J. Ostwald, *Serotonin modulates auditory information processing in the cochlear nucleus of the rat.* Neurosci Lett, 1992. **145**(1): p. 51-4.

14. Endo, T., et al., *Novel strategy for treatment of inner ears using a biodegradable gel.* Laryngoscope, 2005. **115**(11): p. 2016-20.

15. Tamura, T., et al., *Drug delivery to the cochlea using PLGA nanoparticles.* Laryngoscope, 2005. **115**(11): p. 2000-5.

16. Kim, D.H. and D.C. Martin, *Sustained release of dexamethasone from hydrophilic matrices using PLGA nanoparticles for neural drug delivery.* Biomaterials, 2006. **27**(15): p. 3031-3037.

17. Ito, J., et al., *A new method for drug application to the inner ear.* ORL J Otorhinolaryngol Relat Spec, 2005. **67**(5): p. 272-5.

18. Alles, M.J., M.A. der Gaag, and R.J. Stokroos, *Intratympanic steroid therapy for inner ear diseases, a review of the literature.* Eur Arch Otorhinolaryngol, 2006. **263**(9): p. 791-7.

19. Seidman, M.D. and P. Vivek, *Intratympanic treatment of hearing loss with novel and traditional agents.* Otolaryngol Clin North Am, 2004. **37**(5): p. 973-90.

20. Shirwany, N.A., M.D. Seidman, and W. Tang, *Effect of transtympanic injection of steroids on cochlear blood flow, auditory sensitivity, and histology in the guinea pig.* Am J Otol, 1998. **19**(2): p. 230-5.

21. Silverstein, H., *Use of a new device, the MicroWick, to deliver medication to the inner ear.* Ear Nose Throat J, 1999. **78**(8): p. 595-8, 600.

22. Silverstein, H., et al., *Silverstein MicroWick.* Otolaryngol Clin North Am, 2004. **37**(5): p. 1019-34.

23. Noushi, F., et al., *Delivery of neurotrophin-3 to the cochlea using alginate beads.* Otol Neurotol, 2005. **26**(3): p. 528-33.

24. Burdick, J.A., et al., *Stimulation of neurite outgrowth by neurotrophins delivered from degradable hydrogels.* Biomaterials, 2006. **27**(3): p. 452-9.

25. Nakagawa, T. and J. Ito, *Cell therapy for inner ear diseases.* Curr Pharm Des, 2005. **11**(9): p. 1203-7.

26. Sekiya, T., et al., *Rebuilding lost hearing using cell transplantation.* Neurosurgery, 2007. **60**(3): p. 417-33; discussion 433.

27. Sekiya, T., et al., *Cell transplantation to the auditory nerve and cochlear duct.* Exp Neurol, 2006. **198**(1): p. 12-24.

28. Coleman, B., M.G. de Silva, and R.K. Shepherd, *Concise review: the potential of stem cells for auditory neuron generation and replacement.* Stem Cells, 2007. **25**(11): p. 2685-94.

29. Rejali, D., et al., *Cochlear implants and ex vivo BDNF gene therapy protect spiral ganglion neurons.* Hear Res, 2007. **228**(1-2): p. 180-7.

30. Patel, N.P., A.N. Mhatre, and A.K. Lalwani, *Biological therapy for the inner ear.* Expert Opin Biol Ther, 2004. **4**(11): p. 1811-9.

31. Lalwani, A., et al., *Long-term in vivo cochlear transgene expression mediated by recombinant adeno-associated virus.* Gene Ther, 1998. **5**(2): p. 277-81.

32. Leake, P.A., et al., *Chronic intracochlear electrical stimulation induces selective survival of spiral ganglion neurons in neonatally deafened cats.* Hear Res, 1991. **54**(2): p. 251-71.

33. Leake, P.A., et al., *Chronic intracochlear electrical stimulation in neonatally deafened cats: effects of intensity and stimulating electrode location.* Hear Res, 1992. **64**(1): p. 99-117.

34. Hartshorn, D.O., J.M. Miller, and R.A. Altschuler, *Protective effect of electrical stimulation in the deafened guinea pig cochlea.* Otolaryngol Head Neck Surg, 1991. **104**(3): p. 311-9.

35. Shepherd, R.K., et al., *Cochlear pathology following chronic electrical stimulation of the auditory nerve: II. Deafened kittens.* Hear Res, 1994. **81**(1-2): p. 150-66.

36. Zhong, Y., et al., *Stabilizing electrode-host interfaces: a tissue engineering approach.* J Rehabil Res Dev, 2001. **38**(6): p. 627-32.

37. Duan, Y.Y., G.M. Clark, and R.S. Cowan, *A study of intra-cochlear electrodes and tissue interface by electrochemical impedance methods in vivo.* Biomaterials, 2004. **25**(17): p. 3813-28.

38. Williams, J.C., et al., *Complex impedance spectroscopy for monitoring tissue responses to inserted neural implants.* Journal of Neural Engineering, 2007. **4**(4): p. 410-423.

39. Comisar, W.A., et al., *Engineering RGD nanopatterned hydrogels to control preosteoblast behavior: a combined computational and experimental approach.* Biomaterials, 2007. **28**(30): p. 4409-17.

40. Rowley, J.A. and D.J. Mooney, *Alginate type and RGD density control myoblast phenotype.* J Biomed Mater Res, 2002. **60**(2): p. 217-23.

41. Alsberg, E., et al., *Cell-interactive alginate hydrogels for bone tissue engineering.* J Dent Res, 2001. **80**(11): p. 2025-9.

42. Cui, X.Y. and D.C. Martin, *Electrochemical deposition and characterization of poly(3,4-ethylenedioxythiophene) on neural microelectrode arrays.* Sensors and Actuators B-Chemical, 2003. **89**(1-2): p. 92-102.

43. Richardson-Burns, S.M., et al., *Polymerization of the conducting polymer poly(3,4-ethylenedioxythiophene) (PEDOT) around living neural cells.* Biomaterials, 2007. **28**(8): p. 1539-52.

44. Abidian, M.R. and D.C. Martin, *Experimental and theoretical characterization of implantable neural microelectrodes modified with conducting polymer nanotubes.* Biomaterials, 2008. **29**(9): p. 1273-1283.

# Chapter 6

# Conclusions and future research

## 6.1. Summary

The success of neural prostheses including deep brain stimulation, auditory prostheses, cortical implants, and robotic prosthetic limbs relies on the ability to safely, selectively, and reliably record and stimulate bio-electrical activity. The properties of the tissue-electrode interface, including electrical and mechanical integration, are crucial in determining the longterm reliability and function. One of the major roadblocks for chronic use of many implantable neural prostheses is the multi-stage immune and inflammatory tissue response that occurs after device implantation. This response results in the electrical and mechanical isolation of the device from tissue by a dense fibrous sheath that typically extends 60-100 μm. Additionally, there is an increase in glial cell density for approximately 250 μm and often a decrease in the viability of target neurons for roughly 100 μm. Thus, methods to direct the biological response and promote integration between the device and tissue can support the longterm success of a variety of neural prostheses.

This thesis has presented several coatings designed to promote biological and electrical integration at the neuron-electrode interface. These include the deposition of conducting polymer around living cells and into hydrogels containing cells, the immobilization of adhesion molecules and growth factors in

conducting polymers to direct cell growth, the use of laser patterning to create surface topographies capable of directing cellular attachment and growth, and the use of hydrogels to mechanical buffer tissue from stiff electrodes, as well as to deliver growth factors to promote the viability and growth of target neurons. Development of this technology included morphological, electrochemical, biocompatibility, and *in vitro* characterization, and finally implementation in an *in vivo* model.

## 6.2. Chapter 2 – Interactions of bioactive, biomimetic neural electrode coatings with living cells

One approach to promote integration at the neuron-electrode interface is to incorporate cells or cellular components into the electrode to direct the tissue response. Living cells can secrete growth factors and other compounds to promote the growth and viability of nearby neuronal cells while serving as a living bridge between the electrode and tissue. Conducting polymer coatings make this possible as they are both cytocompatible and electrically conductive. Deposition of conducting polymers around living SY5Y neuroblastoma and primary mixed cortical cells was performed to produce an electrode with cells partially encased within. Monomer toxicity was evaluated prior to electrochemical deposition. At the EDOT concentration used for deposition, 0.01 M, 87 % of SY5Y cells were viable after 24 hours, and 76 % after 72 hours. 24 hours after deposition of PEDOT-PSS around cells, 3 % showed signs of apoptosis; 72 hours after deposition, 11 % were apoptotic. In addition, the cytoskeleton of encapsulated cells slowly deteriorated over the course of a week. Strategies to preserve the cytoskeleton and increase cell viability were achieved by incorporating adhesion peptides or other extracellular components into the conducting polymer matrix. Another method of integrating living cells onto biomedical electrodes is to encapsulate the cells first in a hydrogel scaffold that is then coated onto the electrode. Conducting polymer fibers can then be grown from the electrode through the hydrogel scaffold, resulting in a three-dimensional gel electrode containing living cells. This can be used to help promote the

healing and integration of implantable electrodes, and also serves as a mechanical buffer to reduce the mechanical stresses that occur when stiff materials such as silicon or metals are implanted into brain or other soft tissue.

In addition to providing increased biocompatibility and integration, the conducting polymer coatings also reduce the electrode impedance for improved recording, and increase the charge storage capabilities of the electrode for enhanced stimulation. Transition electron microscopy studies reveal that the conducting polymer is aggregating around the alginate polymer fibrils and increases fiber diameter from 5.1 ± 1.2 nm to 7.5 ± 1.8 nm.

Future efforts will be to further characterize the response of cells to the deposition of conducting polymer around them and the development of methods to retain cell viability throughout the process. These studies will investigate the effects on the cytoskeleton reconstruction, including the polymerization and deconstruction of f-actin fibers. Initial efforts have shown that electrically active cells including neurons, nerve cell lines, and myocytes withstand the deposition process at higher rates than non-electrically active cells. Thus efforts to transfect non-electrically active cells with neuronal ion channels may help protect these cells while revealing the underlying mechanisms of the cellular response. Incorporation of extracellular components into the PEDOT film has shown increased cell viability, therefore further studies using immobilized adhesion molecules and cell components may be pursued. Chemically modified EDOT monomers with side groups capable of functionalization with neurotrophins or adhesion molecules may be implemented to increase neuronal attachment and viability. These surfaces may also be tailored to selectively attract neurons and repel other cell types based on the functional molecules used. For example, in peripheral nerve applications it is desirable to selectively connect to sensory or motor neurons and not attract reactive astrocytes or other immune cells, thus electrodes could be functionalized with adhesion molecules specific to these neuronal type.

Studies are currently underway to further understand the characteristics of PEDOT deposition in three-dimensional matrices including hydrogels and tissue.

The scaffold composition and density, electrical field gradient, and local electrolyte environments are all thought to play roles in the deposition process and resulting conducting polymer morphology. Finite element and molecular modeling of the deposition process could further determine the contributions of these parameters. Elucidating each of these roles will help in the reproducible production of three-dimensional conducting polymer electrodes, injectable gel electrodes, and deposition in living tissue.

### 6.3. Chapter 3 – Laser interference patterning of PEDOT-PSS for neuronal guidance

Direct laser writing and laser interference patterning are two useful methods for patterning PEDOT-PSS and other biomaterials with microscale features to direct the attachment, orientation, and growth of neurons and muscle cells. Direct laser writing is extremely adaptable at creating different patterns with varying shapes and lengths. In our studies, portions of PEDOT-PSS substrates were ablated to form channels with widths of 2 – 60 µm. This technique was compared to laser interference patterning, in which two or more laser beams are overlapped to create periodic interference patterns with ablation at the maxima. Interference patterning offers the ability to pattern larger areas with identical features in a single shot. In our studies, interference patterning produced channels in PEDOT-PSS films with two periods: 7.82 and 13.5 µm. The laser fluences used in both laser patterning methods can be tailored to selectively remove conducting polymer layers without removing the underlying metallic substrates. This results in smooth-bottomed channels. Cell culture studies revealed the orientation of neuroblastoma on patterned substrates. Laser interference patterned channels with 7.82 µm periodicity on 825 nm thick PEDOT-PSS provided the highest degree of SY5Y neurite alignment of any patterned substrate, with 87 % of neurites aligned within 10 ° of the pattern direction. These conditions also resulted in the longest average neurite length. Orientation and elongation seems to be driven by neurite attachment and extension along the interface between PEDOT-PSS and ITO/AuPd. Channels

were also created in thicker PEDOT-PSS films in which the underlying ITO/AuPd was not exposed. These all-PEDOT channels produced less orientation than those with exposed ITO/AuPd.

Future studies will further characterize the effects of laser-modification on the chemical and electrical properties of PEDOT-PSS films. Fourier transform infrared spectroscopy, x-ray photoelectron spectroscopy, and secondary ion mass spectroscopy may be used to investigate changes in the chemical composition due to modification with nanosecond and femtosecond lasers. AFM studies have provided insight into the structural reorganization that occurs, but conductive AFM studies may also reveal characteristics of the surface conductivity and charge of these patterned PEDOT-PSS electrodes.

To further develop these laser patterning techniques for central and peripheral nerve regeneration, it will be necessary to repeat these studies with primary cell lines, possibly mixed neuronal/glial co-cultures, and potentially stem cells. Additional measurements may include quantifying neurite branching, cell proliferation, differentiation, and cell death. These studies will provide further information on the mechanisms for neuronal attraction, attachment , neurite elongation, and guidance, as well as optimal pattern dimensions and geometries for regeneration. Various pattern geometries including islands, diamonds, rhombuses, and channels can easily be created and compared using laser patterning techniques. Variation of the substrate materials and roughness measurements may also provide insight into the nature of neurite attachment and elongation along the PEDOT/ITO/AuPd interface.

Eventually these patterned surfaces could be adapted for a specific neural prosthetic application such as cochlear implants, with channels for neuronal attachment that direct processes towards individual electrodes. They would then be tested for their ability to selectively attract and promote adhesion of spiral ganglion neuronal processes as well as their ability to stimulate neuronal activity. Another possible application is the use of electrodes to record and sort signals sent from motor neurons to control prosthetic limbs for amputees. By promoting the formation of neuro-muscular junctions onto the electrode using adhesion

molecules found in the post synaptic complex, these patterned electrodes may selectively attract and integrate with motor neurons, while complimentary electrodes could be used to send sensory information through other neurons. Laser-patterned guidance channels may also be used to guide cell processes towards a defined target where PEDOT will then be deposited around the cell process, using methods from Chapter 2, to form an intimate connection on a specific region of the cell.

### 6.4. Chapter 4 – Bioactive conducting polymer coatings for cochlear stimulating electrodes

Coatings developed to improve the tissue integration and charge transfer of cochlear implant electrodes were made from the conducting polymer, PEDOT-PSS, as well as a layer of RGD-functionalized hydrogel. SEM studies reveal that the conducting polymer layer provides a high surface area for improved charge transfer between the electrode and electrolyte. Impedance spectroscopy indicates reduced impedance across a broad frequency range, while cyclic voltammetry shows increased charge delivery capabilities of the coated electrodes. Coatings on cochlear electrodes reduced the electrode impedance by 80 and 99 % at 1 kHz and 10.7 Hz, respectively. Under biphasic stimulation, the highest charge density achieved with PEDOT-PSS coated electrodes was 16 $mC/cm^2$.

The hydrogel layer re-swells when implanted in order to provide a mechanical buffer between the cochlea and metallic implant, and was functionalized with the adhesion polypeptide RGD to induce neuronal fixation onto the implant. Sterilization with ethylene oxide gas had no effect on the electrical, chemical or structural properties of the coating. These coated implants can also be used to deliver growth factors, such as BDNF, to promote neuronal viability and proximity, or anti-inflammatory steroids to reduce inflammation and fibrous tissue growth.

Cochlear electrode coatings should be applied to commercially-available electrode arrays for further development. These cochlear electrode coating studies were performed using home-made platinum-iridium ball electrodes, which are affordable and easy to use. Despite these advantages, they have much variability in starting impedance due to the variability of the electrode fabrication process. Commercial implants also contain higher numbers of electrodes and will present new difficulties in selectively applying PEDOT and hydrogel coatings to individual electrodes, but will provide more data for each array that is more directly applicable to clinical applications.

Continued refinement of the coating process will include methods to coat large arrays, methods to improve coating adhesion to a variety of substrates, testing with other sterilization techniques including gamma irradiation, and accelerated aging studies on coating stability. With slight re-engineering, these coatings designed for stimulation of the cochlear nerve will also be useful for other stimulation applications including cardiac arrhythmia management, cardiac defibrillation, deep brain stimulation, diaphragm pacing, bladder and bowel control, chronic pain applications, and peripheral sensory nerve stimulation.

### 6.5. Chapter 5 – Performance of BDNF-secreting, PEDOT-coated cochlear implants *in vivo*

Studies confirm that PEDOT, hydrogel, BDNF-coated cochlear electrodes have lower and more stable impedance across a broad frequency range than uncoated implants throughout 6 months implanted in an animal. Animals that received uncoated electrodes were more likely to have electrode failure that included extremely high electrode impedances. The nature of the failure is still uncertain. Explanted uncoated electrodes were intact and functional, indicating that insulating tissue reactions might be responsible. Explanted coated implants were also intact. Histological evaluation is ongoing and should provide more information about neuronal viability, neuronal proximity to the electrode, fibrous

and bony tissue growth around the electrode, and the extent of immune or inflammatory response.

BDNF delivery was monitored *in vivo* and indicated that levels of the neurotrophin increased to 30.3 ng/ml after one week compared to 1.7 ng/ml in animals that received control implants without BDNF. Histological sections will further elucidate the effects of localized cochlear BDNF delivery on neuronal viability and neurite extension. In future work, electrophysiological studies will be performed and related to BDNF delivery.

Electrochemical impedance spectroscopy of implanted electrodes also provided useful information about the electrode quality and the tissue response in real time. Coated cochlear implants had reduced failure than uncoated implants and had a final average 1 kHz impedance of 5870 Ω compared to $1.2 * 10^6$ Ω for uncoated implants after 6 months. Equivalent circuit models based on impedance spectroscopy results provide a good fit for coated and uncoated electrode performance and predictions about the extent of tissue encapsulation. At the failure point of uncoated electrodes, the model no longer holds up, indicating limitations of our measuring equipment. The models also indicate that at low frequencies there is approximately 50 % more surface area for coated electrodes. This conservative estimate could be used to produce future electrodes which are smaller and more closely spaced, but can still safely deliver comparable amounts of charge to produce neuronal activation.

Ongoing histological evaluation to quantify neuronal viability and fibrous tissue growth will provide insight into the effects of BDNF delivery and RGD hydrogel coatings as well as the failure mechanism of the uncoated electrodes. The optimal time course for BDNF delivery and the use of other growth factors will be assessed. Future studies will also investigate the effects of conducting polymer coatings on electrophysiological effects, including effects on the electrically-evoked auditory brainstem response (eABR). It is hypothesized that PEDOT coatings will reduce the voltage and charge necessary to induce auditory neuronal activity, thereby paving the way for the testing of smaller PEDOT-coated electrodes. Preliminary studies indicate that the hydrogel coating acts as

a shunt pathway, particularly during bipolar stimulation; thus, hydrogel thickness will be minimized.

Future studies incorporating the use of commercial multichannel electrodes will increase data production from each animal and allow for control sites within on each array to minimize the variability between animals. *Ex vivo* implantation of coated cochlear electrodes in model cochleae will provide information about the optimal electrode composition for safe implantation and low electrophysiological thresholds. Improvements to the production of three-dimensional PEDOT-hydrogel electrode coatings will be pursued to produce expandable spongy electrodes that can reduce the distance between the electrode and neurons.

## 6.6. Future research and development goals

In order to promote the formation of safe, permanent, and highly selective neuron-electrode interfaces for neuronal stimulation and recording, certain properties are necessary. Ideally, electrodes will communicate with individual neurons in the brain or peripheral nervous system. In order to accomplish this, electrodes must be extremely small, sensitive, and addressable. The neuronal population should be healthy and as close as possible to the electrode for high selectivity. When possible, materials with mechanical properties equal to those of tissue should be selected. Any mismatches in mechanical stiffness should be mediated by smooth gradients of stiffness between the tissue and device to mitigate interfacial stresses [1]. Electrodes should also be capable of rapidly and safely converting electronic charge to the ionic charges used in tissue. Efforts to do so have produced small ionic pumps capable of shuffling biological electrolytes [2]. While fibrous encapsulation surrounding implanted devices often limits the electrical conductivity of the interface, it also helps to fix the device to the tissue which is important in preventing device migration and repeated injury. The use of bioactive surfaces functionalized with adhesion molecules, extracellular components, polypeptides or cell components may be used to

promote tissue adhesion and fixation. One of the most difficult problems with implanted devices is the initial surgical implantation. Even the most skilled surgeons produce trauma, bleeding and cellular damage that initiates immune and inflammatory responses. Efforts should be made to reduce this initial trauma because it is correlated with the long term tissue response in cochlear implants and other devices. Some implants have been designed to deploy at the rate of a moving cell [3] while others contain lubricious coatings [4]. Implementing these design goals will require advanced materials research, along with biomedical engineering and neuroscience expertise. Interdisciplinary communication and collaboration are vital for development of optimal neural interfaces.

Conducting polymer electrode coatings offer many advantages over currently used materials for biological electrodes. The impedance of PEDOT-coated electrodes is as low or lower than IrOx, TiN, and platinum black coated electrodes that are currently the most often used electrode coatings for improved electrical transfer. The charge density for stimulation is higher than IrOx, the material most often used on the surface of implantable stimulating electrodes. In addition, their mechanical properties are much more similar to biological tissue—soft and fuzzy—making them an ideal material to have at the device-tissue interface. They can also deliver small amounts of pharmaceutical agents to reduce swelling, scarring, and cell death directly at the electrode site, where they are needed the most. Delivery can also be controlled electrically so that drug is released only when it is needed. Despite these advantages, there are many hurdles to its widespread clinical use. Since these materials have no history of use in human, their safety and biocompatibility must be approved by FDA testing and ISO 10993 compliance. The FDA approval process is quite lengthy and costly. Once approved for a given device, abridged testing must be repeated for use on other devices. Each application will require adaptation of the coatings for a specific device geometry and function.

Many potential commercial applications exist for conducting polymer coatings. In addition to cortical and cochlear implants, other devices that communicate electrically with cells or tissue can benefit from these low-

impedance biologically functionalized coatings. Such devices include biosensors, cell culture electrodes, drug screening, water toxin monitoring, deep brain stimulation, cardiac arrhythmia management, cardiac defibrillation, chronic pain management, nerve regeneration, glucose monitoring, bladder and bowel control, diaphragm pacing, retinal implants, prosthetic limb interfaces, and treatment of movement disorders. As the ability to selectively promote permanent integration at the neuron-electrode interface progresses, this technology will be useful for tailoring the integration of any implantable device and may make possible the next generation of prostheses.

### 6.7. Final remarks

The results of this thesis provide useful tools to improve the safety and function of traditional bio-electrodes. In particular, conducting polymer coatings improve the electrical properties of bio-electrodes while incorporated adhesion molecules, growth factors and microscale patterned features direct the biological response. These coatings can be used to create sensitive, low-impedance recording electrodes, or to deliver higher charge and current densities at lower voltages than traditional materials. Higher density arrays with smaller PEDOT-coated electrodes could thus be used for many applications. *In vitro* testing has demonstrated the biocompatibility of these coatings, as well as their ability to direct cell viability, proliferation, orientation, and adhesion. *In vivo* testing indicates that coated electrodes have more consistent electrical performance and lower impedance than uncoated implants. By addressing the integration and conductivity of the neural interface using these conducting polymer coatings, current neural prosthetic devices can be made safer, more reliable, and more efficient, while providing the experience and technology for future devices.

# References


1. Miserez, A., et al., *The transition from stiff to compliant materials in squid beaks.* Science, 2008. **319**(5871): p. 1816-9.

2. Isaksson, J., et al., *Electronic control of $Ca^{2+}$ signalling in neuronal cells using an organic electronic ion pump.* Nat Mater, 2007. **6**(9): p. 673-9.

3. Sharp, A.A., et al., *Toward a self-deploying shape memory polymer neuronal electrode.* J Neural Eng, 2006. **3**(4): p. L23-30.

4. Laszig, R., G.J. Ridder, and M. Fradis, *Intracochlear insertion of electrodes using hyaluronic acid in cochlear implant surgery.* J Laryngol Otol, 2002. **116**(5): p. 371-2.